POLITECNICO DI MILANO

Polo Regionale di Lecco

Faculty of Engineering

Mechanical Engineering Department

Heat Transfer Analysis of PEMFC System Using FEM

A Thesis Submitted to the Mechanical Engineering Department in the Partial Fulfillment of the Requirements for the Master of Science Degree in Mechanical Engineering.

Submitted By: Hafiz Muhammad Fahid Amin (737589)

University Tutors: Prof. Giovanni Dotelli

Prof.ssa Barbara Rivolta

Company Tutor: Ing. Paolo Fracas

Academic Year 2009/2010

ACKNOWLEDGEMENT

I would like also to express my gratitude to my university tutors, Prof. Giovanni Dotelli and Prof. Barbara Rivolta whose expertise, understanding, and patience, added considerably to my graduate experience. I appreciate his vast knowledge and skill in many areas and his assistance in writing my thesis. I would like to thank all my Professors for their assistance they provided at all levels during my study and specially many thanks to Luca Omati, assistant of my university tutor.

I would like to acknowledge my company tutors Ing. Paolo Fracas and my colleagues Stefano Limonta, Fabio Musio and all members of Genport for their terrific instruction and their dedication for sharing their wealth of knowledge and experience with me.

Very special thanks goes out to Politicnico Di Milano – Lecco campus, and to the all staff for all the instances in which their assistance helped me a lot along my studies.

As well, I would like to gratefully acknowledge to my parents and my family for the support they provided me through my entire life and during my study period. Finally I must acknowledge my best friends, without their encouragement and editing assistance, I would not have finished this work.

INDEX

Introduction

For the economic growth and standard of living, modern industrialized society is dependent upon the energy and 85 % of the energy is obtained from fossil fuels [DOE/EIA, 2001]. Not only the availability of these fuels is limited but also having a harmful effect on environment, which in turn cause direct and indirect effect on the global economy and the environment [Stern, 2007].Necessary steps need to be taken towards the development of new energy production methods before these fuels become scarce or irreversibly change the planet. Investing in sustainable energy production will also hedges against fossil fuel uncertainty and carbon policy, by fixing the cost of production, which intern creates economic stability. Therefore, there is an impelling need for a sustainable energy approach capable of maintaining future economic standards and minimizing the environmental impact due to energy production.

The interest in fuel cells (FCs) has increased during the past decade because this new technology can fulfill all of these requirements; fuel cells are now closer to commercialization than ever, and they have the ability to satisfy all of the global power needs while meeting efficacy and environmental expectations.

Proton exchange membrane fuel cells, also known as polymer electrolyte membrane (PEM) fuel cells (PEMFC), are a type of fuel cell being developed for transport applications as well as for stationary fuel cell applications and portable fuel cell applications. Their distinguishing features include lower temperature/pressure ranges (50 to 100°C) and a special polymer electrolyte membrane. They use hydrogen as fuel.

In this thesis is presented the literature review of PEM Fuel Cell System of what is already known. Then the parametric analysis of Genport 300W fuel cell system is done at various operating temperature and various stoichiometric ratios. With this analysis the optimum operating temperature and stoichiometric ratio for this fuel cell system is found. Moreover at this optimum operating condition the power output and power losses of the system are analysed.

In the last part of the thesis FEM analysis of the fuel cell system is performed in order to know the thermal balance of the system. A very important computation is done to know the best possible configuration of the system to improve the cooling system’s performance.

Section 1

Introduction to Fuel Cell

The current movement towards environmentally friendlier and more efficient power production has caused an increased interest in alternative fuel and power sources. Fuel cells are one of the older energy conversion technologies, but only within the last decade have they been extensively studied for commercial use. The reliance upon the combustion of fossil fuels has resulted in severe air pollution, and extensive mining of the world oil resources. In addition to being hazardous to the health of many species (including our own), the pollution is indirectly causing the atmosphere of the world to change (global warming). In addition to health and environmental concerns, the world's fossil fuel reserves are decreasing day by day. The world needs a power source that has low pollutant emissions, is energy efficient, and has an unlimited supply of fuel for a growing world population. Fuel cells have been identified as one of the most promising technologies to accomplish these goals.

Many other alternative energy technologies have been researched and developed. These include solar, wind, hydroelectric power, bioenergy, geothermal energy, and many others. Each of these alternative energy resources have their advantages and disadvantages, and are in varying stage of development. In addition most of these energy technologies cannot be used for transportation or portable electronics. Other portable power technologies, such as batteries and supercapacitors also are not suitable for transportation technologies, military applications, and the long term need for future applications.

The ideal option for a wide variety of applications is using a hydrogen fuel cell combined with solar or hydroelectric power. Compared to other fuels, hydrogen does not produce carbon monoxide or other pollutants. When it is fed into a fuel cell the

only byproducts are oxygen and heat. The oxygen is again combined with hydrogen to form water when power is needed.

Fossil fuels are limited in supply, and are located in selected regions throughout the world. This leads to regional conflict and wars, which threaten peace. The limited supply and large demand dries up the cost of fossil fuels tremendously. The end of low cost is rapidly approaching. Other types of alternative technology such as fuel cells can last indefinitely when non fossil fuel based hydrogen is used.

The 19th Century was the century of the steam engine and the 20th Century was the century of the internal combustion engine; it is likely that the 21st Century will be the century of the fuel cell.

Full cells are now on the verge of being introduced commercially, revolutionizing the way we presently produce power. Fuel cells can use hydrogen as a fuel, offering the prospect of supplying the world with clean, sustainable electrical power.

1.1 A Very Brief History of Fuel Cells

The timeline of fuel cell development history is shown in Figure 1-1. The discovery of the fuel cell operating principle—the gaseous fuels that generate electricity, is attributed to Sir William Grove in 1839, although it appears that a Swiss scientist Christian F. Shoenbein independently discovered the very same effect at about the same time (or even a year before). However, in spite of sporadic attempts to make a practical device, the fuel cell, or the "gaseous voltaic battery" as it was called by Grove, remained nothing more than a scientific curiosity for almost a century. It was another Englishman, Francis T. Bacon, who started working on practical fuel cells in 1937, and he developed a 6kW fuel cell by the end of the 1950s. However, the first practical fuel cell applications were in the U.S. Space Program. General Electric developed the first polymer membrane fuel cells that were used in the Gemini Program in the early 1960s. This was followed by the Apollo Space Program, which used the

fuel cells to generate electricity for life support, guidance, and communications. These fuel cells were built by Pratt and Whitney based on license taken on Bacon's patents (Figure 1-2).

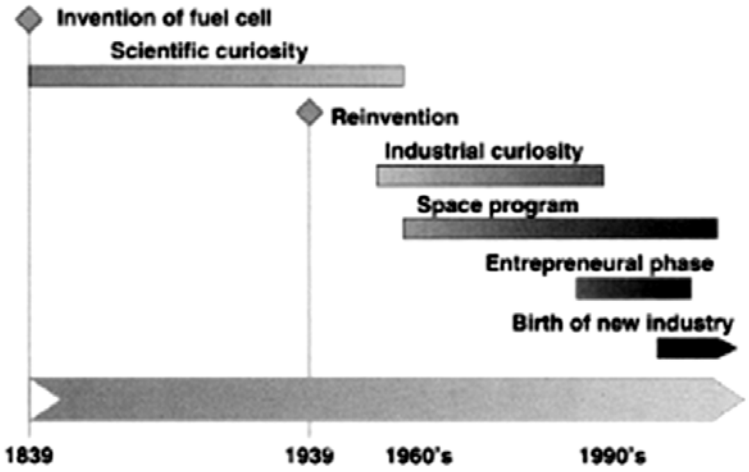

FIGURE 1-1: Fuel cell history timeline.

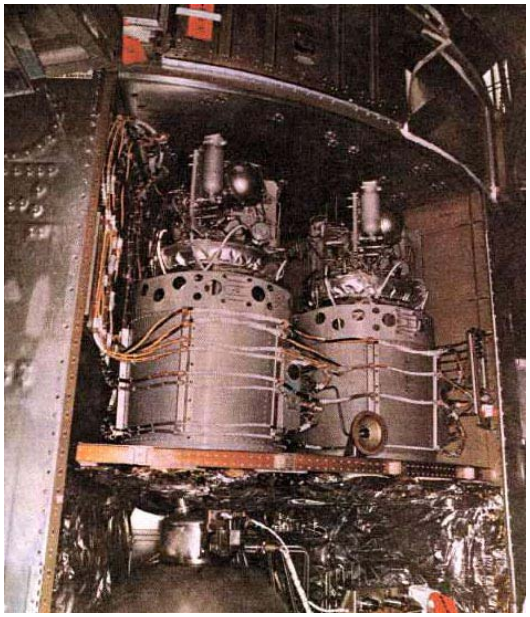

FIGURE 1-2: Apollo fuel cells. (Courtesy of UTC Fuel Cells).

In the mid-1960s General Motors experimented with a fuel cell-powered van (these fuel cells were developed by Union Carbide). Although fuel cells have continued to be

successfully used in the U.S. Space Program until today, they were again "forgotten" for terrestrial applications until the early1990s. In 1989, Perry Energy Systems, a division of Perry Technologies, working with Ballard, a then emerging Canadian company, successfully demonstrated a polymer electrolyte membrane (PEM) fuel cell-powered submarine (Figure 1-3). In 1993, Ballard Power Systems demonstrated fuel cell-powered buses. Energy Partners, a successor of Perry Energy Systems,

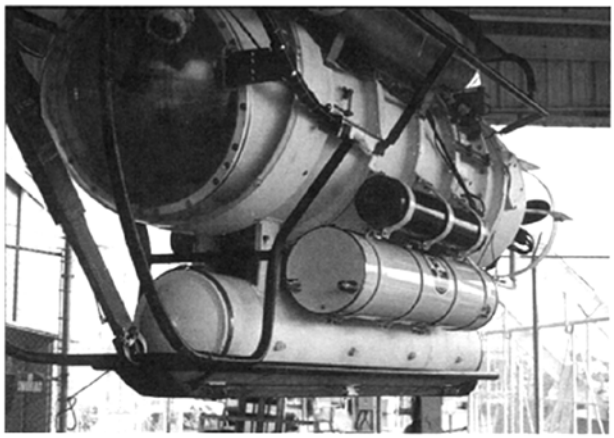

FIGURE 1-3. PC 1401 by Perry Group powered by PEM fuel cells (1989). (Courtesy of Teledyne Energy Systems.)

demonstrated the first passenger car running on PEM fuel cells in 1993. The car companies, supported by the U.S. Department of Energy, picked up on this activity and by the end of the century almost every car manufacturer had built and demonstrated a fuel cell-powered vehicle. A new industry was born. The stocks of fuel cell companies, such as Ballard and Plug Power, soared in early 2000, based on a promise of a new energy revolution (eventually in 2001 they came down with the rest of the market). The number of fuel cell-related patents worldwide, but primarily in the United States and Japan, is increasing dramatically showing continuous interest and involvement of the scientific and engineering community.

1.2 Types of fuel cells

A brief description of various electrolyte cells of interest follows.

1.2.1 Proton Exchange Membrane Fuel Cells (PEMFC)

Proton Exchange Membrane Fuel Cells (PEMFC) are believed to be the best type of fuel cell as the vehicular power source to eventually replace the gasoline and diesel internal combustion engines. First used in the 1960s for the NASA Gemini program, PEMFCs are currently being developed and demonstrated for systems ranging from 1W to 2kW.PEM fuel cells use a solid polymer membrane (a thin plastic film) as the electrolyte. This polymer is permeable to protons when it is saturated with water, but it does not conduct electrons.

Compared to other types of fuel cells, PEMFCs generate more power for a given volume or weight of fuel cell. This high-power density characteristic makes them compact and lightweight. In addition, the operating temperature is less than 100ºC, which allows rapid start-up. These traits and the ability to rapidly change power output are some of the characteristics that make the PEMFC the top candidate for automotive power applications.

Other advantages result from the electrolyte being a solid material, compared to a liquid. The sealing of the anode and cathode gases is simpler with a solid electrolyte, and therefore, less expensive to manufacture. The solid electrolyte is also more immune to difficulties with orientation and has fewer problems with corrosion, compared to many of the other electrolytes, thus leading to a longer cell and stack life.

1.2.2 Alkaline Fuel Cell (AFC)

The electrolyte in this fuel cell is concentrated (85 wt%) KOH in fuel cells operated at high temperature (~250 ˚C, or less concentrated (35-50 wt%) KOH for lower temperature (<120˚C) operation. The electrolyte is retained in a matrix (usually

asbestos), and a wide range of electro catalysts can be used (e.g., Ni, Ag, metal oxides, spinels, and noble metals). The fuel supply is limited to non-reactive constituents except for hydrogen. CO is a poison, and CO2 will react with the KOH to form K2CO3, thus altering the electrolyte. Even the small amount of CO2 in air is detrimental to the alkaline cell.

1.2.3 Phosphoric Acid Fuel Cell (PAFC)

Phosphoric acid concentrated to 100% is used for the electrolyte in this fuel cell, which operates at 150 to 220˚C. At lower temperatures, phosphoric acid is a poor ionic conductor, and CO poisoning of the Pt electrocatalyst in the anode becomes severe. The relative stability of concentrated phosphoric acid is high compared to other common acids; consequently the PAFC is capable of operating at the high end of the acid temperature range (100 to 220 C). In addition, the use of concentrated acid (100%) minimizes the water vapor pressure so water management in the cell is not difficult. The matrix universally used to retain the acid is silicon carbide, and the electrocatalyst in both the anode and cathode is Pt.

1.2.4 Molten Carbonate Fuel Cell (MCFC)

The electrolyte in this fuel cell is usually a combination of alkali carbonates, which is retained in a ceramic matrix of LiAlO2. The fuel cell operates at 600 to 700˚C where the alkali carbonates form a highly conductive molten salt, with carbonate ions providing ionic conduction. At the high operating temperatures in MCFCs, Ni (anode) and nickel oxide (cathode) are adequate to promote reaction. Noble metals are not required.

1.2.5 Solid Oxide Fuel Cell (SOFC)

The electrolyte in this fuel cell is a solid, nonporous metal oxide, usually Y2O3-stabilized ZrO2. The cell operates at 600-1000˚C where ionic conduction by oxygen

ions takes place. Typically, the anode is Co-ZrO2 or Ni-ZrO2 cermet, and the cathode is Sr-doped LaMnO3.

1.3 Fuel cell applications

Why do we need fuel cell

Power traditionally relies upon fossil fuels, which have several limitations: (1) they produce large amounts of pollutants, (2) they are of limited supply, and (3) they cause global conflict between regions. Fuel cells can power anything from a house to a car to a cellular phone. They are especially advantageous for applications that are energy-limited. For example, power for portable devices is limited; therefore, constant recharging is necessary to keep a device working. Table 1-1 compares the weight, energy, and volume of batteries to a typical PEM fuel cell. The fuel cell system can provide a similar energy output to batteries with a much smaller system weight and volume. This is especially advantageous for portable power system. Future markets for fuel cells include the portable, transportation and stationary sectors (basically every sector!). Each market needs fuel cells for varying reasons.

TABLE 1-1

General Fuel Cell Comparison with Other Power Sources

	Weight	Energy	Volume
Fuel Cell	9.5 lb	2190 Whr	4.0 L
Zinc-air cell	18.5lb	2620 Whr	4.0 L
Other battery types	24 lb	2200 Whr	9.5 L

1.3.1 Portable Sector

One of the major future markets for fuel cells is the portable sector. There are numerous portable devices that would use fuel cells in order to power the device for longer amounts of time. Some of these devices include laptops, cell phones, video recorders, ipods, etc. Fuel cells will power a device as long as there is fuel supplied to it. The current trend in electronics is the convergence of devices, and the limiting factor of these devices is the amount of power required. Therefore, power devices that can supply greater power for a longer period of time will allow the development of new, multifunctional devices. The military also has a need for high power, long-term devices for soldiers' equipment. Fuel cells can easily be manufactured with greater power and less weight for military applications. Other military advantages include silent operation and low heat signatures.

1.3.2 Transportation Market

The transportation market will benefit from fuel cells because fossil fuels will continue to become scarce, and because of this, there will be inevitable price increases. Legislation is becoming stricter about controlling environmental emissions. There are certain parts of countries that are passing laws to further reduce emissions and to sell a certain number of zero emission vehicles annually. Fuel cell vehicles allow a new range of power use in smaller vehicles and have the ability to be more fuel efficient than vehicles that are powered by other fuels.

1.3.3 Stationary Sector

Large stationary fuel cells can produce enough electricity to power a house or business. These fuel cells may also make enough power to sell back to the grid. This fuel cell type is especially advantageous for businesses and residences where no electricity is available. Fuel cell generators are also more reliable than other generator types. This can benefit companies by saving money when power goes down for a short time.

1.4 How Does a PEM Fuel Cell Work?

PEM stands for polymer electrolyte membrane or proton exchange membrane. Sometimes, they are also called polymer membrane fuel cells, or just membrane fuel cells. In the early days (1960s) they were known as solid polymer electrolyte (SPE) fuel cells. This technology has drawn the most attention because of its simplicity, viability, quick startup, and the fact that it has been demonstrated in almost any conceivable application, as shown in the following sections.

At the heart of a PEM fuel cell is a polymer membrane that has some unique capabilities. It is impermeable to gases but it conducts protons (hence the name, proton exchange membrane). The membrane that acts as the electrolyte is squeezed between the two porous, electrically conductive electrodes. These electrodes are typically made out of carbon cloth or carbon fiber paper. At the interface between the porous electrode and the polymer membrane there is a layer with catalyst particles, typically platinum supported on carbon. A schematic diagram of cell configuration and basic operating principles is shown in Figure 1-4

Electrochemical reactions happen at the surface of the catalyst at the interface between the electrolyte and the membrane. Hydrogen, which is fed on one side of the membrane, splits into its primary constituents— protons and electrons. Each hydrogen atom consists of one electron and one proton. Protons travel through the membrane, whereas the electrons travel through electrically conductive electrodes, through current collectors, and through the outside circuit where they perform useful work and come back to the other side of the membrane. At the catalyst sites between the membrane and the other electrode they meet with the protons that went through the membrane and oxygen that is fed on that side of the membrane. Water is created in the electrochemical reaction, and then pushed out of the cell with excess flow of oxygen. The net result of these simultaneous reactions is current of electrons through an external circuit—direct electrical current.

The hydrogen side is negative and it is called the anode, whereas the oxygen side of the fuel cell is positive and it is called the cathode.

Because each cell generates about 1V, as will be shown subsequently, more cells are needed in series to generate some practical voltages. Depending on application, the output voltage may be between 6V and 200 V or even more.

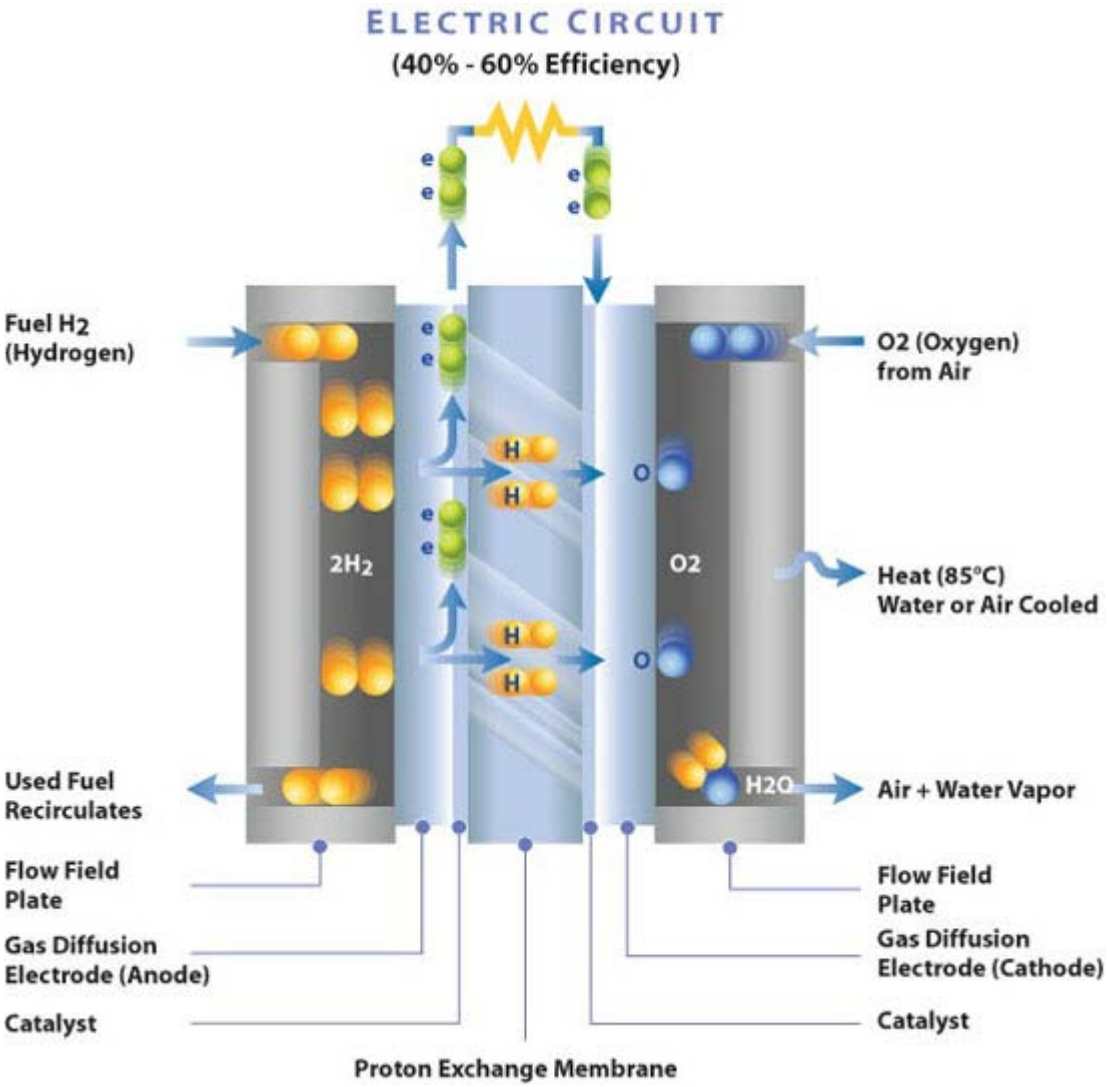

FIGURE 1-4. The basic principle of operation of a PEM fuel cell.

A fuel cell stack needs a supporting to:

• Handle the supply of reactant gases and their exhaust, including the products;

• Take care of waste heat and maintain the stack temperature,

• Regulate and condition power output;

• Monitor the stack vital parameters; and

• Control the start-up, operation, and shutdown of the stack and system components.

Reference:

[1]http://www.ika.rwth-aachen.de/r2h/index.php/Hydrogen_and_Fuel_Cells_in_Portable_Applications

[2] Spiegel C., ***"PEM Fuel Cell Modelling and Simulation Using MATLAB",*** *Elsevier, 2008.*

[3] James Larminie., **''Fuel Cell Systems Explained'',**

[4] http://www.fctec.com/fctec_types_pem.asp

[5] Frano Barbir., " PEM Fuel Cells Theory and Practice.

[6] http://galaxywire.net/wp-content/uploads/2009/05/fuel_cell_bay_4_apollo_sm.jpg

[7] http://www.ballard.com/files/images/aboutballard/How-a-fuel-cell-works.jpg

Section 2

Hydrogen as energy carrier

2.1 Introduction

PEM fuel cells need hydrogen as fuel. Hydrogen is not a source of energy, and hydrogen is not a readily available fuel. Hydrogen is more like electricity—an intermediary form of energy or an energy carrier. Just like electricity, it can be generated from a variety of energy sources, be delivered to the end users, and at the user end, it can be converted to useful energy efficiently and cleanly. However, although electricity infrastructure is already in place, hydrogen infrastructure is practically nonexistent. It is this lack of hydrogen infrastructure that is considered one of the biggest obstacles to fuel cell commercialization. Commercialization of fuel cells, particularly for transportation and stationary electricity-generation markets, must be accompanied by commercialization of hydrogen energy technologies, that is, technologies for hydrogen production, distribution, and storage. In other words, hydrogen must become a readily available commodity (not as a technical gas but as an energy carrier) before fuel cells can be fully commercialized. On the other hand, it may very well be that the fuel cells will become the driving force for development of hydrogen energy technologies. Fuel cells have many unique properties, such as high energy efficiency, no emissions, no noise, modularity, and potentially low cost, which may make them attractive in many applications even with a limited hydrogen supply.

2.2 Hydrogen as a sustainable source of energy:

Energy resources are essentially used to satisfy human needs and improve quality of life, but may generally lead to environmental impacts. For instance, the United Nations indicates that effective atmosphere-protection strategies must address the energy sector by increasing efficiency and shifting to environmentally benign energy systems. Reduced CO2 emissions can be achieved directly via increased efficiency, reductions

in the fossil fuel component of the energy mix and the introduction of alternative energy sources. The motivation for writing about hydrogen is due to the key facts like: (i) sustainable energy sources and energy carriers are required due to the limited availability of fossil fuel reserves and some unavoidable environmental impacts of their utilization; (ii) hydrogen will play a key role in replacing fossil fuels; (iii) hydrogen as a fuel is more exergetically efficient in power generation systems (including fuel cells) ; (iv) environmentally benign and sustainable hydrogen production and utilization will be one of the potential solutions in combating global warming.

It is obvious that current use of fossil fuels in various sectors for heat and power generation (including hydrogen production from them) continues threatening global stability and sustainability. These are locally, regionally and globally more evident than before. This concern is even further compounded by increasing world population, rapid technological development, increasing energy demand, etc. Although in the past fossil fuels were prime in meeting the energy needs, the current global picture does not allow any further potential use. So, there is an urgent need to switch to sustainable energy carriers, such as hydrogen.

Hydrogen can be produced from many fossil based sources including coal, natural gas, hydrocarbons, etc., by applying different production techniques such as gasification, reforming, pyrolysis, etc. However, it should be particularly known that, in this century, the required energy for hydrogen production, storage, distribution and transportation is mostly supplied from fossil fuel sources. In such a way that, given the advantages inherent in fossil fuels, such as their availability, relatively low cost, and the existing infrastructure for delivery and distribution, they are likely to play a major role for hydrogen production in the near to medium-term future. If so, the fossil fuel use for hydrogen production will not decrease, on the contrary, may increase. In this case, as a result of fossil fuel consumption, CO2, NOx, SOx and other pollutants will cause considerable damage to the environment. Therefore, in order to reduce the utilization of fossil fuel sources for hydrogen activities such as production, storage,

etc., and thus to save fossil fuel sources, the sustainable energy based hydrogen production, storage, distribution and transportation should be commonly encouraged, and also, the use of sustainable energy resources required for hydrogen activities should be absolutely increased and diversified. If done, hydrogen produced through non-fossil fuel sources such as water by using the different forms of sustainable energy sources and process heats (even nuclear based process heat) may then be considered to be a prime fuel in meeting energy supply and security, transition to hydrogen economy, environmental betterment, and social, societal, sectoral, technological, industrial, economical and governmental sustainabilities. In this regard, considering long-term environmental damages created by consumption of fossil fuels, sustainable energy based hydrogen energy systems that enable us to store the sustainable energy sources in the form of hydrogen should be particularly put in to practice. If so, it can be considered that hydrogen will play an important role in future energy scenarios and the foremost factor that will determine the specific role of hydrogen energy and technologies will likely be energy demand. However, it should be noted that, in the next one-to-two decades, the sustainable energy based hydrogen production processes be unlikely to yield significant reduction in hydrogen costs. However, the key may be the sustainable energy based hydrogen to reduce the environmental effects of fossil fuel consumption since: Hydrogen may have particularly attractive characteristics with regard to exergetic performance during its use as a fuel, because its combustion reaction is one of a combination of two relatively simple molecules into a more complicated one.

_ Hydrogen generally causes less or no environmental impact. The variety of hydrogen energy resources provides a flexible array of options for their use.

_ Hydrogen cannot be depleted. If used carefully in appropriate applications, hydrogen energy system can provide a reliable and sustainable supply of energy almost indefinitely.

_ It can provide environmental sustainability because hydrogen is high quality and environmental benign energy and a non-toxic clean energy carrier, and produces non-toxic exhaust emissions.

_It can also provide environmental stability because hydrogen can be safely transported in pipelines.

_It can be appropriate for the utilization of the sustainable energy sources and present long period-energy use, and thus ensure energy resource sustainability because hydrogen can be produced from non-fossil fuel sources by using different production techniques, and can be stored over relatively long periods of time, compared to electricity.

Considering these important advantages of a sustainable energy based hydrogen energy system, it can be said that, in order to protect the environment and save fossil fuel reserves, it will be useful to produce hydrogen from non-fossil fuel sources such as water, clean biomass, etc. For this purpose, the environmentally benign hydrogen production system including sustainable energy sources such as solar, hydro, and wind should have the electrolysis, thermolysis and gasification techniques with the lower exhaust or non-exhaust emissions.

2.3 How is hydrogen produced?

As mentioned before that one of the benefits of hydrogen fuel is that it can be produced from a diverse array of potential feed stocks including water, fossil fuels and organic matter. Described below are the most common and best understood hydrogen production pathways. Each of these pathways has its own pros and cons that should be considered in terms of cost, emissions, feasibility, scale, and logistics.

Table 1- Hydrogen Production Pathways

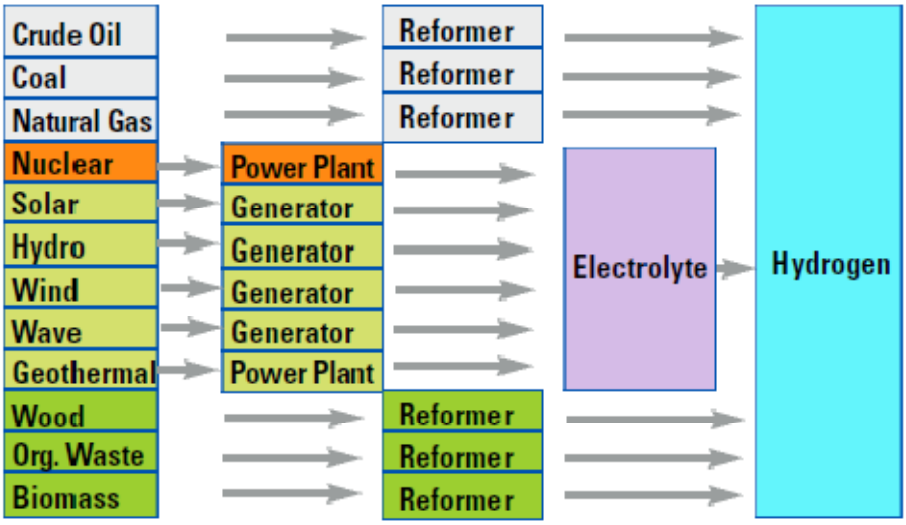

2.3.1 Reformation of Natural Gas

Process - In this process, natural gas (for example methane, propane, or ethane) is combined with high temperature steam (700-1000°C) where it reacts in presence of a catalyst, thereby breaking the bonds of the natural gas and creating hydrogen, carbon monoxide, and carbon dioxide. A subsequent shift reaction then treats the carbon monoxide with more high temperature steam thereby producing more hydrogen and carbon dioxide. The unwanted carbon dioxide is then removed from the mixture using absorption or membrane separation and the final result is pure hydrogen.

2.3.2 Biomass Gasification

Process - In this process, biomass such as forestry byproducts, straw, municipal solid waste or sewage is heated at high temperatures in a reactor where the bonds in the molecules forming the biomass are broken. This creates gas consisting mainly of hydrogen, carbon monoxide, and methane (CH4). Using the same steam reformation process described above, the methane is converted into hydrogen and carbon dioxide.

2.3.3 Electrolysis of Water

Process – Electrolysis of water involves passing an electric current though water, thereby splitting the water molecules into their basic elements of hydrogen and oxygen. Hydrogen gas rises from the negative cathode and oxygen gas collects at the positive anode.

2.3.4 Coal Gasification

Process - The basic process of coal gasification begins with converting the coal into a gaseous state by heating the coal in a reactor at very high temperatures. The gaseous coal is then treated with steam and oxygen and the result is the formation of hydrogen gas, carbon monoxide, and carbon dioxide.

2.3.5 From NaBH4

Sodium borohydride (NaBH4) is currently being investigated due to its potential as a new hydrogen carrier for advanced mobile applications. NaBH4 is very stable and easy to handle compared with other chemical hydrides. Moreover, it can be obtained from borax, which is a globally abundant natural substance. The solubility of NaBH4 in water at 25˚C is 55 g/ 100 g (NaBH4/water). Therefore, large amounts of NaBH4 can be stored in aqueous solutions under ambient condition. Solid state NaBH4 belongs to a group of chemical hydrides based on metal–hydrogen complex that can react with water in the presence of catalysts and release pure hydrogen via hydrolysis reaction, as follows :

$$NaBH_4 + 2H_2O + \text{catalyst} \rightarrow 4H_2 + NaBO_2, \qquad \Delta H \text{ ¼} = -217 \text{ kJ/ mol}$$

The hydrolysis reaction of NaBH4 is exothermic. Therefore, there is no need to supply external heat for hydrogen generation and the heat of reaction is sufficient to vaporize some of the water present. A sodium metaborate (analogous to borax) could be formed as a by-product during the reaction, but it is water-soluble and environmentally benign.

Hence, NaBH4 is regarded as a promising hydrogen source with the prediction that the water vapor presented in the H2 gas stream can be used to humidify the PEMFC membranes.

Solid metal catalysts such as Pt/Li, CoO, Ni based alloy, and Co-based alloy are generally required to generate hydrogen at room temperature. Recently, significant progress was reported in the use of organic acids dissolved in an aqueous solution as catalysts. SEIKO Instruments has developed a small air-breathing PEMFC system that was operated by the hydrogen generated from NaBH4 catalyzed with an organic acid aqueous solution, malic acid. This concept was thought to be capable of controlling the hydrogen generation and improving cell performance at room temperature.

2.4 Technologies for Hydrogen Storage

• Bulk storage in distribution system: It is expected that any large-scale hydrogen distribution system should address the problem of bulk storage, to provide a buffer between production facilities and fluctuations in demand. Low-cost and efficient bulk storage techniques are a major research goal. One can store hydrogen as either a gas or a liquid. The most widely studied options for storing gaseous hydrogen are underground caverns and depleted underground natural gas formations. Although hydrogen is more prone to leak than most other gases, leakage is shown not to be a problem for these techniques.

• Compressed gaseous hydrogen storage is at room temperature in a high-strength pressure tank. Including the weight of the tank, compressed gas storage holds about 1–7% hydrogen by weight, depending on the type of tank used. Lighter, stronger tanks, capable of holding more hydrogen with less weight, are more expensive. Compressing the hydrogen gas at the filling station requires about 20% as much energy as is contained in the fuel.

• Cryogenic liquid storage is at 20 K in a heavily insulated tank at ordinary atmospheric pressure. As a liquid, hydrogen contains almost 3 times more energy than an equal weight of gasoline, and takes up only about 2.7 times as much space for an equal energy content. Including the tank and insulation, this technique can hold as much as 16% hydrogen by weight. Furthermore, liquefaction at the filling station requires about 40% as much energy as is contained in the fuel. Another disadvantage is the so-called "dormancy problem": despite the insulation, some heat leaks into the tank, eventually boiling of the hydrogen.

• Metal hydride systems store hydrogen in the inter atom spaces of a granular metal. Various metals can be used. The hydrogen is released by heating. Metal hydride systems are reliable and compact, but can be heavy and expensive.

• Other techniques are still in the early stages of development. One uses powdered iron and water. At high temperatures these react to produce rust and hydrogen. Other methods are similar to the metal hydride option, but substitute certain liquid hydrocarbons (also known as "recyclable liquid carriers") or other chemicals for the metal.

References:

[1] Frano Barbir, " **PEM Fuel Cells Theory and Practice**".

[2] http://www.princeton.edu/~chm333/2002/spring/FuelCells/H_storage.shtml

[3] http://www.anl.gov/PCS/acsfuel/preprint%20archive/Files/48_2_New%20York_10-03_0784.pdf

[4] http://www.energyindependencenow.org/pdf/fs/EIN-hereDoesHydrogenFuelCo.pdf

[5] Ibrahim Dincer Technical, "**Environmental and exergetic aspects of hydrogen energy systems.**"

[6] Adnan Midillia,b,*, Ibrahim Dincera,b "**Hydrogen as a renewable and sustainable solution in reducing global fossil fuel consumption.**"

[7] Jin-Ho Kim a,b, Kyoung-Hwan Choi a, Yeong Suk Choi a,*. **"Hydrogen generation from solid NaBH4 with catalytic solution for planar air-breathing proton exchange membrane fuel cells."**

Section 3

Fuel Cell Thermochemistry and Voltage losses

3.1 Introduction

The predictions that can be made using thermodynamic equations are essential for understanding and modeling fuel cell performance since fuel cells transform chemical energy into electrical energy. Basic thermodynamic concepts allow one to predict states of the fuel cell system, such as potential, temperature, pressure, volume, and moles in a fuel cell.

A fuel cell is an electrochemical energy converter; it converts chemical energy of fuel (hydrogen) directly into electrical energy.

Describing the laws of thermodynamics, it will be clear how the system works.

The reactions are:

Anode side $$H_2 \rightarrow 2H^+ + 2e^- \quad (3\text{-}1)$$

Cathode side $$2H^+ + \frac{1}{2}O_2 + 2e^- \rightarrow H_2O \quad (3\text{-}2)$$

Overall $$H_2 + \frac{1}{2}O_2 \rightarrow H_2O + heat \quad (3\text{-}3)$$

3.2 Higher and Lower Heating Value of Hydrogen

The enthalpy of hydrogen combustion reaction *(i.e.,* 286kJ/mol) is also called the hydrogen's heating value. It is the amount of heat that may be generated by a complete combustion of 1 mol of hydrogen. The measurement of a heating value is conducted in a calorimetric bomb. If 1 mol of hydrogen is enclosed in a calorimetric bomb with 1/2 mol of oxygen, ignited, fully combusted, and allowed to cool down to 25°C, at atmospheric pressure there will be only liquid water left in the bomb (Figure 3-1). The measurement should show that 286kJ of heat was released. This is

known as hydrogen's higher heating value. However, if hydrogen is combusted with sufficient excess of oxygen (or air) and allowed to cool down to 25 °C, the product water will be in the form of vapor mixed with unburned oxygen and/or nitrogen in case that air was used (Figure 3-2). The measurement should show that less heat was released, exactly 241 kJ. This is known as hydrogen's lower heating value.

$$H_2 + \frac{1}{2}O_2 \rightarrow H_2O(g) + 241KJ / mol \tag{3-4}$$

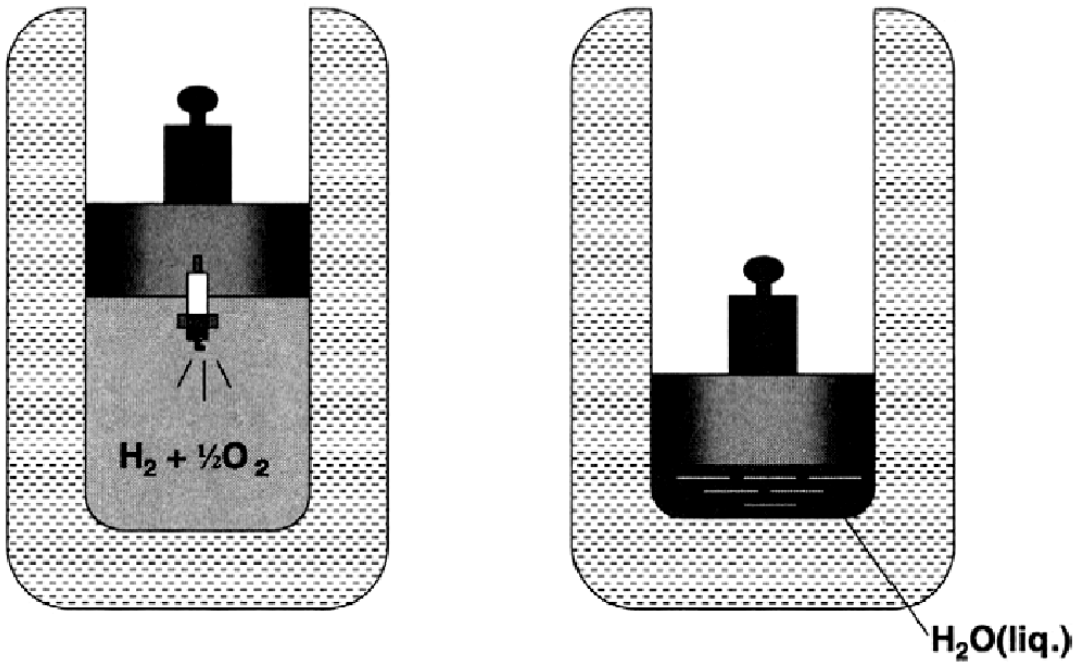

FIGURE 3-1: Combustion of H2 + $\frac{1}{2}$ 02 in a calorimetric bomb - measurement of higher heating value.

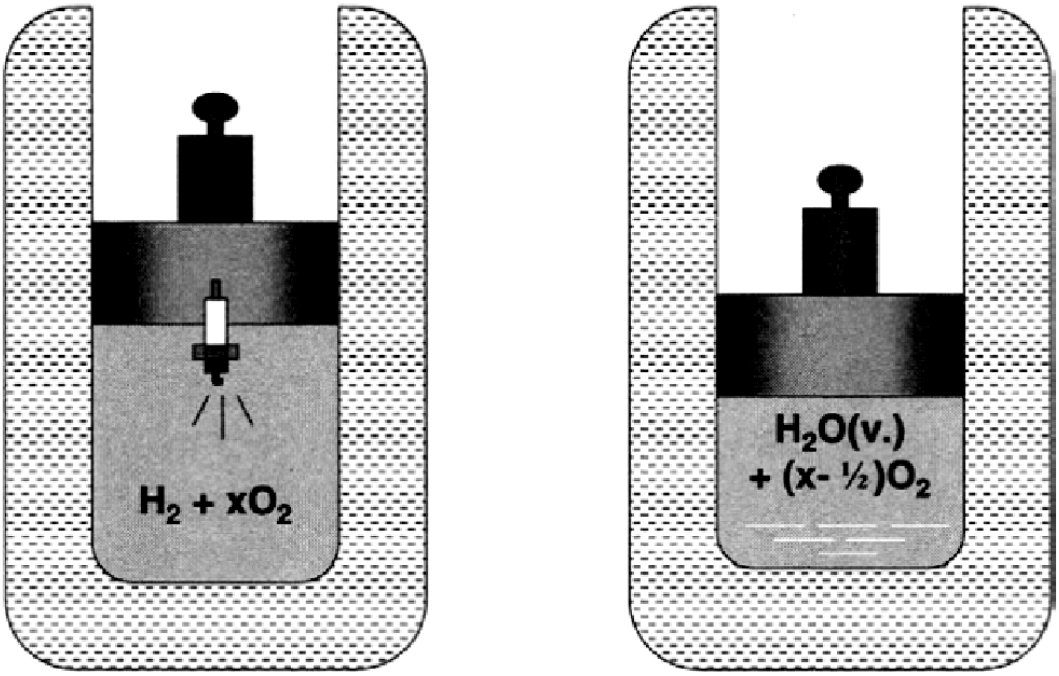

FIGURE 3-2: Combustion of H2 with excess O2 in a calorimetric bomb—measurement of lower heating value.

The difference between higher and lower heating value is the heat of evaporation of water (at 25°C):

$$H_{fg} = 286 - 241 = 45 \text{ kj/mol}$$

Hydrogen heating value is used as a measure of energy input in a fuel cell. This is the maximum amount of (thermal) energy that may be extracted from hydrogen. However, electricity is produced in a fuel cell. All the energy input cannot be converted into electricity. In every chemical reaction some entropy is produced, and because of that, a portion of the hydrogen's higher heating value cannot be converted into useful work—electricity. The portion of the reaction enthalpy (or hydrogen's higher heating value) that can be converted to electricity in a fuel cell corresponds to Gibbs free energy and is given by the following equation:

$$\Delta G = \Delta H - T\Delta S \qquad (3\text{-}5)$$

In other words, there are some irreversible losses in energy conversion due to creation of entropy, ΔS. Similarly, as ΔH for the reaction (Equation 3-3) is the difference between the heats of formation of products and reactants, ΔS is the difference between entropies of products and reactants:

$$\Delta S = (S_f)_{H20}-(S_f)_{H2}-1/2(S_f)_{O2} \quad (3\text{-}6)$$

3.3 Theoretical Fuel Cell Potential

In general, electrical work is a product of charge and potential:

$$W_{ei}=qE \quad (3\text{-}8)$$

where:

W_{ei} = electrical work ($Jmol^{-1}$)

q = charge (Coulombs mol^{-1})

E = potential (Volts)

The total charge transferred in a fuel cell reaction (Equations 3-1 through 3-3) per mol of H_2 consumed is equal to:

$$q = nN_{Avg}q_{ei} \quad (3\text{-}9)$$

Where:

n = number of electrons per molecule of H_2 = 2 electrons per molecule

N_{Avg} = number of molecules per mole (Avogadro's number) = 6.022 $x10^{23}$ molecules/mol

q_{ei} = charge of 1 electron = 1.602 x 10^{-19} Coulombs/electron

The product of Avogadro's number and charge of 1 electron is known as Faraday's constant:

F = 96,485 Coulombs/electron-mol

Electrical work is therefore:

$$W_{ei}=nFE \tag{3-10}$$

As mentioned previously, the maximum amount of electrical energy generated in a fuel cell corresponds to Gibbs free energy, ΔG:

$$W_{ei} =-\Delta G \tag{3-11}$$

The theoretical potential of fuel cell is then:

$$E = \frac{-\Delta G}{nF} \tag{3-12}$$

Because ΔG, n, and F are all known, the theoretical fuel cell potential of hydrogen/oxygen can also be calculated:

$$E = \frac{-\Delta G}{nF} = \frac{237340}{2*96485} = 1.23\ Volts \tag{3-13}$$

At 25°C, the theoretical hydrogen/oxygen fuel cell potential is 1.23 Volts.

This potential, obviously, changes with the temperature, in fact combining equation (3-12) with (3-5) yields:

$$E = -\left(\frac{\Delta H}{nF} - \frac{T\Delta S}{nF}\right) \tag{3-14}$$

At 25°C and pressure of 1 atm, the theoretical potential can be calculated as:

$$E = \frac{-\Delta G}{nF} = \frac{237340}{2*96485}\frac{Jmol^{-1}}{Asmol^{-1}} = 1.229\ \ Volts \tag{3-15}$$

It can be seen that the theoretical cell potential decreases with temperature. However, in operating fuel cells, in general, a higher cell temperature results in a higher cell potential. This is because the voltage losses in operating fuel cells

decrease with temperature, and this more than compensates for the loss of theoretical cell potential.

This previous equations were valid at atmospheric pressure. However, a fuel cell may operate at any pressure, typically from atmospheric all the way up to 6-7 bar.

For an isothermal process, the Gibbs free energy may be shown to be:

$$dG = V_m dP \tag{3-16}$$

where V_m is the molar volume in m^3mol^{-1} and P is the pressure in Pa.

Now, introducing the law for ideal gas:

$$PV_m = RT \tag{3-17}$$

Therefore:

$$dG = RT\frac{dP}{P} \tag{3-18}$$

After integration:

$$G = G_0 + RT\ln\left(\frac{P}{P_0}\right) \tag{3-19}$$

where G_0 is Gibbs energy at the standard temperature and pressure (25°C and 1 atm), and P_0 is the standard pressure of 1 atm.

For any chemical reaction between A and B (reactant) to give C and D (products):

$$jA + kB \rightarrow mC + nD \tag{3-20}$$

The Gibbs free energy is the change between products and reactants Gibbs free energy of formation:

$$\Delta G = mG_C + nG_D - jG_A - kG_B \tag{3-21}$$

Substituting into equation (3-18):

$$\Delta G = \Delta G_0 + RT \ln \left[\frac{\left(\frac{P_C}{P_0}\right)^m \left(\frac{P_D}{P_0}\right)^n}{\left(\frac{P_A}{P_0}\right)^j \left(\frac{P_B}{P_0}\right)^k} \right] \tag{3-22}$$

Then, for the hydrogen and oxygen reaction (3-3), the equation becomes:

$$\Delta G = \Delta G_0 + RT \ln \left(\frac{P_{H_2O}}{P_{H_2} P_{O_2}^{0.5}} \right) \tag{3-23}$$

This is known as Nernst equation; now introducing equation (3-14) into (3-23):

$$E = E_0 - \frac{RT}{nF} \ln \left(\frac{P_{H_2O}}{P_{H_2} P_{O_2}^{0.5}} \right) \tag{3-24}$$

In this form Nernst equation is valid only for gaseous products and reactants, but it is possible to adapt to liquid water produced in the fuel cell with P_{H2O}=1.

To calculate correctly this equation is important to notice that P_{O2} is the partial pressure of oxygen, and then, if in the fuel cell is used air instead of pure oxygen, the partial pressure is proportional to its concentration.

3.4 Theoretical Fuel Cell Efficiency

The efficiency for any energy conversion device is defined as the ratio between the useful energy output and the total energy input.

For a fuel cell, the useful energy output is the electrical energy produced, whereas the input can be represented by the enthalpy of fuel (hydrogen), which is hydrogen's higher heating value.

Therefore, the efficiency results the ratio between the Gibbs free energy and the enthalpy of hydrogen, assuming that the first can be all converted into electrical energy.

$$\eta = \frac{\Delta G}{\Delta H} \tag{3-25}$$

If both *ΔG* and *ΔH* are divided by *nF*, the fuel cell efficiency may be expressed as a ratio of two potentials:

$$\eta = \frac{-\Delta G}{-\Delta H} = \frac{\frac{-\Delta G}{nF}}{\frac{-\Delta H}{nF}} = \frac{1.23}{1.482} = 0.83 \tag{3-26}$$

Where 1.23 is the theoretical cell potential at standard pressure and temperature and 1.482 is the potential corresponding to hydrogen's higher heating value.

The Carnot efficiency is at the same time the maximum efficiency that a heat engine may have operating between two temperatures.

$$\eta = 1 - \sqrt{\frac{T_C}{T_H}} \tag{3-27}$$

This efficiency does not apply to a fuel cell because it is not a heat engine, but an electrochemical converter.

As shown in figure3.3, the fuel cell may have efficiency significantly higher than any engine operating between the same temperatures.

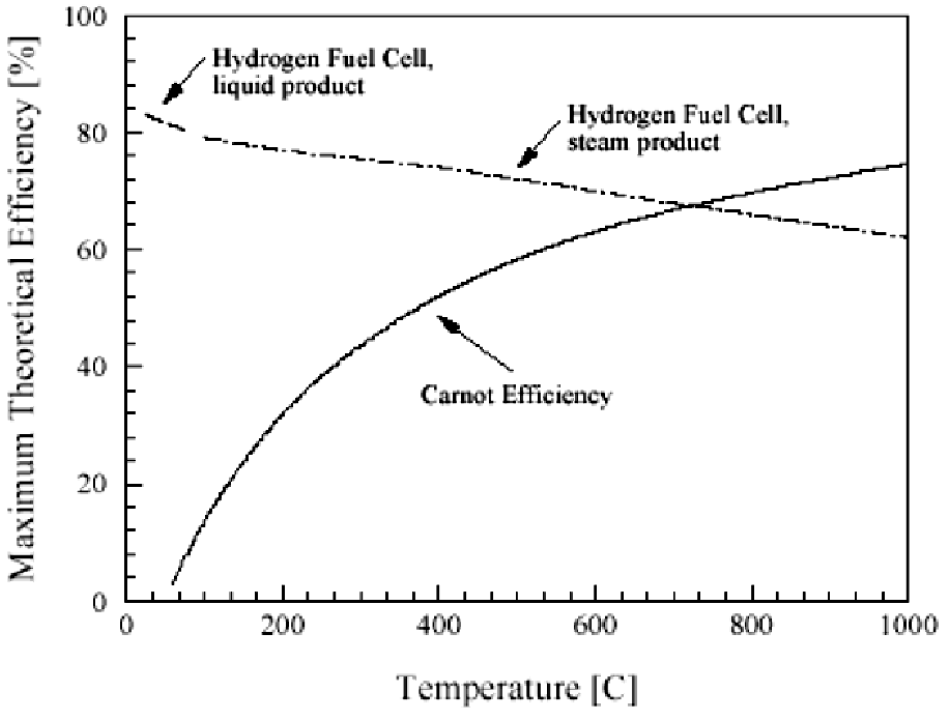

Figure 3.3: Theoretical efficiency of Carnot engine and fuel cell as a function of temperature

3.5 Voltage Losses

Typical voltage losses seen in a fuel cell are illustrated in Figure 3-4. The single fuel cell provides a voltage dependent on operating conditions such as temperature, applied load, and fuel/oxidant flow rates. The standard measure of performance for fuel cell systems is the polarization curve, which represents the cell voltage behavior against operating current density.

When electrical energy is drawn from the fuel cell, then actual cell voltage drops from the theoretical voltage due to several irreversible loss mechanisms. The loss is defined as the deviation of the cell potential (V_{irrev}) from the theoretical potential (V_{rev}) as mentioned above

$$V(i) = V_{rev} - V_{irrev} \qquad (3\text{-}28)$$

The actual voltage of a fuel cell is lower than the theoretical model due to species crossover from one electrode through the electrolyte and internal currents.

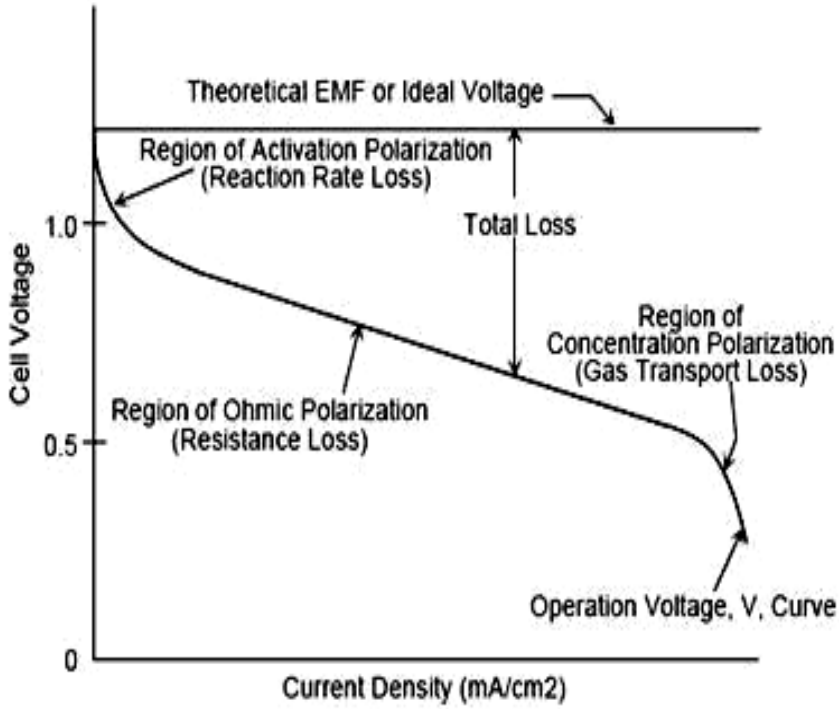

FIGURE 3-4. Generalized polarization curve for a fuel cell.

The three major classifications of losses that result in the drop from open-circuit voltage is (1) activation polarization, (2) ohmic polarization, and (3) concentration polarization. Therefore, the operating voltage of the cell can be represented as the departure from ideal voltage caused by these polarizations:

$$V(i) = V_{rev} - u_{act\_anode} - u_{act\_cath} - u_{ohmic} - u_{conc\_anode} - u_{conc\_cath} \quad (3\text{-}29)$$

Where u_{act}, u_{ohmic}, u_{conc} represent activation, ohmic (resistive), and mass concentration polarization. As seen in Equation 3-29, activation and concentration polarization occur at both the anode and cathode, while the resistive polarization represents ohmic losses throughout the fuel cell.

The equation for the fuel cell polarization curve is the relationship between the fuel cell potential and current density, as illustrated in Figure 3-9, and can be written as:

$$E = E_r - \frac{RT}{aF}\ln\left(\frac{i+i_{loss}}{i_o}\right) - \frac{RT}{nF}\ln\left(\frac{i_L}{i_L-i}\right) - iR_i \quad (3\text{-}30)$$

3.5.1 Activation losses

The voltage overpotential required to overcome the energy barrier for the electrochemical reaction to occur is activation polarization. As described previously this type of polarization dominates losses at low current density and measures the catalyst effectiveness at a given temperature. This type of voltage loss is complex because it involves the gaseous fuel, the solid metal catalyst, and the electrolyte. The catalyst reduces the height of the activation barrier, but a loss in voltage remains due to the slow oxygen reaction. The total activation polarization overpotential often ranges from 0.1 to 0.2 V, which reduces the maximum potential to less than 1.0 V even under open-circuit conditions. Activation overpotential expressions can be derived from the Butler-Volmer equation. The activation overpotential increases with current density and can be expressed as:

$$\Delta V_{act} = E - Er = \frac{RT}{\alpha n F} \ln\left(\frac{i}{i_0}\right) \tag{3-31}$$

Where 'i' is the current density, and i_0, is the reaction exchange current density. Where n is the number of exchange protons per mole of reactant, F is Faraday's constant, and α is the charge transfer coefficient used to describe the amount of electrical energy applied to change the rate of the electrochemical reaction

The activation losses can also be expressed simply as the Tafel equation:

$$\Delta V_{act} = a + b \ln(i) \tag{3-32}$$

Where

$$a = -\frac{RT}{\alpha F} \ln(i_0) \tag{3-33}$$

$$b = \frac{RT}{\alpha F} \tag{3-34}$$

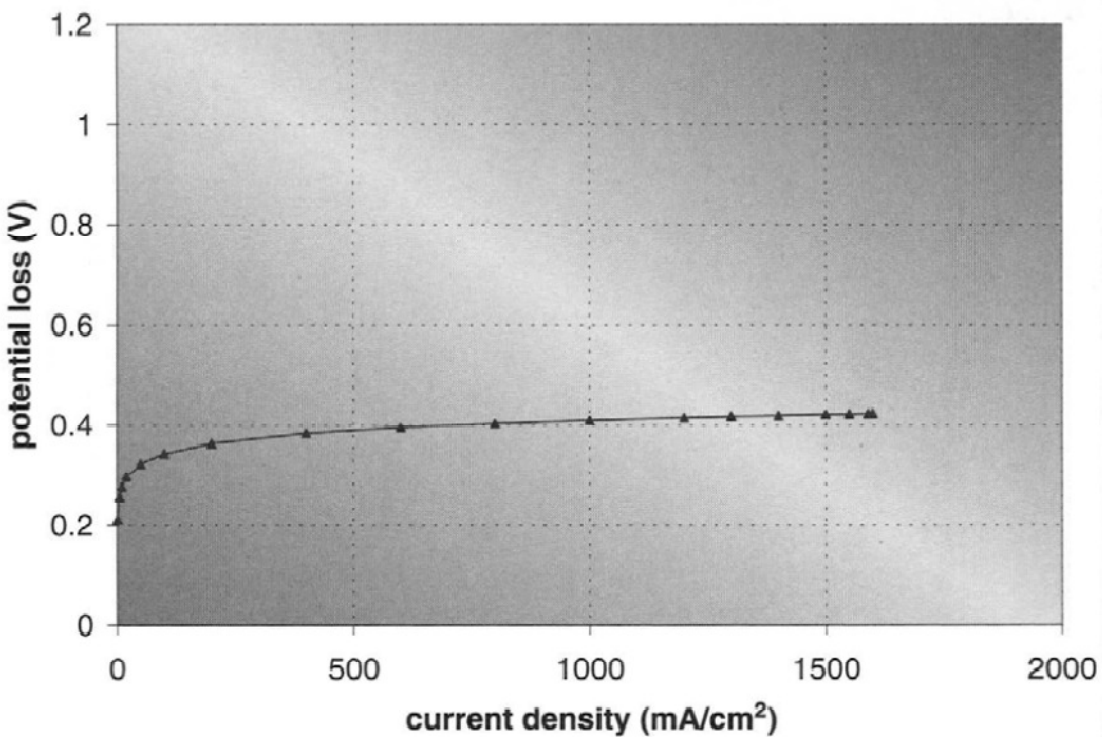

Figure 3.5 Activation losses as a function of current density

The equation for the anode and cathode activation overpotential can be represented by:

$$\Delta V_{act} = \Delta V_{act,c} + \Delta V_{act,a} = \frac{RT}{n\alpha_c F}\ln\left(\frac{i}{i_{0,c}}\right) + \frac{RT}{n\alpha_a F}\ln\left(\frac{i}{i_{0,a}}\right) \tag{3-35}$$

Where n is the number of exchange protons per mole of reactant, F is Faraday's constant, and α is the charge transfer coefficient used to describe the amount of electrical energy applied to change the rate of the electrochemical reaction. The exchange current density, i_o, is the electrode activity for a particular reaction at equilibrium. In PEM fuel cells, the anode i_o for hydrogen oxidation is very high compared to the cathode i_o for oxygen reduction; therefore, the cathode contribution to this polarization is often neglected. Intuitively, it seems like the activation polarization should increase linearly with temperature based upon Equation 3-35, but the purpose of increasing temperature is to decrease activation polarization. In Figure 3-5, activation losses as a function of current density are shown.

3.5.2 Internal Currents and Crossover Losses

Although the electrolyte, a polymer membrane, is not electrically conductive and is practically impermeable to reactant gases, some small amount of hydrogen will diffuse from anode to cathode, and some electrons may also find a "shortcut" through the membranes. Because each hydrogen molecule contains two electrons, this fuel crossover and the so-called internal currents are essentially equivalent. Each hydrogen molecule that diffuses through the polymer electrolyte membrane and reacts with oxygen on the cathode side of the fuel cell results in two fewer electrons in the generated current of electrons that travels through an external circuit. These losses may appear insignificant in fuel cell operation, because the rate of hydrogen permeation or electron crossover is several orders of magnitude lower than hydrogen consumption rate or total electrical current generated. However, when the fuel cell is at open circuit potential or when it operates at very low current densities, these losses may have a dramatic effect on cell potential, as shown in Figure 3-6.

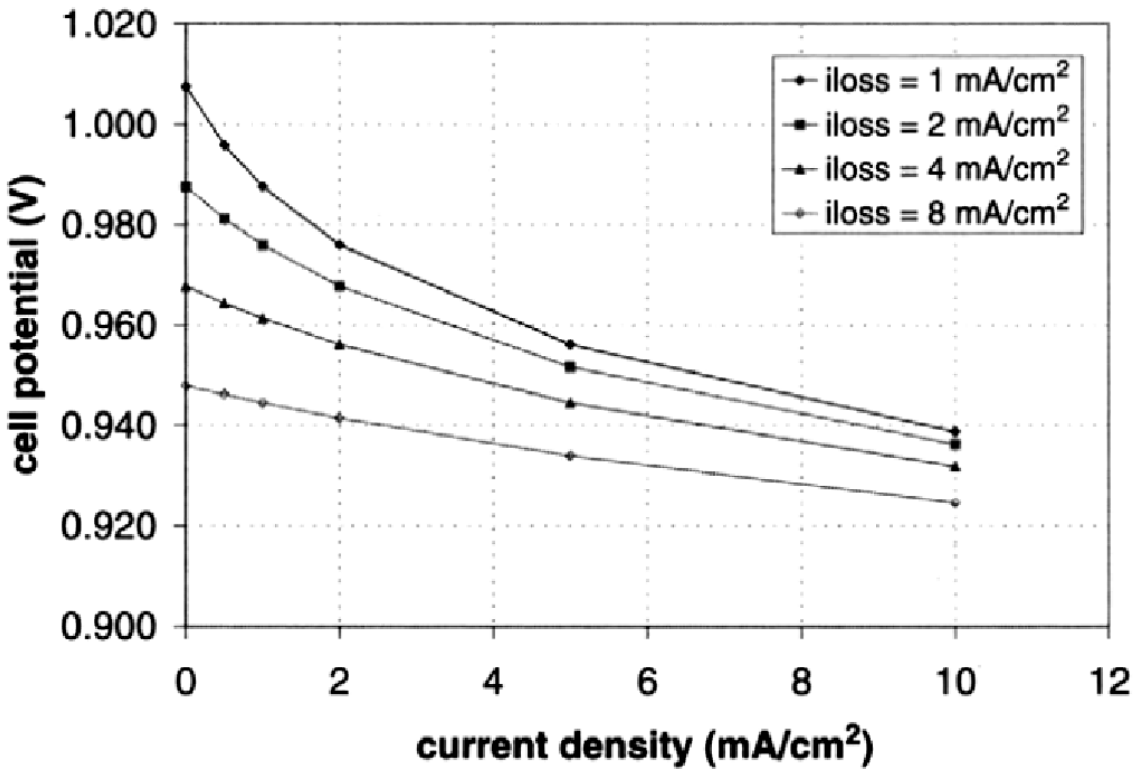

FIGURE 3-6: Effect of internal currents and/or hydrogen crossover loss on open circuit potential.

3.5.3 Ohmic Polarization

Ohmic losses occur because of resistance to the flow of ions in the electrolyte and resistance to flow of electrons through the electrode. The dominant ohmic losses through the electrolyte are reduced by decreasing the electrode separation and enhancing the ionic conductivity of the electrolyte. Because both the electrolyte and fuel cell electrodes obey Ohm's law, the ohmic losses can be expressed by the equation

$$\eta_{ohm} = iR \tag{3-36}$$

Where 'i' is the current flowing through the cell and R is the total cell resistance, which includes electronic, ionic, and contact resistance.

3.5.4 Concentration Polarization

As a reactant is consumed at the electrode by electrochemical reaction, there is a loss of potential due to the inability of the surrounding material to maintain the initial concentration of the bulk fluid. That is, a concentration gradient is formed. Several processes may contribute to concentration polarization: slow diffusion in the gas phase in the electrode pores, solution/dissolution of reactants and products into and out of the electrolyte, or diffusion of reactants and products through the electrolyte to and from the electrochemical reaction site. At practical current densities, slow transport of reactants and products to and from the electrochemical reaction site is a major contributor to concentration polarization.

The rate of mass transport to an electrode surface in many cases can be described by Fick's first law of diffusion:

$$i = \frac{nFD(C_b - C_S)}{\delta} \tag{3-36}$$

Where D is the diffusion coefficient of the reacting species, C_b is its bulk concentration, C_S is its surface concentration, and δ is the thickness of the diffusion

layer. The limiting current (i_L) is a measure of the maximum rate at which a reactant can be supplied to an electrode, and it occurs

when $C_S = 0$, i.e.,

$$i_L = \frac{nFDC_b}{\delta} \tag{3-37}$$

By appropriate manipulation of Equations (3-36) and (3-37),

$$\frac{Cs}{Cb} = 1 - \frac{i}{i_L} \tag{3-38}$$

The Nernst equation for the reactant species at equilibrium conditions, or when no current is flowing, is

$$E_{i=0} = E^\circ + \frac{RT}{nF} \ln C_b \tag{3-39}$$

When current is flowing, the surface concentration becomes less than the bulk concentration, and the Nernst equation becomes

$$E_{i=0} = E^\circ + \frac{RT}{nF} \ln C_s \tag{3-40}$$

The potential difference (ΔE) produced by a concentration change at the electrode is called the concentration polarization:

$$\Delta E = \eta_{conc} = \frac{RT}{nF} \ln \frac{Cs}{Cb} \tag{3-41}$$

Upon substituting Equation (3-38) in (3-41), the concentration polarization is given by the equation

$$\eta_{conc} = \frac{RT}{nF} \ln \left(1 - \frac{i}{i_L}\right) \tag{3-42}$$

In this analysis of concentration polarization, the activation polarization is assumed to be negligible. The charge transfer reaction has such a high exchange current density that the activation polarization is negligible in comparison with the concentration polarization (most appropriate for the high temperature cells).

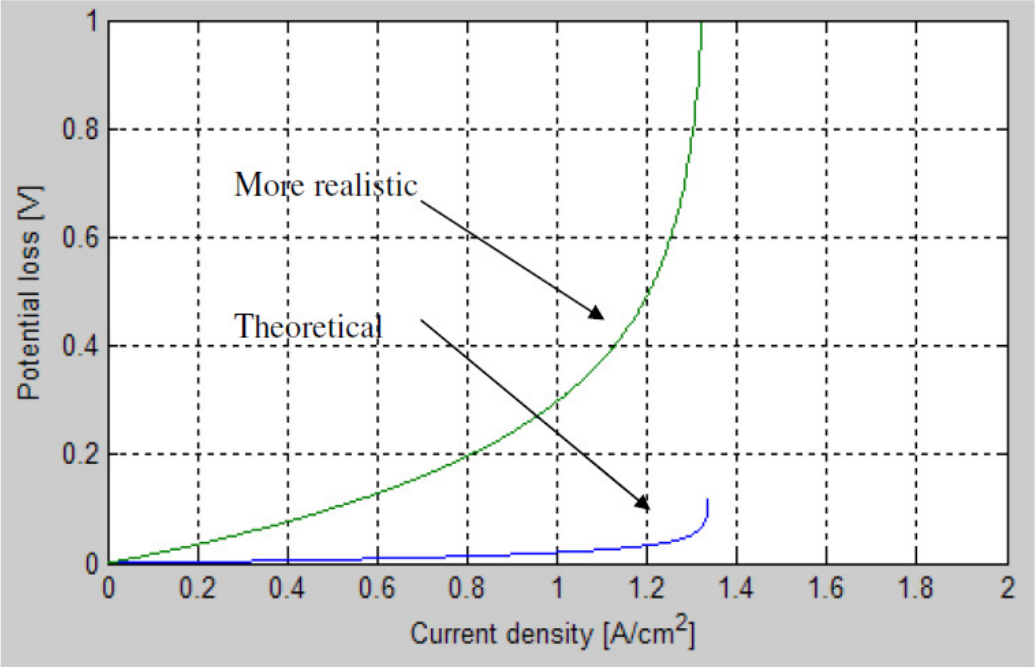

Figure 3-7 Concentration losses in fuel cell

3.6 Polarisation curve

Figure 3-8 shows the proportions between the three types of losses. Activation losses are the largest losses at any current density. Figure 3-9 illustrates potential distribution in a hydrogen and air fuel cell over the cell cross section.

At open circuit, when there is no current being generated, the anode is at reference or zero potential and the cathode is at the potential corresponding to the reversible potential at given temperature, pressure, and oxygen concentration.

As soon as the current is being generated, the cell potential, measured as the difference between cathode and anode solid phase potentials (electrically conductive parts), drops because of various losses, as discussed earlier.

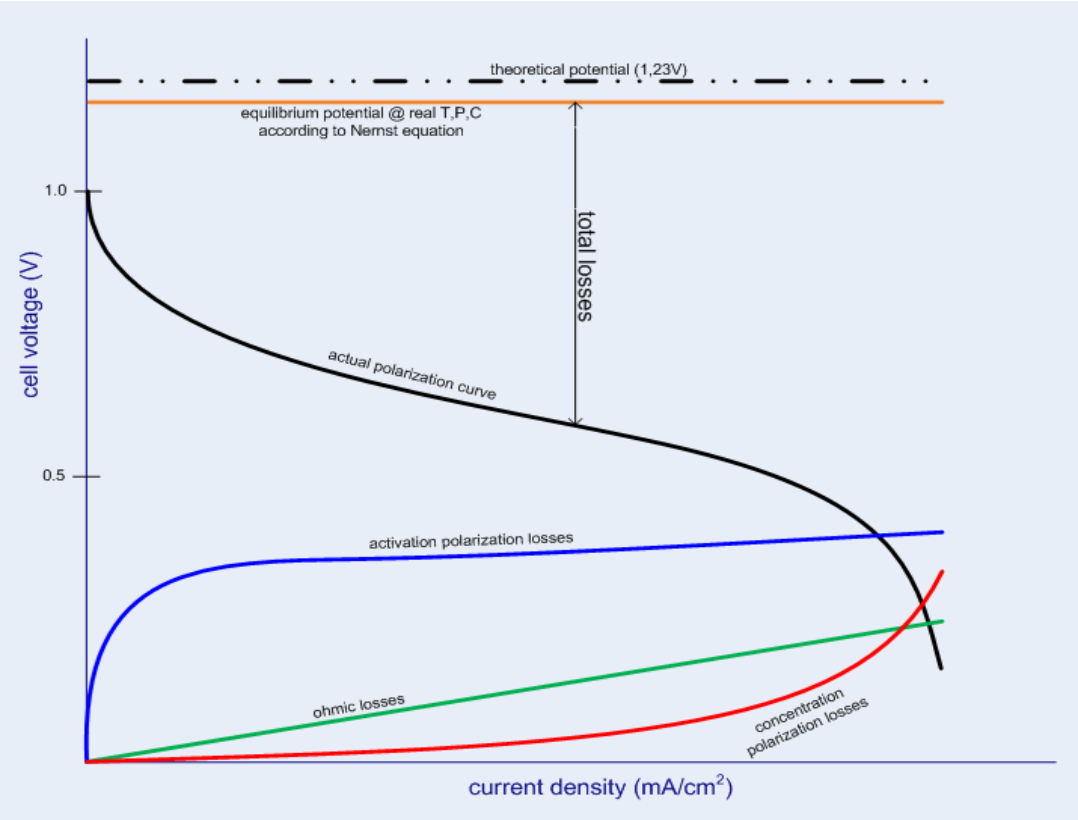

Figure 3-8 Voltage losses in the fuel cell

The cell potential is so equal to the reversible cell potential, reduced by potential losses.

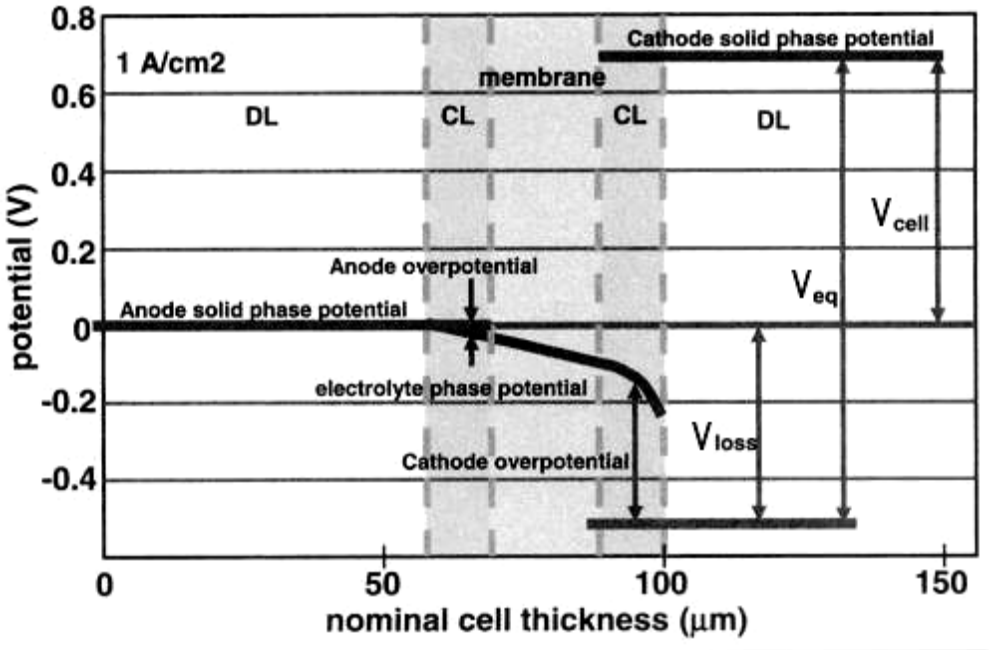

Figure 3-9 Potential distribution in fuel cell cross-section

It is possible modelling the cell voltage as:

$$E_{cell} = E_r - E_{loss} \tag{3-43}$$

Where the losses are composed by activation, ohmic and diffusion polarisation, the first and the third on both sides, anode and cathode:

$$E_{loss} = \left(\Delta V_{act} + \Delta V_{conc}\right)_a + \left(\Delta V_{act} + \Delta V_{conc}\right)_c + \Delta V_{ohm} \tag{3-44}$$

Therefore:

$$E_{cell} = E_r - \left(\Delta V_{act} + \Delta V_{conc}\right)_a - \left(\Delta V_{act} + \Delta V_{conc}\right)_c - \Delta V_{ohm} \tag{3-45}$$

3.7 Implications and Use of Fuel Cell Polarization Curve

Polarization curve is the most important characteristic of a fuel cell. It may be used for diagnostic purposes, as well as for sizing and control of a fuel cell. In addition to potential-current relationship, other information about the fuel cell may also become available just by rearranging the potential-current data.

3.8 Other Curves Resulting from Polarization Curve

For example, Power is a product of potential and current. Similarly, power density (in W/cm^2) is a product of potential and current density:

$$w = V^* I \tag{3-46}$$

Power density vs current density may be plotted together with the polarization curve on the same diagram (Figure 3-10). Such a plot shows that there is a maximum power density a fuel cell may reach. It does not make sense to operate a fuel cell at a point beyond this maximum power point, because the same power output may be obtained at a lower current and higher potential. Although the graph in Figure 3-10 shows maximum power density of about 0.6 W/cm^, power densities in excess of 1 W/cm^2 have been reported with PEM fuel cells.

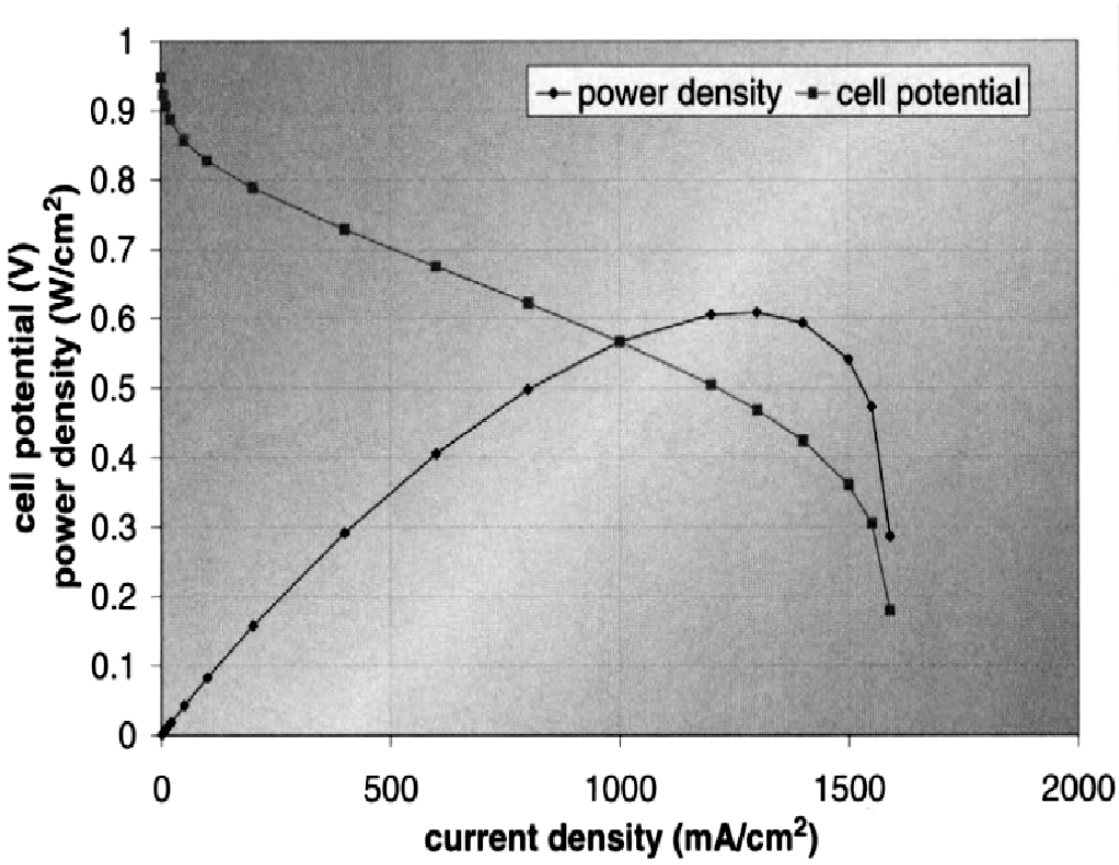

FIGURE 3-10. Typical fuel cell polarization curve and resulting power curve.

If cell potential is plotted vs power density (Figure 3-11), the same information is available—there is a maximum power that the cell can. For a fuel cell with a polarization curve as shown in Figure 3-10, the maximum power is reached at efficiency of 33%. This is significantly lower than the maximum theoretical fuel cell efficiency of 83%. A higher efficiency may be reached with the same fuel cell, but at significantly lower power densities. This means that for a required power output a fuel cell may be made larger (with a larger active area) and more efficient, or more compact but less efficient, by selecting the operating point anywhere on the polarization curve or on the efficiency-power density plot. Typically, a fuel cell is rarely sized anywhere close to the maximum power density.

More commonly, the operating point is selected at cell potential around 0.7V. For the graph in Figure 3-11, this would result in power density of 0.36W/cm^ and efficiency of 47%. For applications where a higher efficiency is required, a higher nominal cell potential may be selected (0.8 V or higher), which would result in a

55% to 60% efficient fuel cell, but the power density would be <0.1 W/cm^2. Similarly, for applications where fuel cell size is important, a lower nominal cell potential may be selected (around 0.6V), which would result in a higher power density, that is, a smaller fuel cell.

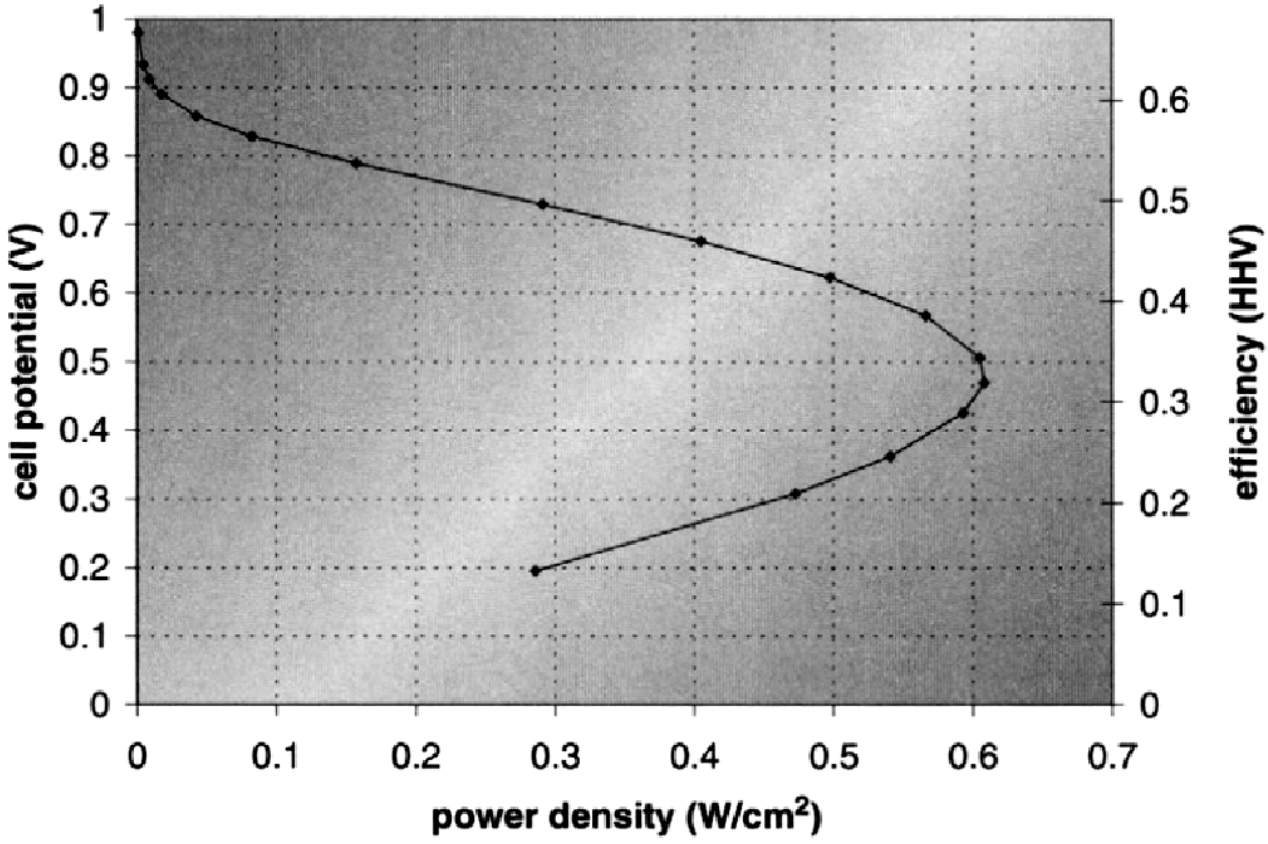

FIGURE 3-11: Cell potential vs power density for a fuel cell with the polarization curve from Figure 3-10

REFERENCES

[1] EG&G Technical Services, Inc. **"Fuel Cell Hand book"**

[2] Spiegel C., ***"PEM Fuel Cell Modelling and Simulation Using MATLAB"***, *Elsevier, 2008*

[3] Barbir F., *"**PEM Fuel Cells Theory and Practice**"*, *Elsevier, 2005*

[4] http://wikiri.upc.es/images/7/72/Pol_curve_with_losses.PNG

Section 4

Components of Cell and Material Properties

4.1 Fuel Cell Description

The heart of a fuel cell is a polymer, proton-conductive membrane. On both sides of the membrane there is a porous electrode. The electrodes must be porous because the reactant gases are fed from the back and must reach the interface between the electrodes and the membrane, where the electrochemical reactions take place in the so-called catalyst layers, or more precisely, on the catalyst surface. Technically, the catalyst layer may be a part of the porous electrode or part of the membrane, depending on the manufacturing process. The multilayer assembly of the membrane sandwiched between the two electrodes is commonly called the membrane electrode assembly or MEA. The MEA is then sandwiched between the collector/separator plates—"collector" because they collect and conduct electrical current, and "separator" because in multi-cell configuration they separate the gases in the adjacent cells. At the same time, in multi-cell configuration they physically/electrically connect the cathode of one cell to the anode of the adjacent cell, and that is why they are also called the bipolar plates. They provide the pathways for flow of reactant gases (so called flow fields), and they also provide the cell structural rigidity. Obviously, the design of the components and properties of materials must accommodate processes with minimum obstruction and losses. Because in some of the components more than one process takes place, very often with conflicting requirements, the properties and the design must be optimized.

Typical schematic of a Proton Exchange Membrane Fuel Cell (PEMFC) is shown in Figure 4-1. The cell is a sandwich of two graphite bipolar plates with micro flow channels separated by MEA (Membrane Electrode Assembly) which consists of a membrane and two electrodes with dispersed Pt catalyst. The gas diffusion layer (GDL) is porous to supply reactants to the electrodes at unexposed areas of micro flow channel.

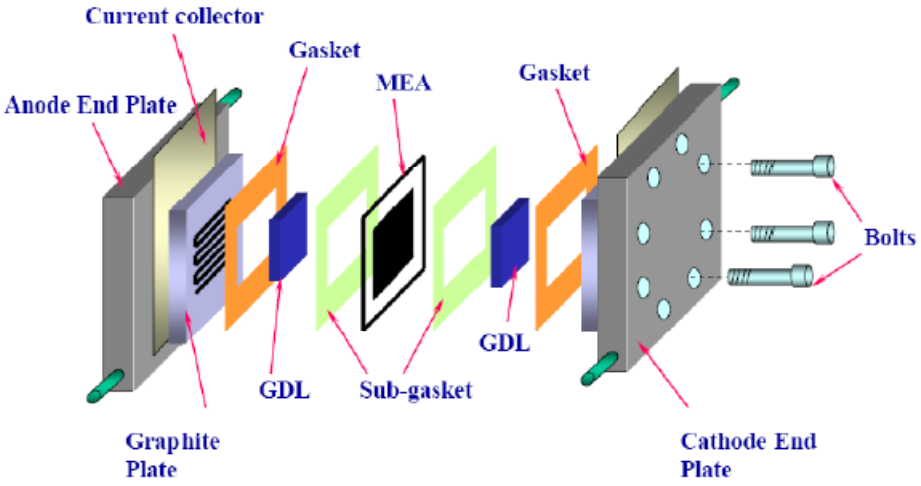

Figure 4-1: *Schematics of a fuel cell assembly displaying different essential components of the system*

4.1.1 Proton Exchange Membrane

The electrolyte layer is essential for a fuel cell to work properly. In PEM fuel cells (PEMFCs), the fuel travels to the catalyst layer and gets broken into protons (H+) and electrons. The electrons travel to the external circuit to power the load, and the hydrogen protons travel through the electrolyte until they reach the cathode to combine with oxygen to form water. The PEM fuel cell electrolyte must meet the following requirements in order for the fuel cell to work properly:

- High ionic conductivity
- Present an adequate barrier to the reactants
- Be chemically and mechanically stable
- Low electronic conductivity
- Ease of manufacturability/availability
- Preferably low cost

The membrane layer contains the solid polymer membrane, liquid water, and may also contain water vapor and trace amounts of H_2, O_2, or CO_2 depending upon the purity of the H_2 coming into the system.

Typically, the membranes for PEM fuel cells are made of perfluorocarbon-sulfonic acid ionomer (PSA). This is essentially a copolymer of tetrafluorethylene (TFE) and

various perfluorosulfonate monomers. The best-known membrane material is Nafion'^{TM} made by Dupont, which uses perfluoro-sulfonylfluoride ethylropylvinyl ether (PSEPVE). Figure 4-2 shows the chemical structure of perfluorosulfonate ionomer such as Nafion^{TM}.

The SO_3H group is ionically bonded, and so the end of the side chain is actually an SO_3^- ion with H^+ ion. This is why such structure is called ionomer. Because of their ionic nature, the ends of the side chains tend to cluster within the overall structure of the membrane. Although the Teflon-like backbone is highly hydrophobic, the sulphonic acid at the end of the side chain is highly hydrophyllic. The hydrophyllic regions are created around the clusters of sulphonated side chains. This is why this kind of material absorbs relatively large amounts of water (in some cases up to 50% by weight). H^+ ions movement within well hydrated regions makes these materials proton conductive.

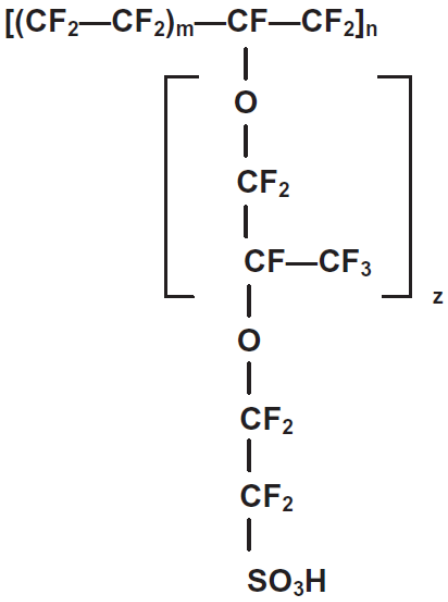

FIGURE 4-2. The chemical structure of Nafion.

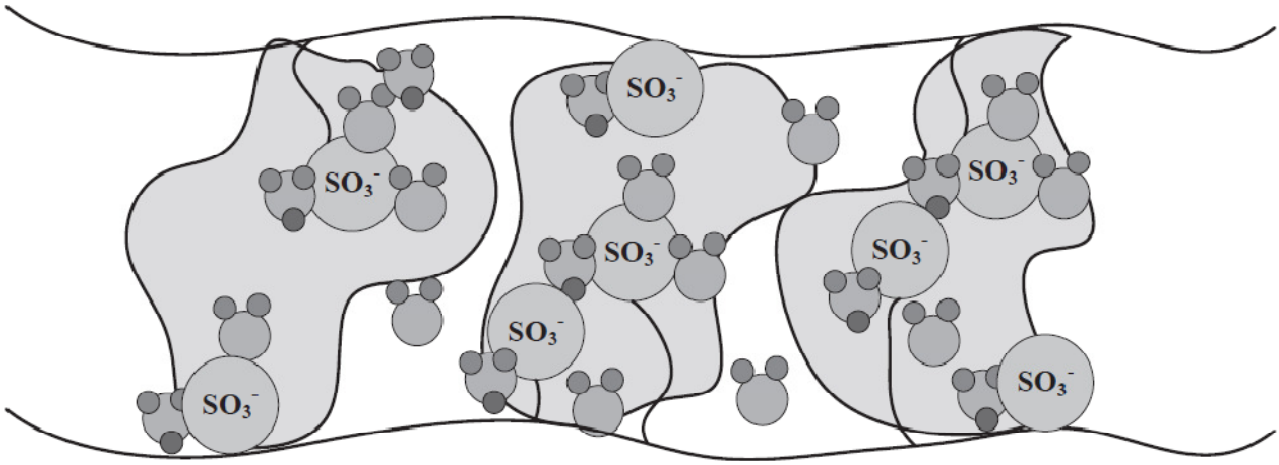

FIGURE 4-3. A pictorial illustration of Nafi on.

4.1.1.1The Role of Water

The conductivities of perfluorinated membranes such as Nafion are strongly dependent on the *level of hydration*. In a fuel cell system, the reactants therefore have to be humidified in order to prevent water evaporation, despite the generation of large quantities of product water at the cathode. When proton exchange membranes are subjected to temperatures above 100°C at atmospheric pressure, their conductivity decreases significantly due to *dehydration*. Somewhat higher temperatures can be reached when reactant pressures exceeding the water vapor pressure are employed. Clearly, pressurizing reactants to more than 1 to 2 bar above ambient is not practical in fuel cell systems due to the high parasitic power requirement for compressors. This, in addition to thermal stability issues, makes this family of proton conducting materials unsuitable for high-temperature (120–200°C) fuel cell applications.

Water transport inside perfluorinated membranes is complex. When a vehicle mechanism is responsible for proton transport, for example in the form of H3O+, the migration of each proton will be linked with the transport of at least one water molecule. In practical fuel cells, a mixed transport process is believed to be operating, leading to a certain *electro-osmotic drag factor* of water molecules per proton. This is thought to be on the order of 0.6 to 2.0. In the net water transport this is largely compensated by back diffusion (from cathode to anode) of neutral water

molecules according to Fick's law. Because the electro-osmotic drag depends primarily on the nature of the polymer and the temperature but not on thickness, thinner membranes tend to establish a more even cross-sectional distribution of water. In addition, thinner membranes open up an additional route for product water removal via the membrane, which helps to reduce mass transport limitations at high current densities.

4.1.2 Electrode

A fuel cell electrode is essentially a thin catalyst layer pressed between the ionomer membrane and porous, electrically conductive substrate. It is the layer where the electrochemical reactions take place. More precisely, the electrochemical reactions take place on the catalyst surface. Because there are three kinds of species that participate in the electrochemical reactions, namely gases, electrons and protons, the reactions can take place on a portion of the catalyst surface where all three species have access. Electrons travel through electrically conductive solids, including the catalyst itself, but it is important that the catalyst particles are somehow electrically connected to the substrate. Protons travel through ionomer,- therefore the catalyst must be in intimate contact with the ionomer. And finally, the reactant gases travel only through voids; therefore the electrode must be porous to allow gases to travel to the reaction sites. At the same time, product water must be effectively removed; otherwise the electrode would flood and prevent oxygen access.

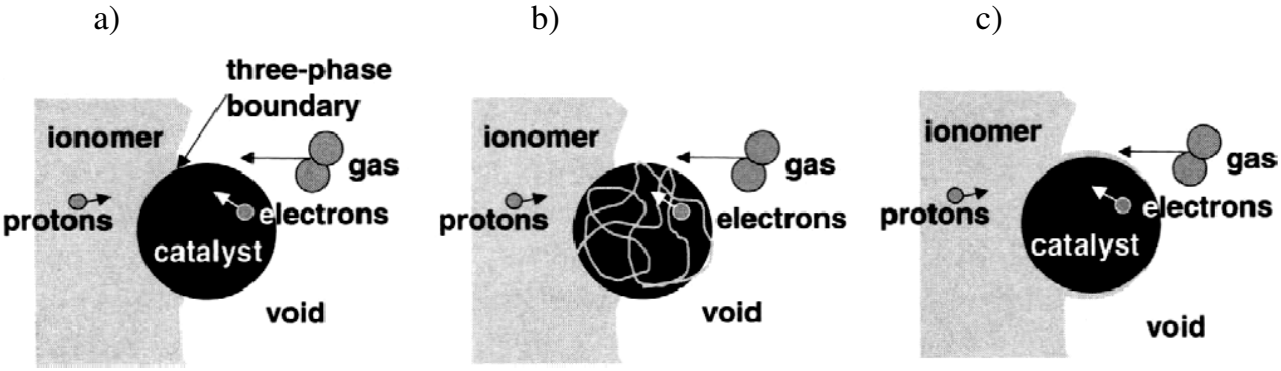

FIGURE 4-4: Graphical representation of the reaction sites.

As shown graphically in Figure 4-4a, the reactions take place at the three-phase boundary, namely ionomer, solid, and void phases. However, this boundary has an infinitesimally small area (essentially it is a line not an area) that would result in infinitely large current densities. In practice, because some gas may permeate through the polymer, the reaction zone is larger than a single three-phase boundary line. The reaction zone may be enlarged by either "roughening" the surface of the membrane or by incorporating ionomer in the catalyst layer (as shown in Figure 4-4b). In an extreme case, the entire catalyst surface may be covered by a thin ionomer layer (Figure 4-4c), except for some allowance for electrical contacts. Obviously, the ratios between the catalyst area covered by ionomer to catalyst area opened to void to catalyst area contacting other catalyst particles or electrically conductive support must be optimized.

The most common catalyst in PEM fuel cells for both oxygen reduction and hydrogen oxidation reactions is platinum. In the early days of PEMFC development large amounts of Pt catalyst were used (up to 28mgcm^{-2}). In the late 1990s, with the use of supported catalyst structure, this was reduced to 0.3-0.4 mgcm^{-2}. It is the catalyst surface area that matters, not the weight, so it is important to have small platinum particles (4nm or smaller) with large surface area finely dispersed on the surface of catalyst support, typically carbon powders (cca 40nm) with high mesoporous area (>75m^{2}g^{-1}).

To minimize the cell potential losses due to the rate of proton transport and reactant gas permeation in the depth of the electrocatalyst layer, this layer should be made reasonably thin. At the same time, the metal active surface area should be maximized, for which the Pt particles should be as small as possible. For the first reason, higher Pt/C ratios should be selected (>40% by wt.); however, smaller Pt particles and consequently larger metal areas are achieved with lower loading. Paganin *et al.* found that the cell's performance remained virtually unchanged when the Pt/C ratio was varied from 10% to 40% with a Pt loading of 0.4mg/cm^2. However, the performance deteriorated as the Pt/C ratio was increased beyond 40%.

This indicates a negligible change in the active catalyst area between Pt/C ratios of 10% and 40% and significant decrease in catalyst active area beyond 40% Pt/C.

In general, higher Pt loading results in voltage gain (Figure 4-5), assuming equal utilization and reasonable thickness of the catalyst layer. However, when current density is calculated per area of Pt surface then there is almost no difference in performance, that is, all the polarization curves fall on top of each other (Figure 4-6). Note that the Tafel slope is about 70mV/decade. The key for improving the PEM fuel cell performance is not in increasing the Pt loading, but rather in increasing Pt utilization in the catalyst layer.

The catalyst surface active area may be greatly increased if ionomer is included in the catalyst layer either by painting it with solubilized PFSA in a mixture of alcohols and water or preferably by premixing catalyst and ionomer in a process of forming the catalyst layer.

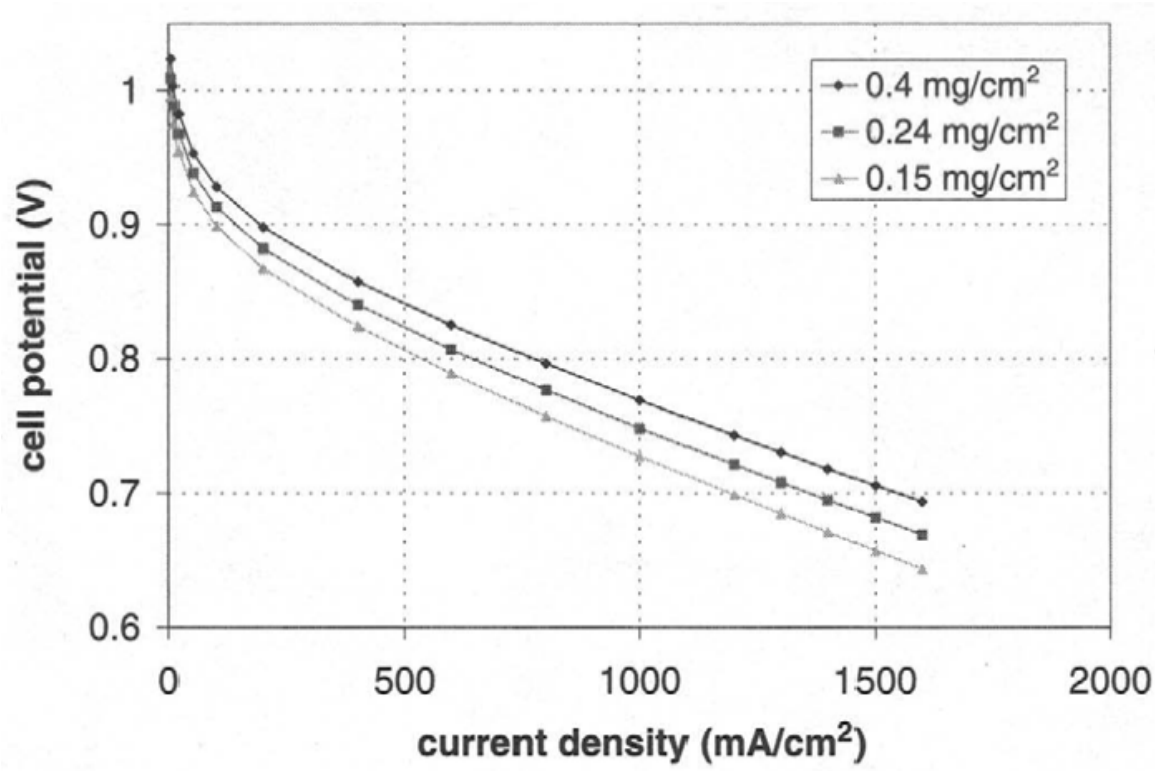

FIGURE 4-5: Effect of Pt loading on fuel cell polarization curve (H_2/O_2 fuel cell).

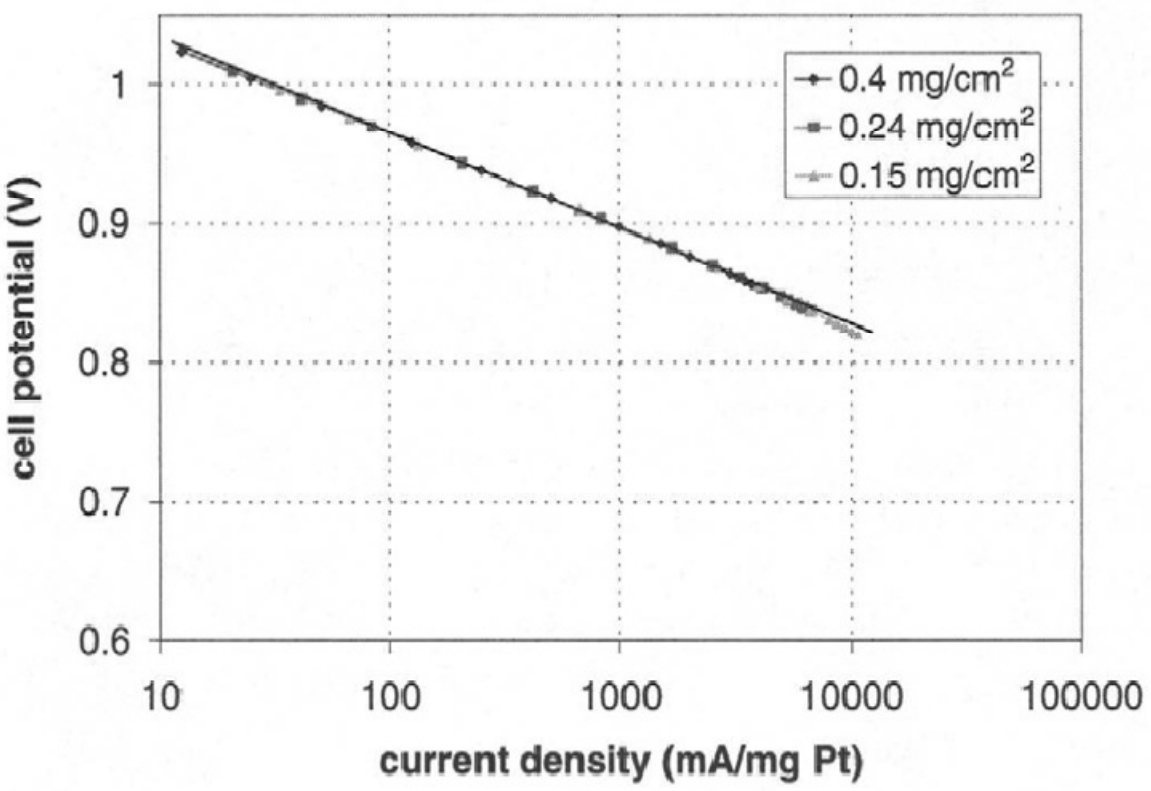

FIGURE 4-6: Cell performance per unit of Pt electrocatalyst.

4.1.3 Gas diffusion media

A gas diffusion layer (GDL) is the mediator between the nanostructured electrode and the flow field which has structures in the millimeter range. Most commonly the GDL consists of carbon fiber paper or carbon cloth (Fig. 4-7).

- A GDL has to fulfill several tasks in a PEM fuel cell (compare Fig. 4-8):
- The GDL must have high electronic conductivity.
- Heat must be transported through the material. Therefore high heat conductivity is desirable.
- The GDL should mechanically support the MEA.
- The GDL should provide gas access from the flow-field channels to the catalyst layer and allow removal of gaseous products.

- Finally the GDL should provide a passage for water removal from the electrode to the flow field.

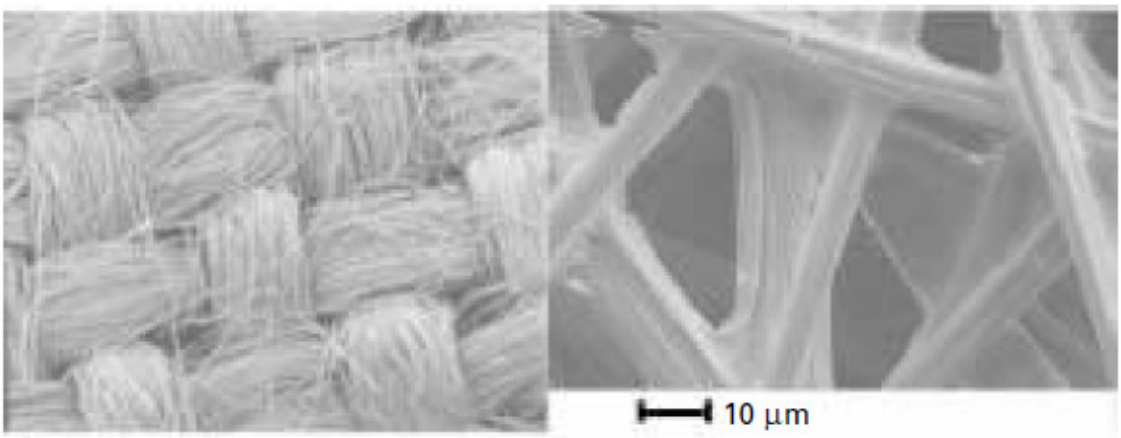

4-7: SEM pictures of GDL substrates. Left: carbon cloth, right: carbon fiber paper.

Several of the features mentioned above are in contradiction to each other. For example a high electronic conductivity of the material would require a dense material, whereas an unhindered gas transport requires a high porosity of the material. Therefore a compromise has to be found for which the material fulfills the required properties for a given cell design and for the projected operating conditions.

The influence of different GDL materials on the characteristic curve of a PEMFC is presented in Fig. 4-9. All cells had the same geometry, were equipped with the same MEA and were operated at the same operating conditions, but the GDL substrate material used in the experiment had a different structure. In order to improve the water transport in the GDL, the samples in Fig. 4-9 were all hydrophobized with PTFE, applying the same procedure. The PTFE content and the thickness of the material were the same. A simultaneous measurement of the electrical resistance proved that the differences can be attributed to water transport and water storage behavior of the material. The use of materials with the same structure but with different PTFE content has a similar influence on the fuel cell behavior. From these findings it becomes obvious that the GDL has a strong impact on fuel cell behavior and that intense research and development effort is required in order to understand the relation between structure and functionality of GDL material.

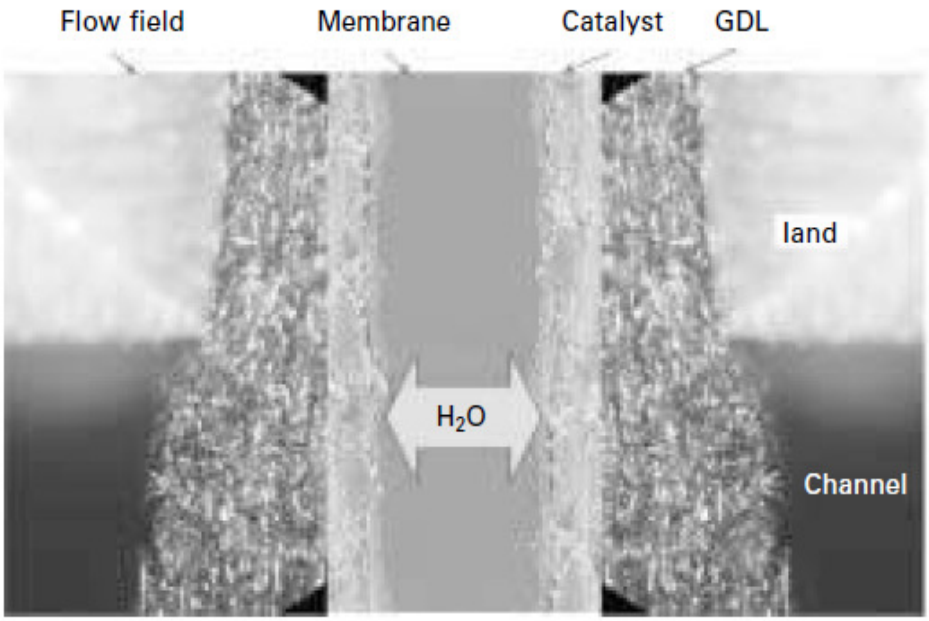

4-8: Cross-section through a PEMFC, GDL compressed under the land, uncompressed under the channel.

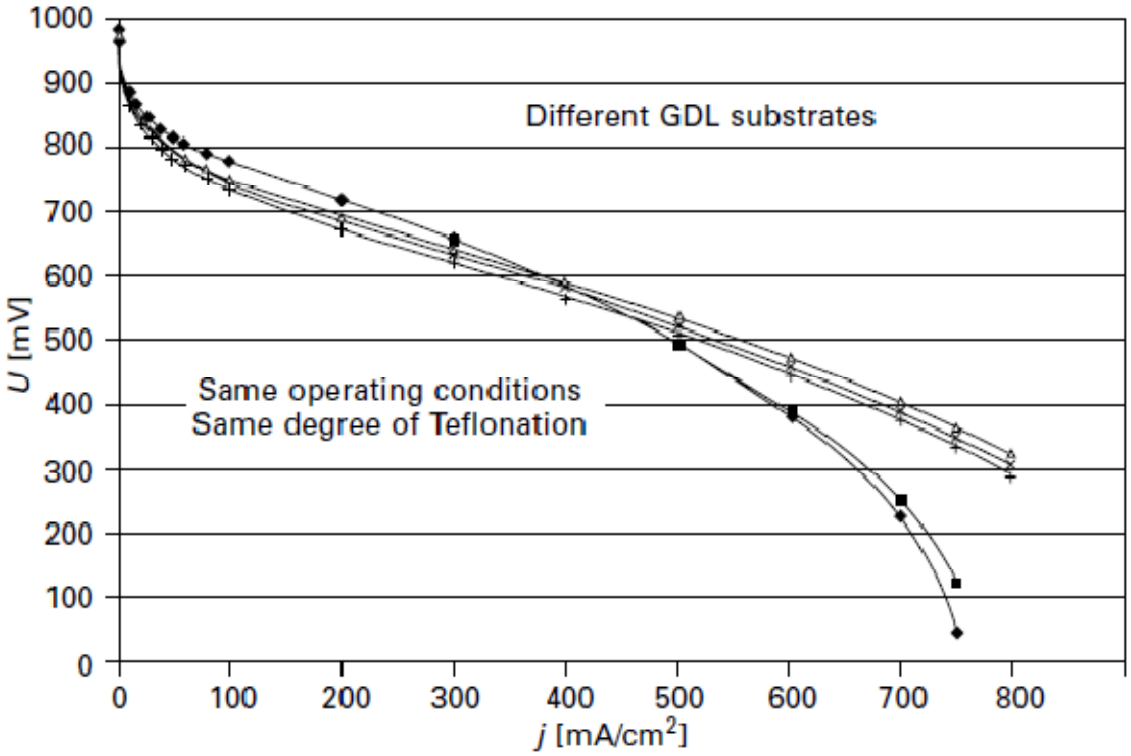

4-9: Characteristic curves of a single cell with different GDL substrate materials.

4.1.4 Bipolar Plates

Flow field plates in early fuel cell designs — and still in use in the laboratory — were usually made of *graphite* into which flow channels were conveniently machined. These plates have high electronic and good *thermal conductivity* and are stable in the chemical environment inside a fuel cell. Raw bulk graphite is made in a high-temperature sintering process that takes several weeks and leads to shape distortions and the introduction of some porosity in the plates. Hence, making flow field plates is a lengthy and labor-intensive process, involving sawing blocks of raw material into slabs of the required thickness, *vacuum-impregnating* the blocks or the cut slabs with some resin filler for *gas-tightness*, and grinding and polishing to the desired surface finish. Only then can the gas flow fields be machined into the blank plates by a standard milling and engraving process. The material is easily machined but abrasive. Flow field plates made in this way are usually several millimeters (1 mm = 0.04 inch) thick, mainly to give them mechanical strength and allow the engraving of flow channels. This approach allows the greatest possible flexibility with respect to designing and optimizing the *flow field.*

When building stacks, flow fields can be machined on either side of the flow field plate such that it forms the cathode plate on one and the anode plate on the other side. Therefore, the term *bipolar plate* in often used in this context. The reactant gases are then passed through sections of the plates and essentially the whole fuel cell stack (see Fig. 4-10).

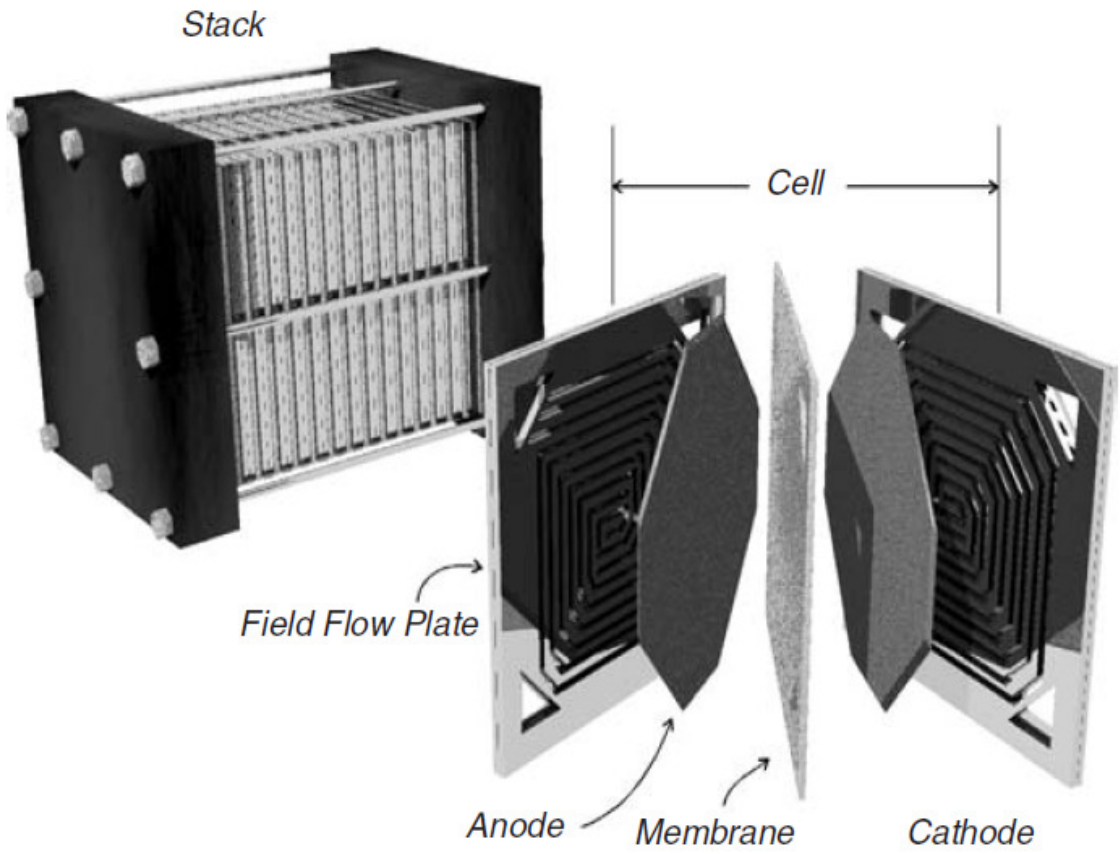

FIGURE 4-10: Fuel cell stack made up of flow field plates (or bipolar plates) and MEAs (shown in the insert).

4.1.4.1 Flow Field Designs and Their Effects on Performance

Let us first consider the main tasks of a flow field plate:

• Current conduction

• Heat conduction

• Control of gas flow

• Product water removal

Figure 4-11 showed that a balance exists between gas supply and current conduction. The best conductor, a solid blank sheet, will not allow any gas access, while an entirely open structure does not allow any current to flow. Therefore, some sort of large-scale "porosity" is needed in flow fields. The rib and channel design shown in Fig. 4-11 is just one way of achieving this. Clearly, the size of the open flow structure (for example channels) depends on the resistivity of the materials

used (including that of the gas diffusion layer), the size of the MEA, the operating pressure, and the current range envisaged. The complex task of achieving the right structure can be done by fluid-dynamic modeling in combination with experimental evaluation of a large number of different designs. Modeling will also give sufficiently accurate treatment of *heat removal* from the power-generating MEA to *heat sinks* within the stack.

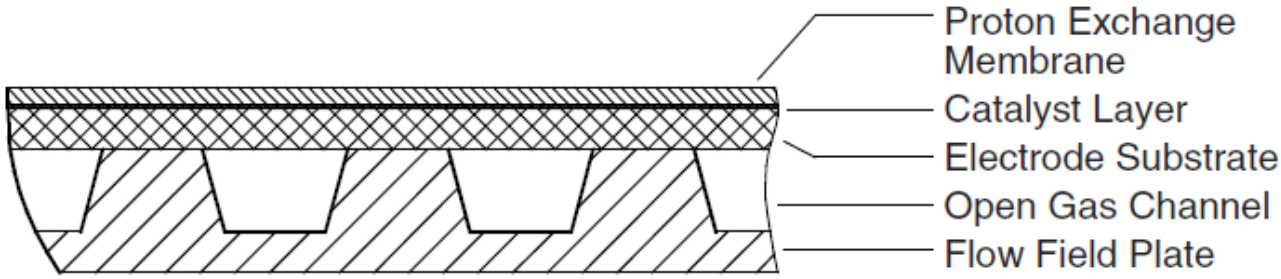

FIGURE 4-11: Cross-section of a MEA (only membrane and one electrode are shown) in contact with a flow field plate. The schematic sketch shows the function of the porous electrode substrate. The open gas channels are needed for reactant supply, but only the landing areas can conduct electric current. Therefore, the substrate conducts the current laterally from electrode areas above the open channels to the landing areas. Likewise, gas is being conducted through the porous material to electrode sections above the landing areas.

Product water removal (at the cathode) is even more complex as this represents a two-phase flow problem. While some *turbulence* may help to release water from the open gas diffusion layer structure, opening up room for gas access, turbulent gas flow leads to larger pressure drops between flow field inlet and outlet. *Pressure differentials* require *compression energy* to drive the reactants through the flow field structure, and this has an impact on systems efficiency. A possible answer is the construction of many parallel gas channels as indicated in Fig. 4.12(a). Parallel flow through many channels will lower the pressure differential between gas inlet and outlet. Unfortunately, water formed at the cathode accumulates in the channels adjacent to the cathode. *Water droplets* tend to coalesce and form larger droplets, partially obstructing the channels. Not all channels will be equally blocked, and the main gas flow will be redistributed through the remaining open channels.

Ultimately, portions of the MEA will no longer be supplied with reactant gas and will become inactive.

The *flow field designs* employed by leading stack developers are well-kept secrets. However, the patent literature gives hints as to what principal concepts are used. The so-called *serpentine flow field* described by Ballard researchers (Watkins et al., 1992) is sketched in Fig. 4.12(b). It is believed to overcome the blockage of certain channels by product water because the differential pressure between inlet and outlet forces *stagnant water* out of the channels. When higher flows are needed and widening of channels is not feasible, the number of channels may be increased. The excellent performance of Ballard stacks probably relies on the use of this concept.

General Motors has patented a flow field design sketched in Fig. 4.12(c) that looks like a compromise between straight parallel channels and a single serpentine flow field (a so-called mirrored flow field).

The patent (Rock, 2000) is also interesting regarding the materials and the integration of cooling within the bipolar plate, which will be discussed below.

Structures of the type shown in Fig. 4.12(d) have been suggested, where the channels are no longer continuous, but the gas is forced to flow through some part of the gas diffusion layer. The *interdigitated* structure shown in Fig. 4.12(d) is just one possibility. This structure helps to induce forced *water removal* from the open structure of the gas diffusion layer but induces higher pressure drops between inlet and outlet than through-flow options do.

Another option is abandoning channels altogether by creating a regular pattern of supporting patches, as shown in Fig. 4.12(e), or dimples, or by using a more or less isotropic gas distribution layer, such as a wire mesh (Wilson and Zawodzinski, 2001) or a foam (Gamburzev et al., 1999), as sketched in Fig. 4.12(f). These two options may work well in a limited current range and single cells or short stacks.

When high power is generated in the MEA, gas flow will focus more and more on the central section of the flow field, leaving inactive patches around the edges. What was said about stagnant water in conjunction with the structure shown in Fig. 4.12(a) applies accordingly.

More importantly, it is very difficult to produce irregular structures of the type shown in Fig. 4.12(f) with absolutely identical porosity properties. In a stack, this

may lead to differences in flow resistance among different cells, particularly at the high performance end. Certain cells may be shut off because of accumulating water and lack of reactant and, possibly, may be destroyed. The technique of "*purging*" the stack by venting the outlet at fixed intervals, which is used by some stack manufacturers, may have been applied to fix this problem.

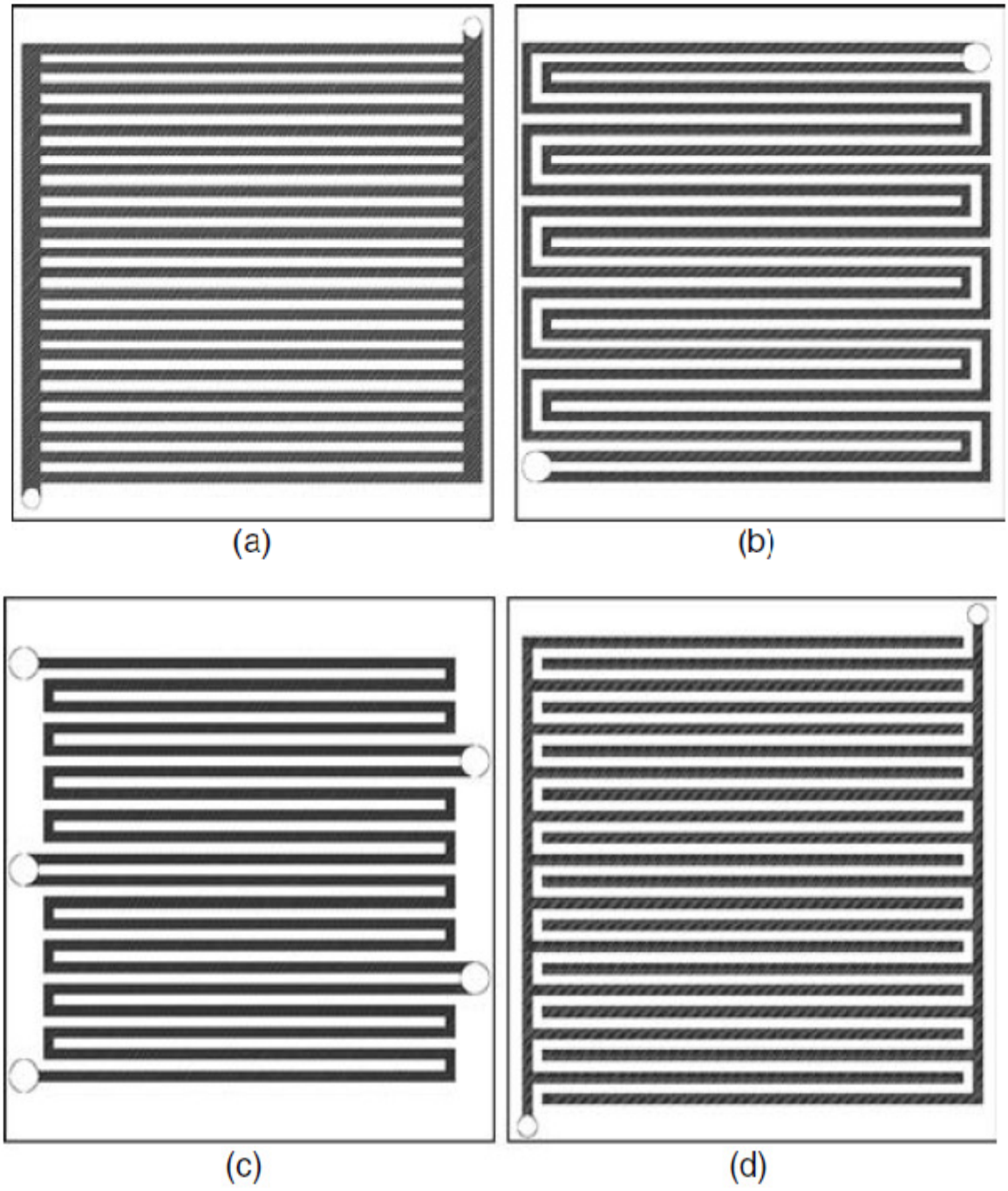

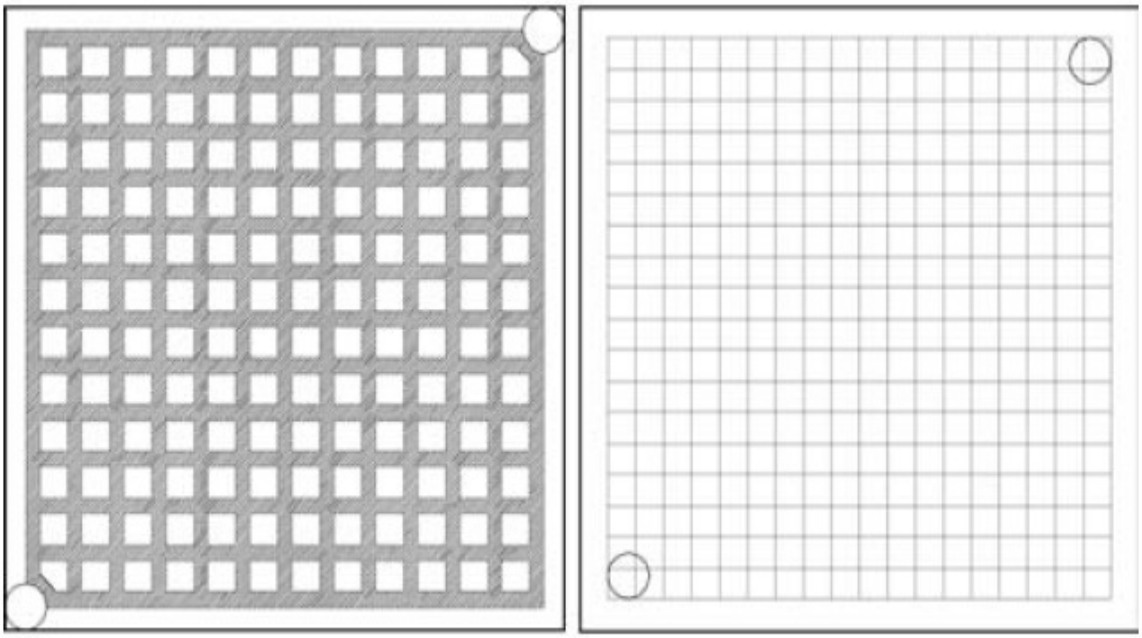

FIGURE 4.12: Various possible flow field designs: (a) Parallel gas channels — this design may lead to pressure imbalances between adjacent channels and gas blockages; (b) serpentine flow field as patented by Ballard Power Systems; (c) mirrored flow field as patented by General Motors; (d) interdigitated flow field with gas conduction through the attached electrode substrate; (e) gas diffusion layer without flow channels (here: ordered support pad structure); (f) metal mesh flow field — the gas passes through the mesh structure below and above the metal wires.

4.1.4.2 Materials and Production Techniques for Bipolar Plates

As far as *materials properties* for bipolar plates are concerned, there are currently two competing approaches, the use of graphite-based flow field materials and the use of metal.

4.1.4.3 Graphite-Based Materials

The choice of materials for producing bipolar plates in commercial fuel cell stacks is dictated not only by performance considerations but also by cost. Currently, blank graphite plates cost between U.S. $20 and U.S. $50 apiece in small quantities, i.e., up to U.S. $1000/m2, or perhaps more than U.S. $100/kW, assuming one plate per

MEA plus cooling plates at an MEA power density of 1 Wcm^{-2}. Again, automotive cost targets are well beyond reach, even ignoring additional machining and tooling time.

4.1.4.4 Metallic Bipolar Plates

Metals are very good electronic and thermal conductors and exhibit excellent mechanical properties. Undesired properties are their limited *corrosion resistance* and the difficulty and cost of machining. The metals contained in the plates bear the risk of leaching in the harsh electrochemical environment inside a fuel cell stack; leached metal may form damaging deposits on the electrocatalyst layers or could be ion-exchanged into the membrane or the ionomer, thereby decreasing the conductivity. Corrosion is believed to be more serious at the anode, probably due to weakening of the protective oxide layer in the hydrogen atmosphere.

Several grades of *stainless steel* (310, 316, 904L) have been reported to survive the highly corroding environment inside a fuel cell stack for 3000 h without significant degradation by forming a protective *passivation* layer. Clearly, the formation of oxide layers reduces the conductivity of the materials employed. Therefore, coatings have been applied in some cases. In the simplest case, this may be a thin layer of gold or titanium. Titanium nitride layers are another possibility and have been applied to lightweight plates made of aluminum or titanium cores with corrosion resistant spacer layers. Whether these approaches are commercially viable depends on the balance between materials and processing cost.

Directing the gas flow is sometimes done by shaping thin metal plates to form *dimples* or other *protrusions*. Alternatively, meshes and metal foams have been used as spacers.

Meanwhile, mechanical machining of flow fields into solid stainless steel plates is difficult. A number of companies such as Microponents (Birmingham, U.K.) and PEM (Germany) attempt to achieve volume production of flow field plates by employing *chemical etching* techniques. Yet etching is a slow process and generates slurries containing heavy metals, and it is hence of limited use for mass production.

4.2 Fuel Cell Stack

There are many alternative stack configurations, however, the materials, designs, and methods of fabricating the components are similar. When considering the design of a fuel cell stack, usually several limitations should be considered. Some of these limitations may include the following:

- Size, weight, and volume at the desired power
- Cost
- Water management
- Fuel and oxidant distribution

Figure 4-13 illustrates a PEM fuel cell stack.

4.2.1 Fuel Cell Stack Sizing

The sizing of a fuel cell stack is very simple; there are two independent variables that must be considered—voltage and current. The known requirements are the maximum power, voltage, and/or current. Recall that power output is a product of stack voltage and current:

$$W_{FC} = V_{st} \cdot I \qquad (4\text{-}1)$$

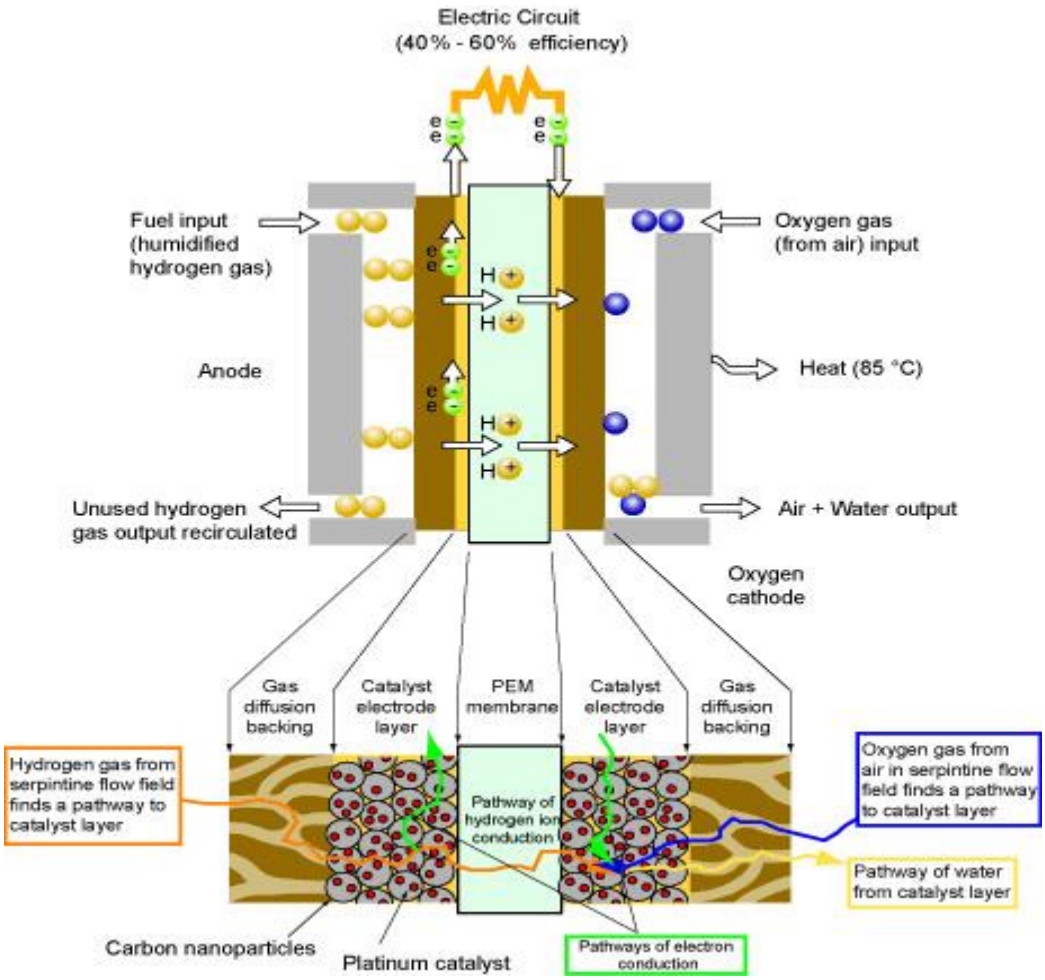

FIGURE 4-13. Schematic of a PEM fuel cell stack.

Other initial considerations that are helpful when designing a fuel cell stack are the current and power density. These are often unavailable initially, and can be calculated from the desired power output, stack voltage, efficiency, and volume and weight limitations. The current is a product of the current density and the cell active area:

$$I = i * A_{cell} \tag{4-2}$$

As mentioned previously, the cell potential and the current density are related by the polarization curve:

$$V_{cell} = f(i) \tag{4-3}$$

Figure 4-14 shows example polarization curves for single PEM fuel cells from the literature. Most fuel cell developers use a nominal voltage of 0.6 to 0.7 V at nominal power. Fuel cell systems can easily be designed at nominal voltages of

0.8V per cell or higher if the correct design, materials, operating conditions, balance-of-plant, and electronics are selected.

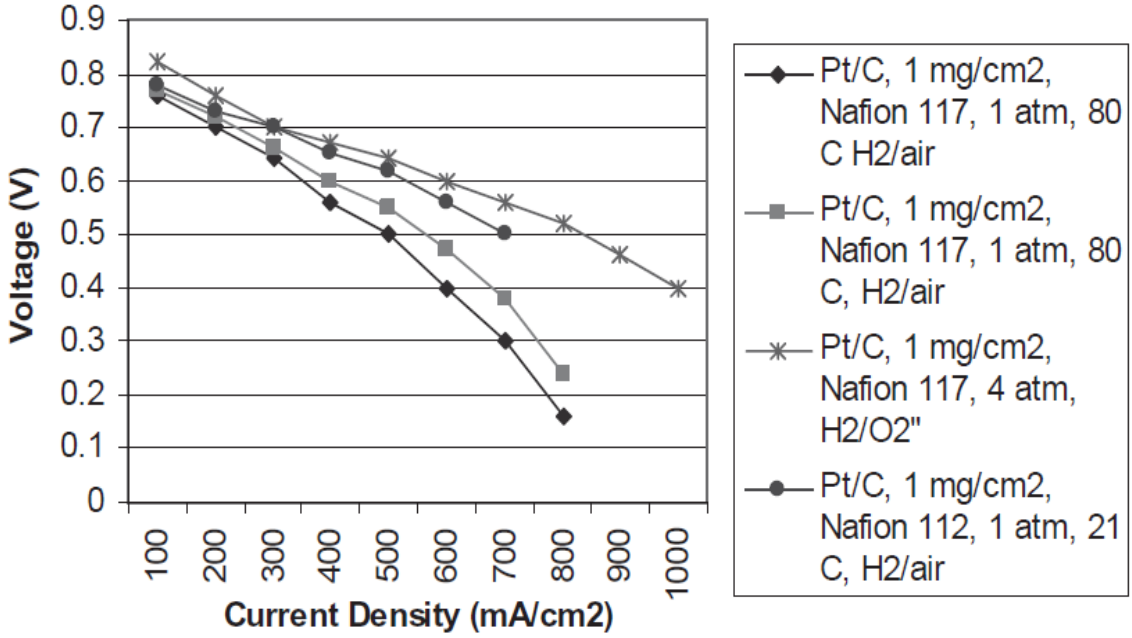

FIGURE 4-14. Polarization curves for PEM fuel cell single cells

4.2.3 Number of Cells

The number of cells in the stack is often determined by the maximum voltage requirement and the desired operating voltage. The total stack potential is a sum of the stack voltages or the product of the average cell potential and number of cells in the stack

$$V_{st} = \sum_{i=1}^{N_{cell}} V_i = \overline{V_{cell}} * N_{cell} \quad (4\text{-}4)$$

The cell area must be designed to obtain the required current for the stack. When this is multiplied by the total stack voltage, the maximum power requirement for the stack will be obtained. The average voltage and corresponding current density selected can have a large impact upon stack size and efficiency. The fuel cell stack efficiency can be approximated with the following equation:

$$\eta_{stack} = \frac{V_{cell}}{1.482} \quad (4\text{-}5)$$

4.2.4 Stack Configuration

In the traditional bipolar stack design, the fuel cell stack has many cells in series, and the cathode of one cell is connected to the anode of the next cell. The MEAs, gaskets, bipolar plates, and end plates are the layers of the fuel cell. The stack is held together by bolts, rods, or another pressure device to clamp the cells together. When contemplating a fuel cell design, the following should be considered:

• Fuel and oxidant should be uniformly distributed through each cell, and across its surface area.

• The temperature must be uniform throughout the stack.

• If designing a fuel cell with a polymer electrolyte, the membrane must not dry out or become flooded with water.

• The resistive losses should be kept to a minimum.

• The stack must be properly sealed to ensure no gas leakage.

• The stack must be sturdy and able to withstand the necessary environments it will be used in.

The most common fuel cell configuration is shown in Figure 4-15. Each cell (MEA) is separated by a plate with flow fields on both sides to distribute the fuel and oxidant. The fuel cell stack end plates have only a single-sided flow field. The majority of fuel cell stacks, regardless of fuel cell type, size, and fuels used is of this configuration.

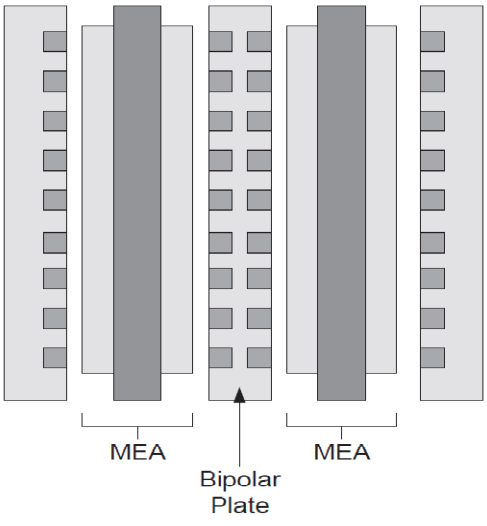

FIGURE 4-15: Typical fuel cell stack confi guration (a two-cell stack).

4.2.5 Distribution of Fuel and Oxidants to the Cells

Fuel cell performance is dependent upon the flow rate of the reactants. Uneven flow distribution can result in uneven performance between cells. Reactant gases need to be supplied to all cells in the same stack through common manifolds. Some stacks rely on external manifolds, while others use an internal manifolding system. One advantage of external manifolding is its simplicity, which allows a low pressure drop in the manifold, and permits good flow distribution between cells. A disadvantage is that the gas flow may flow in crossflow, which can cause uneven temperature distribution over the electrodes and gas leakage. Internal manifolding distributes gases through channels in the fuel cell itself. An advantage of internal manifolding is more flexibility in the direction of flow of the gases. One of the most common methods is ducts formed by the holes in the separator plates that are aligned once the stack is assembled. Internal manifolding allows a great deal of flexibility in the stack design. The main disadvantage is that the bipolar plate design may get complex, depending on the fuel flow channel distribution design. The manifolds that feed gases to the cells and collect gases have to be properly sized. The pressure drop through the manifolds should be an order of magnitude lower than the pressure drop through each cell in order to ensure uniform flow distribution.

When analyzing the flow for the cells:

1. The flow into each junction should equal the flow out of it.
2. The flow in each segment has a pressure drop that is a function of the flow rate and length through it.
3. The sum of the pressure drops around a closed loop must be zero.

Some of the factors that need to be considered when designing manifold stacks include manifold structure, size, number of manifolds, overall gas flow pattern, gas channel depth, and the active area for electrode reactions.

The manifold holes can vary in shape from rectangular to circular. The area of the holes is important because it determines the velocity and type of flow. The flow pattern is typically a U-shape (reverse flow), where the outlet gas flows in the opposite direction to the inlet gas, or a Z-shape (parallel flow), where the directions of the inlet and outlet gas flows are the same as shown in Figures 4-16 and 4-17.

The pressure change in manifolds is much lower than that in the gas channels on the electrodes in order to ensure a uniform flow distribution among cells piled in a stack.

The pressure drop can be calculated from the Bernoulli equation as follows:

$$\Delta P(i) = -\rho \frac{[u(i)]^2 - [u(i-1)]^2}{2} + f.\rho \frac{L_S}{D_H} \frac{[u(i)]^2}{2} + K_f.\rho \frac{[u(i-1)]^2}{2} \qquad (4\text{-}5)$$

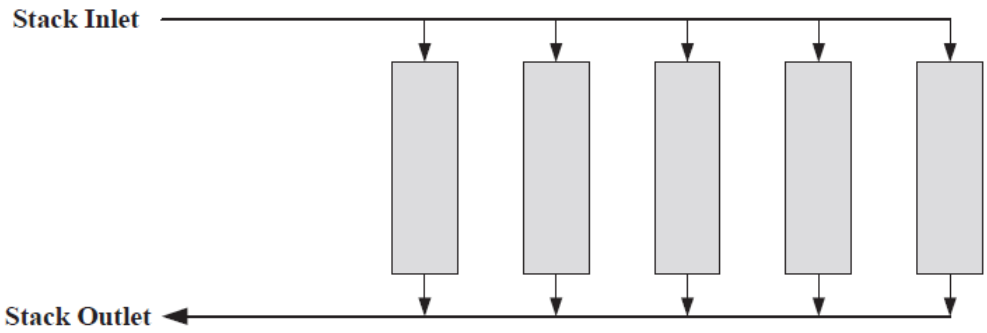

FIGURE 4-16: A U-type manifold

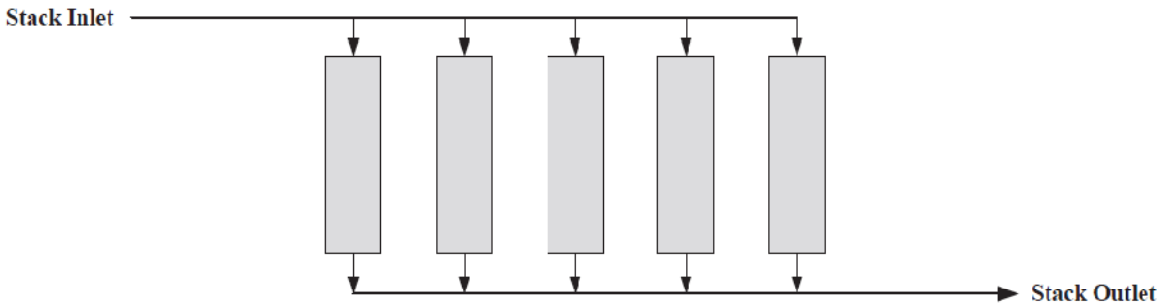

FIGURE 4-17. A Z-type manifold.

Where r is the density of the gas (kg/m3), n is the velocity (m/s), f is the friction coefficient, Ls is the length of the segment (m), DH is the hydraulic diameter of the manifold segment (m), and K_f is the local pressure loss coefficient. For laminar flow (Re < 2300), the friction coefficient f for a circular conduit (as mentioned previously) is:

$$f = \frac{64}{Re} \qquad (4\text{-}6)$$

The walls of the fuel cell manifolds are considered "rough" when the stack has bipolar plates that are clamped together. The friction coefficient for turbulent flow is a function of wall roughness. The friction coefficient is

$$f = \frac{1}{\left(1.14 - 2log\frac{\varepsilon}{D}\right)^2} \tag{4-7}$$

Where $\frac{\varepsilon}{D}$ is the relative roughness, which can be as high as 0.1.

References:

[1] Spiegel C., ***"PEM Fuel Cell Modelling and Simulation Using MATLAB",*** *Elsevier, 2008.*

[2] Frano Barbir., " **PEM Fuel Cells Theory and Practice**."

[3] Hoogers, Gregor "**Fuel cell Technology handbook**"

[4] Bei Gou, Woon Ki Na, Bill Diong. – 2009. "**Fuel Cells**"

[5] http://physics.nist.gov/MajResFac/NIF/Images/FuelCellBasic.gif

Section 5

Fuel Cell System Design

5.1 Introduction

In order to obtain optimum performance from a fuel cell stack, the hydrogen and oxidant flow, water removal, and the voltage output should be optimized using external plant components. Fuel cell system designs range from very simple to very complex depending upon the fuel cell application and the system efficiency desired. A fuel cell system can be very efficient with a few plant components, as shown in Figure 5-1. Usually, the larger the fuel cell stack, the more complex the fuel cell plant subsystem.

The part of the fuel cell system that is responsible for air flow includes a particulate filter for cleaning the system, humidification module, and a pressure transducer. There is also a pump to ensure an adequate supply of air into the fuel cell stack. The hydrogen flows into the fuel cell stack using a pressurized tank. A mass flow controller should be installed in this system to monitor the flow rate. Other additional components often found in fuel cell plant include: heat exchangers, pumps, fans, blowers, compressors, electrical power inverters, converters and conditioners, water handling devices, and control systems.

Only a few sensors and pressure transducers are included in Figure 5-1. A fully developed control system will consist of thermocouples, pressure transducers, hydrogen sensors, and mass flow controllers, which will measure and control data using a data acquisition program.

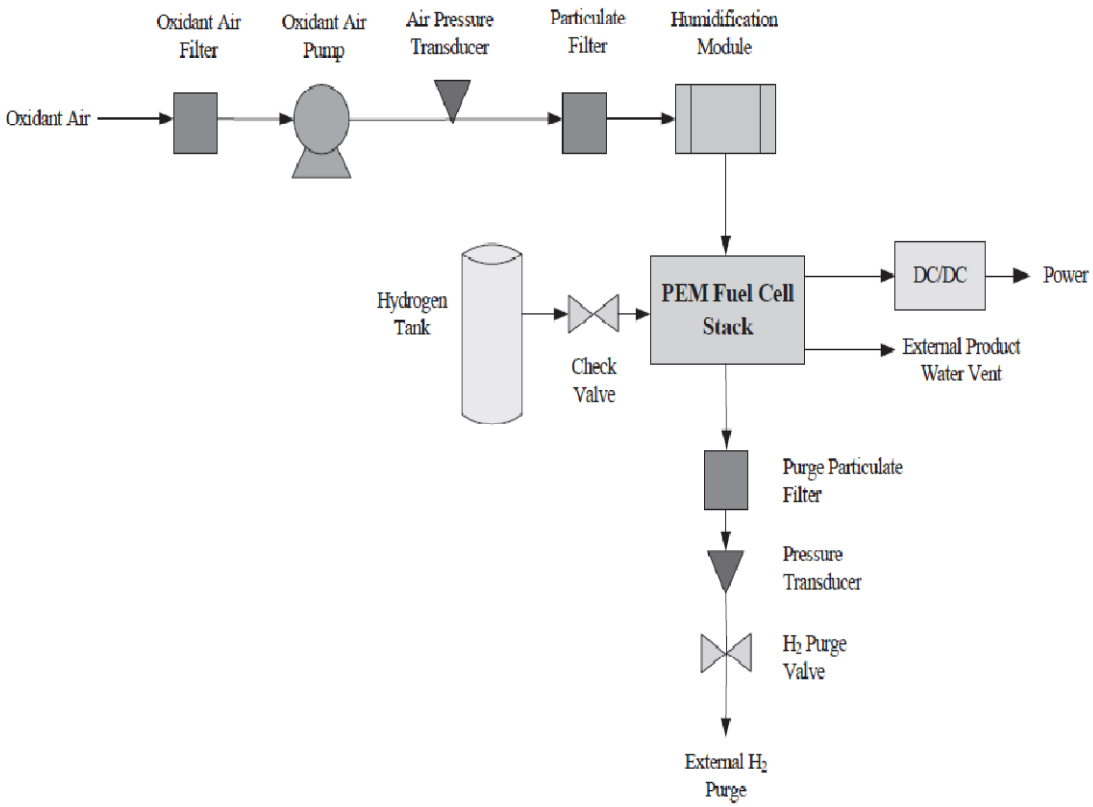

Figure5- 1: Simple PEM fuel cell system

5.2 Fuel Subsystem

As seen in Figure 5-1, the fuel subsystem is very important because the reactants may need to undergo several processes before they are ultimately delivered to the fuel cell with the required conditions. Plant components such as blowers, compressors, pumps, and humidification systems have to be used to deliver the gases to the fuel cell with the proper temperature, humidity, flow rate, and pressure.

5.2.1 Hydrogen-Air Systems

For most terrestrial systems it is more practical to use oxygen from air than to carry oxygen as a part of the fuel cell system. Oxygen content in air is 20.95% by volume. This dilution has a penalty on fuel cell voltage (about 50 mV). Additional penalty in

both power output and efficiency is because oxygen and almost four times that of nitrogen must be somehow pumped through the fuel cell.

5.2.2 Air Supply

In hydrogen-air systems, air is supplied by a fan or a blower (for lowpressure systems) or by an air compressor (for pressurized systems). In the former case, the exhaust from the fuel cell is opened directly into the environment (Figure 5-2a), whereas in a pressurized system, pressure is maintained by a preset pressure regulator (Figure 5-2b).

In any case, a fan, blower, or compressor is run by an electric motor that requires electrical power and thus represents power loss or parasitic load. Compression may be either isothermal or adiabatic. The former implies an infinitesimally slow process allowing temperature equilibration with the environment. The latter implies quite the opposite—a process so fast that no heat is exchanged with the environment during the compression.

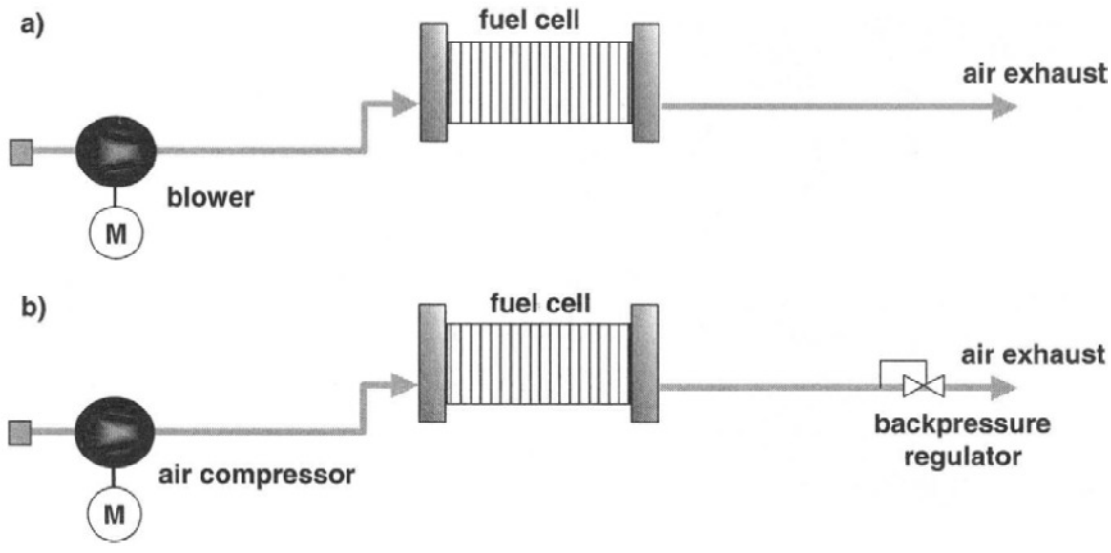

Figure5- 2: Air supply for a fuel cell system: a) ambient pressure; b) pressurized system.

The ideal power needed for adiabatic compression of air from pressure P_1 to pressure P_2 is:

$$W_{comp,ideal} = \dot{m}_{Airin}.C_p.T_1\left[\left(\frac{P_2}{P_1}\right)^{\frac{k-1}{k}} - 1\right] \quad (5\text{-}1)$$

Where:

m_{Airin} = Air flow rate, gs^{-1}

Cp = specific heat, J/g/K

T_1 = temperature before compression, K

P_2 = pressure after compression, Pa

P_1 = pressure before compression. Pa

k = ratio of specific heats (for diatomic gases k = 1.4)

However, no compression is ideal, that is, there are inefficiencies associated with the compression process that result in more power needed:

$$W_{comp} = \frac{\dot{m}_{Airin}.C_p.T_1}{\eta_{Comp}}\left[\left(\frac{P_2}{P_1}\right)^{\frac{k-1}{k}} - 1\right] \quad (5\text{-}2)$$

where the efficiency, η_{comp}, is defined as a ratio between ideal (adiabatic) and actual compression power.

At higher pressures, above 150kPa, a compressor's electric motor may consume a significant portion of the fuel cell power output, depending not only on the compressor efficiency but also on the stichiometric ratio and cell operating voltage, as shown in Figure 5-3. The net power output, W_{net}, is the fuel cell power, W_{pc}, less the power

delivered to the auxiliary components, W_{aux}, which includes the compressor or the blower:

$$W_{net} = W_{FC} - W_{aux}$$

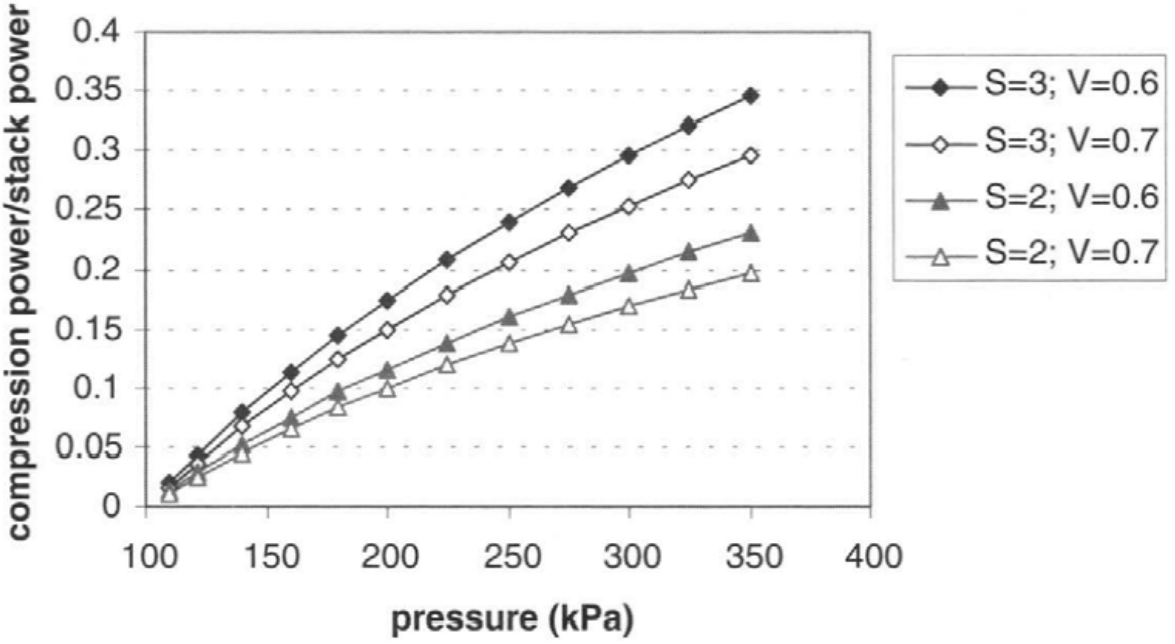

Figure 5-3: Compression power as a function of pressure (assuming inlet pressure is atmospheric, inlet temperature of 20°C, and compressor efficiency of 70%).

The net system efficiency is then:

$$\eta_{sys} = \eta_{FC} \frac{W_{net}}{W_{FC}} = \eta_{FC}(1 - \xi_{aux}) \quad (5\text{-}3)$$

Where ξ_{aux} is the ratio between auxiliary power (also called parasitic losses) and fuel cell power output is $W_{aux}/W_{FC.}$ One of the main reasons for operating a fuel cell at an elevated pressure is to get more power out of it. However, when compression power is taken into account, operation at higher pressure may not result in more Power.

5.2.3 Hydrogen Supply

The properties and storage method of hydrogen have already been discussed in section 2. Once hydrogen is released from the storage reservoir, the simplest way to supply hydrogen to a fuel cell is in the dead-end mode (Figure 5-4a). Such a system would only require a preset pressure regulator to reduce the pressure from the stack to the fuel cell operating pressure. The long-term operation in a dead-end mode may be possible only with extremely pure gases, both hydrogen and oxygen. Any impurities present in hydrogen will eventually accumulate in the fuel cell anode. This also includes water vapor that may remain (when the back diffusion is higher than the electroosmotic drag), which may be the case with very thin membranes and when operating at low current densities. In addition, inerts and impurities may diffuse from the air side until an equilibrium concentration is established. To eliminate this accumulation of inerts and impurities, purging of the hydrogen compartment may be required (Figure 5-4b). This may be programmed either as a function of cell voltage or as a function of time.

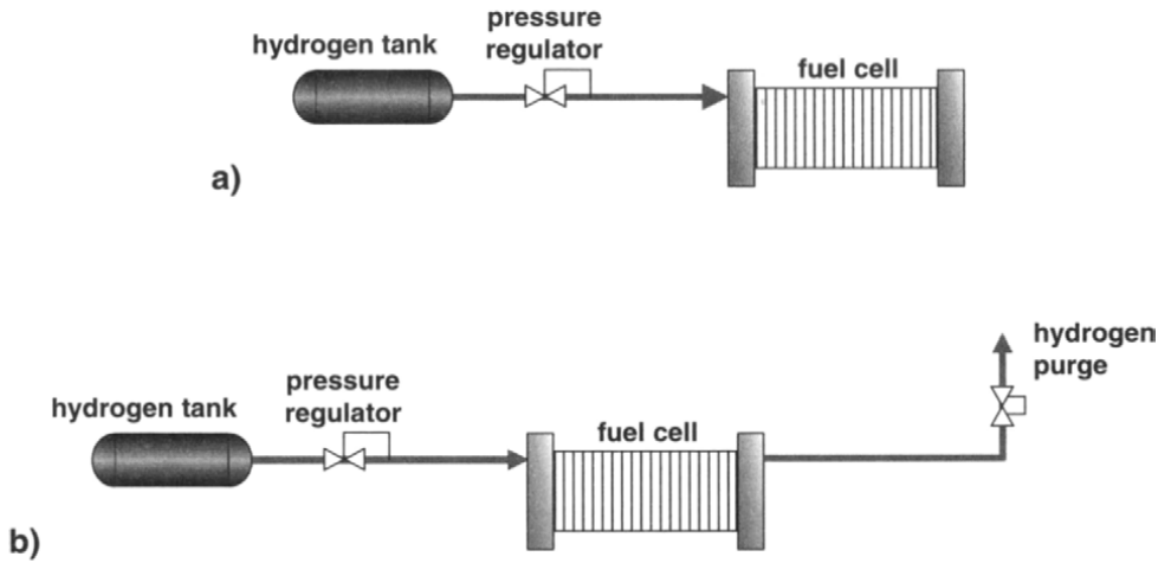

Figure: 5-4: Hydrogen supply schemes: a) dead-end; b) dead-end with intermittent purging.

5.2.4 Humidification Systems

In PEM fuel cells, a hydrogen humidification system may be required to prevent the fuel cell PEM from dehydrating under the load. Water management is a challenge in the PEM fuel cell because there is ohmic heating under high current flow, which will dry out the polymer membrane and slow ionic transport. Some fuel cell stacks may not require any humidification due to water generation at the cathode. In larger fuel cell systems, either the air or the hydrogen or both the air and hydrogen must be humidified at the fuel inlets. The following are the ways to humidify the gases:

- Bubbling the gas through water (dew point humidification)
- Water or steam injection
- Exchange of water and heat through a water permeable medium
- Exchange of water and heat on an absorbent surface

Example of these humidification methods are shown in figure 5-5 below

a):

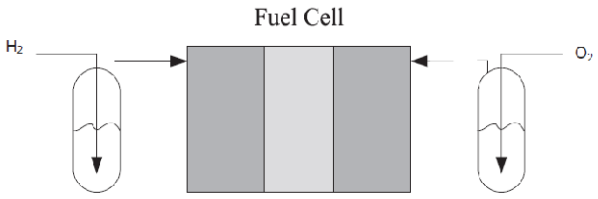

Dewpoint Humidification

b):

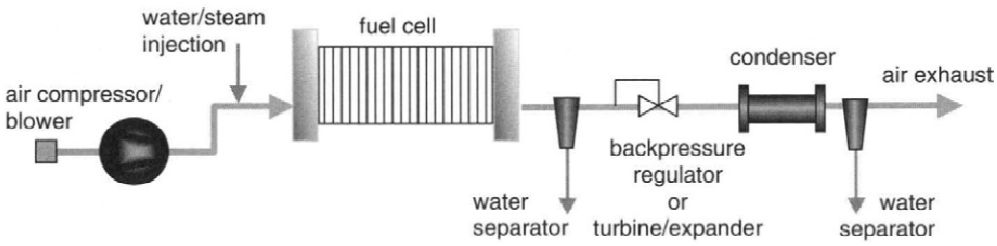

c):

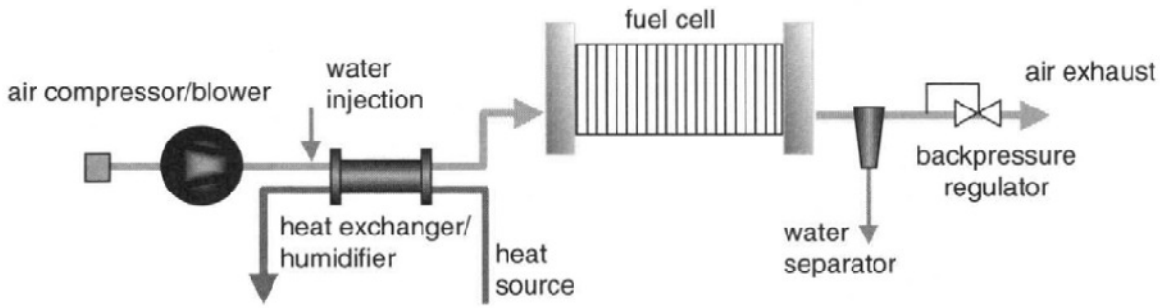

d):

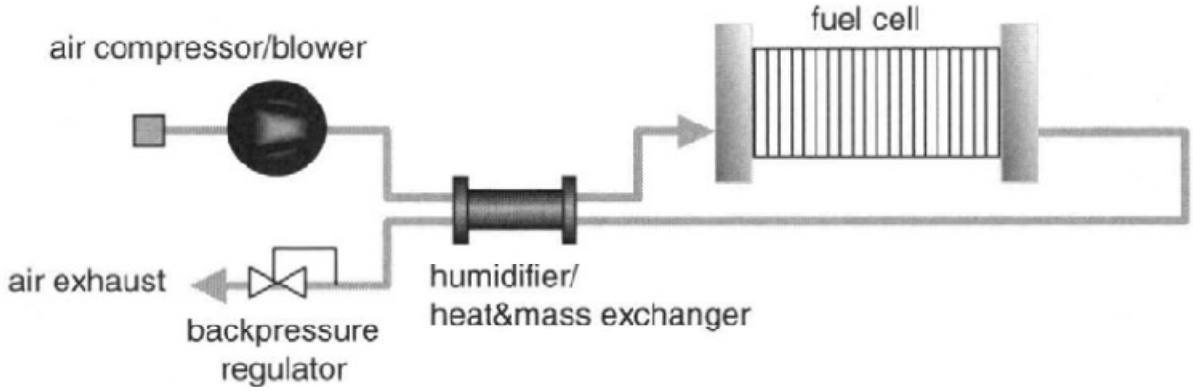

FIGURE 5-5. Dew point humidification: a) Practical air humidification schemes: b) water/steam injection, c) water injection with heat exchange, d) exchange of water and heat with the cathode exhaust.

In laboratory systems, bubbling or dew point humidification is the most common method. In this method, air is dispersed through a porous tube immersed in heated liquid water. In this way, bubbles of air in water form a relatively large contact area between gas and liquid water where the evaporation process can take place. The desired level of humidification is achieved by controlling the temperature of water with heaters. The device should be designed so the fuel cell does not carry water droplets. The following are the few points for designing the humidification systems:

- Minimize the heat loss in the system.
- The water should be delivered in the vapor phase at or near the inlet gas temperature required by the fuel cell. This may mean heating the piping after the humidification unit to the fuel cell.
- The level of humidification may need to be controlled depending upon the fuel cell system design.

Direct water injection is a more elegant, more compact, and easier to control method (Figure -5b). The required amount of water to be injected can be easily calculated for any combination of operating conditions (temperature, pressure, gas flow rate, and desired relative humidity):

$$\dot{m}_{H_2O} = \dot{m}_{Air} \frac{M_{H_2O}}{M_{Air}} \left(\frac{\varphi . P_{sat}(T)}{P - \varphi . P_{sat}(T)} - \frac{\varphi_{amb} . P_{sat}(T_{amb})}{P_{amb} - \varphi_{amb} . P_{sat}(T_{amb})} \right) \quad (5\text{-}4)$$

where (φ, T, P, and φ_{amb}, T_{amb}, P_{amb} are relative humidity, temperature, and pressure at the fuel cell inlet and of the ambient air, respectively. The exact amount of water may be dosed by a metering pump. It is important that water is injected in the form of fine mist, so that a large contact area between water and air facilitates evaporation. However, simple injection of liquid water in the gas stream may not be sufficient to actually humidify the gas, because humidification also requires heat for evaporation. The enthalpy of water, even if the water is hot, is usually not sufficient and additional heat is required.

The sources of heat may be the air compressor (obviously applicable only in pressurized systems) and the fuel cell stack itself. In most of the operating conditions, there is sufficient amount of heat generated in the fuel cell stack. It is the duty of the system to transfer a portion of that heat to the humidification process (Figure 5-5c).

Water injection during the compression process may actually improve the efficiency of the compression process by simultaneously cooling the compressed gas; however, this method is not applicable for all kinds of compressors.

Direct steam injection eliminates the need for additional heat exchange; however, steam must be generated somewhere in the system, which means that this method is applicable only for the systems where heat is generated at a temperature above the water boiling temperature (l00˚C at 101.3 kPa).

Exchange of heat and water from the cathode exhaust with incoming air is an elegant way of taking advantage of water and heat produced in the fuel cell stack (Figure 5-5d). This can be achieved through a water permeable medium, such as porous plate (metal, ceramic, or graphite), or a water-permeable membrane (such as Nafion), or through an enthalpy wheel. These devices are essentially mass and heat exchangers, allowing both heat and water to be exchanged between warm and oversaturated fuel cell exhaust and dry incoming air. The heat and water fluxes in a humidifier at low fuel cell operating pressure are in the same direction (from fuel cell exhaust to inlet), whereas at elevated pressure due to compression, the inlet gas may be hot, and in that case the heat and water flow in opposite directions. In either case, it is not possible to humidify the incoming gas to 100% relative humidity at stack operating temperature with this method, because of finite temperature and water concentration differences between the two sides of the humidifier needed for heat and mass transfer.

5.2.5 Fuel Cell Pumps

Pumps, like blowers, compressors, and fans, are among the most important components in the fuel cell plant system. These components are required to move fuels, gases, and condensate through the system and are important factors in the fuel cell system efficiency. Small- to medium-sized PEM fuel cells for portable applications have a back pressure of about 10 kPa or 1 m of water. This is too high for most axial or centrifugal fans, as discussed earlier.

Choosing the correct pump for the fuel cell application is important. As in fans, blowers, and compressors, factors to consider are efficiency, reliability, corrosion-free materials, and the ability to work with the required temperatures, pressures, and flow

rates for the specific fuel cell system. The appropriate matching of a high-efficiency pump with the appropriate motor speed/torque curve may allow for a more efficient fuel cell stack and system.

Figure 5-6: Example of a water circulating pump which is a part of the cooling system

5.3 Water and Heat Management—System Integration

Water and heat are the by-products of the fuel cell operation, and the supporting system must include the means for their removal. Both water and heat from the fuel cell stack may be at least partially reused, for example for humidification of the reactant gases, or for facilitating hydrogen release from metal hydride storage tanks.

Water and heat handling may be integrated into a single subsystem if deionized water is used as a stack coolant. In that case water removes the heat from the stack and the same water and heat are used to humidify the reactant gases. The remaining heat has to be discarded to the surrounding through a heat exchanger, for hydrogen-air systems that is typically a radiator. The amount of heat to be discarded must be calculated from the stack and humidifier energy balances.

The flow rate of the coolant is

$$\dot{m}_{coolant} = \frac{Q}{C_p \Delta T} \tag{5-5}$$

ΔT is typically a design variable. Most typically, ΔT is below 5°C, and rarely above 10°C. Smaller ΔT results in more uniform stack temperature distribution, but it requires larger coolant flow rate, which in turn increases parasitic losses. Sometimes larger stack temperature variations are needed to maintain the water in the desired state; in that case, the coolant ΔT is dictated by the stack temperature requirements.

The size of the radiator heat exchanger depends on the temperature difference between the coolant and the ambient air. For that reason, it is preferred to operate the fuel cell system at a higher temperature, for systems where the size of the components is critical.

A hydrogen-air fuel cell system must be designed so that it does not need any backup water supply. Water is generated inside the stack, but water is needed for humidification of one or both reactant gases. Sometimes, depending on the intended operation of the fuel cell system, and depending on the stack's capabilities of recirculating water internally *{e.g.* with the use of thinner membranes and with hydrogen and air in counterflow), humidification of only one of the reactants may be sufficient. Water for humidification must be collected at the stack exhaust, on the cathode side (although sometimes it is necessary on both cathode and anode exhausts). Depending on the fuel cell operating conditions (pressure, temperature, and flow rates), water at the exhaust may be in either liquid or gaseous form. Liquid water is relatively easily separated from the gaseous stream in liquid/gas separators. If liquid water collected at the stack exhaust is not sufficient for humidification, the exhaust must be cooled so that additional water may condense and be separated. On the system level, water balance is very simple: the amount of water entering the system in ambient air, plus water generated inside the fuel cell, must be larger than or equal to the amount of water leaving the system with exhaust air and hydrogen. Hydrogen exhaust can be

either continuous (flow-through mode) or periodic stream (dead-end or recirculation with periodic purging).

System water balance is given with the following equation:

$$\dot{m}_{H_2o,Airin} + \dot{m}_{H_2o,gen} = \dot{m}_{H_2o,Airout} + \dot{m}_{H_2o,out} \quad (5\text{-}5)$$

Where:

$\dot{m}_{H_2o,Airin}$ = Water entering the system with ambient air intake:

$\dot{m}_{H_2o,gen}$ = water generated inside the stack.

Water balance therefore depends on:

• The oxygen (and hydrogen) flow rate, that is, stichiometric ratio,

• stack operating temperature, that is, temperature of the exhaust,

• stack operating pressure, or more precisely the stack outlet pressure, that is, the pressure at which the liquid water is separated from the exhaust gases,

• Ambient conditions (pressure, temperature, and relative humidity).

It should be noted that water balance on the system level does not depend on current and number of cells.

Figure 5-7 shows the required exhaust temperature that results in neutral water balance as a function of air flow rate and operating pressure (ambient conditions are assumed to be 20°C, 101.3 kPa, and 60% relative humidity). For the ambient pressure operation and oxygen stichiometry of 2.0, the stack should not be operated above 60°C. If it is necessary to operate at a higher temperature, then a higher operating pressure should be selected or additional heat exchanger may be needed to achieve neutral water balance (which may defeat the purpose of operating at a higher temperature).

It should be noted that hydrogen does not carry much water out of the system. The dashed lines in Figure 5-7 take into account water taken away from the system by hydrogen exhaust assuming hydrogen stichiometry of 1.2. Presence of water in the system makes fuel cell systems susceptible to freezing if used outdoors in cold climate. In such case, the coolant loop is separated from the water system, which allows for antifreeze coolants (such as aqueous solutions of ethylene-glycol or propylene-glycol) to be used instead of deionized water. Nevertheless, water cannot be completely eliminated from the system,- after all, the PSA membrane contains up to 35% water. Operation, or actually, survival and start-up, of a fuel cell system in a cold environment is an issue that must be addressed by the system design.

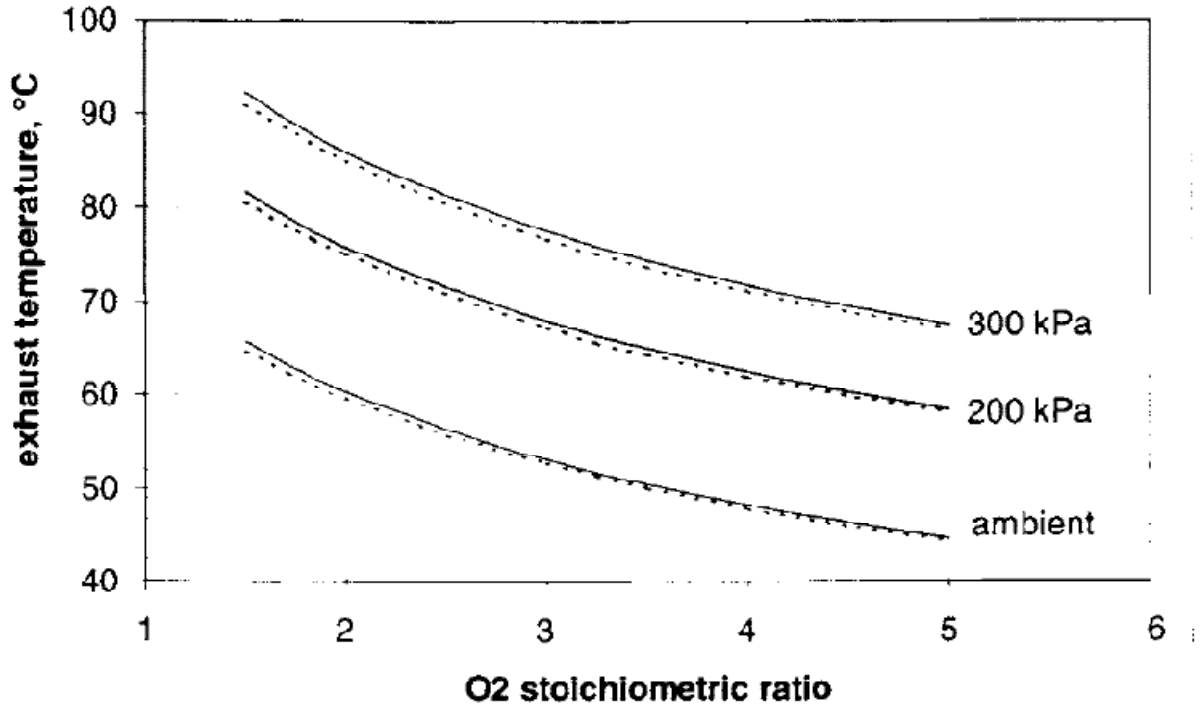

Figure 5-7: Required stack exhaust temperature to achieve neutral system water balance.

References:

[1] Spiegel C., **"PEM Fuel Cell Modelling and Simulation Using MATLAB",** Elsevier, 2008.

[2] Frano Barbir., " **PEM Fuel Cells Theory and Practice**."

[3] Colleen S. Spiegel "**Designing and building Fuel cells**"

Section 6

Heat Transfer In a Fuel Cell System

6.1 Introduction

Temperature in a fuel cell is not always uniform, even when there is a constant mass flow rate in the channels. Uneven fuel cell stack temperatures are due to a result of water phase change, coolant temperature, air convection, the trapping of water, and heat produced by the catalyst layer. In order to precisely predict temperature-dependent parameters and rates of reaction and species transport, the heat distribution throughout the stack needs to be determined accurately. The specific topics to be covered are as follows:

• Fuel cell energy balances

• Fuel cell heat management

The first step in determining the heat distribution in a fuel cell stack is to perform energy balances on the system. The total energy balance around the fuel cell is based upon the power produced, the fuel cell reactions, and the heat loss that occurs in a fuel cell. Convective heat transfer occurs between the solid surface and the gas streams, and conductive heat transfer occurs in the solid and/or porous structures. The reactants, products, and electricity generated are the basic components to consider in modeling basic heat transfer in a fuel cell, as shown in Figure 6-1.

The general energy balance states that the enthalpy of the reactants entering the cell equals the enthalpy of the products leaving the cell plus the sum of the heat generated by the power output, and the rate of heat loss to the surroundings. The basic heat transfer calculations will aid in predicting the temperatures and heat in overall fuel cell stack and stack components.

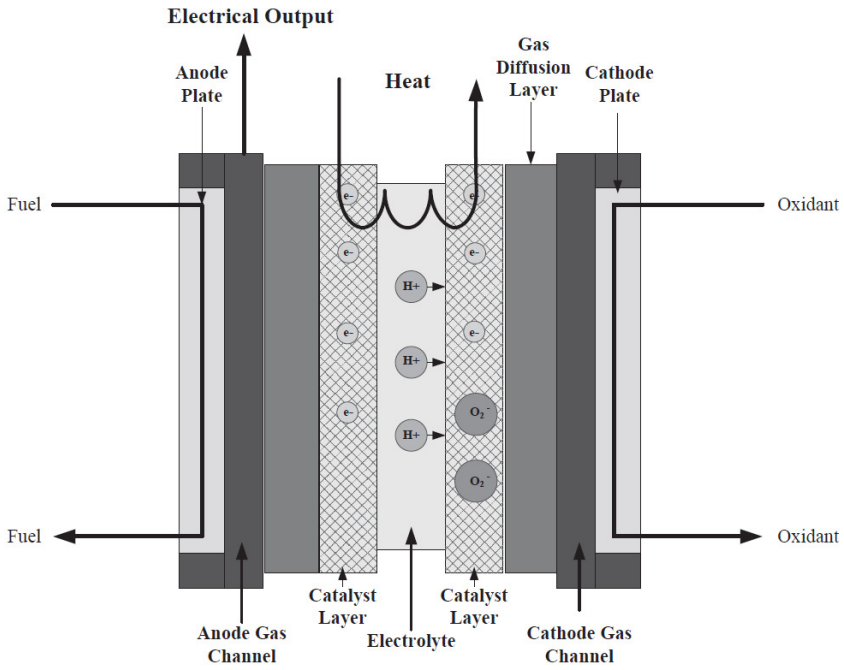

FIGURE 6-1. Stack illustration for heat fl ow study1.

6.2 Heat Removal from a Fuel Cell Stack

To maintain the desired temperature inside the cells, the heat generated as a by-product of the electrochemical reactions must be taken away from the cells and from the stack. Different heat management schemes (Figure 6-2) may be applied, such as:

• Cooling with a coolant flowing between the cells. Coolant may be deionized water, antifreeze coolant, or air. Cooling may be arranged between each cell, between the pair of cells (in such configuration one cell has the cathode and other cell has the anode next to the cooling arrangement), or between a group of cells (this is feasible only for low-power densities because it results in higher temperatures in the center cells). Equal distribution of coolant may be accomplished by the manifolding arrangement similar to that of reactant gases. If air is used as a coolant, equal distribution may be accomplished by a plenum.

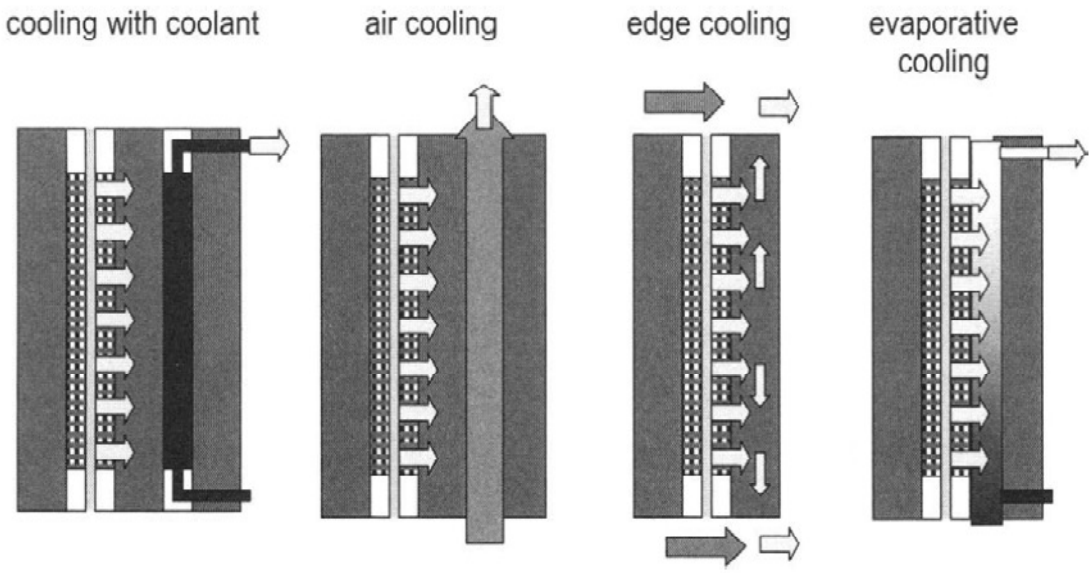

FIGURE 6-2. Different cell/stack cooling options.

• Cooling with coolant at the edge of the active area (with or without fins).

The heat is conducted through the bipolar plate and then transferred to the cooling fluid, typically air. To achieve relatively uniform temperature distribution within the active area, the bipolar plate must be a very good thermal conductor. In addition, the edge surface may not be sufficient for heat transfer and fins may need to be employed. This method results in a much simpler fuel cell stack and fewer parts, but it has heat transfer limitations and is typically used for low-power outputs.

• Cooling with phase change.

Coolant may be water or another phase-change medium. Use of water simplifies the stack design, because water is already used in both anode and cathode compartments.

Stack Heat Balance

There are several ways to set the fuel cell stack energy balance. In general, energy of fuel (higher heating value) is converted into either electricity or heat:

Energy of fuel reacted = Heat generated + Electricity generated

Or

$$\frac{I}{2F} H_{HHV}.n_{cell} = Q_{gen} + IV_{cell}n_{cell} \quad (6\text{-}1)$$

Heat generated in a fuel cell stack is then:

$$Q_{gen} = (1.482 - V_{cell})I.n_{cell} \quad (6\text{-}2)$$

The previous equation assumes that all the product water leaves the stack as liquid at 25°C, which may be the case if the inlet is fully saturated at the stack operating temperature. If all of the product water leaves the stack as vapor, then the following equation is more appropriate:

$$Q_{gen} = (1.254 - V_{cell})I.n_{cell} \quad (6\text{-}3)$$

The previous equations (6-1 through 6-3) are just approximations. A complete stack energy balance should take into account the heat (enthalpy) brought into the stack with reactant gases, as well as the heat of the unused reactant gases leaving the stack, including both latent and sensible heat of water at the stack inlet and stack outlet:

Enthalpy of reactant gases in = electricity generated -H enthalpy of unused reactant gases including heat of product water + heat dissipated to the surrounding + heat taken away from the stack by active cooling

or

$$\sum Q_{in} = W_{el} + \sum Q_{out} + Q_{dis} + Q_c \quad (6\text{-}4)$$

On closer examination of this energy balance, it is clear that some of the heat generated in the stack is carried away by reactant gases and product water, some is lost to the surrounding by natural convection and radiation, and the rest must be taken away from the stack by active cooling. Because heat generation is associated with the (voltage) losses in a fuel cell, most heat is generated in the catalyst layers, predominantly on the cathode side, then in the membrane due to ohmic losses, and

also in the electrically conductive solid parts of the fuel cell (also due to ohmic losses). This heat is first carried by heat conduction through solid parts of the fuel cell, namely porous electrode structures, including the gas diffusion layer and bipolar plates (Figure 6-3). Some heat is transferred to the reactant gases (depending on their temperature), some is transferred to the cooling medium through convection, and some is conducted to the edge of the stack where it is transferred to the surrounding air through radiation and natural convection (or, in some cases, forced convection when this is the primary way of stack temperature control).

6.3 Active Heat Removal

From the heat removal point of view, a fuel cell stack may be considered as a heat exchanger with internal heat generation. The walls of the fuel cell cooling channels may be neither at constant temperature nor have the constant heat flux, but these two cases are often used as boundary cases for heat transfer analyses.

The heat to be removed by active cooling is

$$Q_c = \sum Q_{in} - W_{el} - \sum Q_{out} - Q_{dis} \tag{6-5}$$

The same heat, Qc, has to be transferred to the cooling fluid:

$$\frac{dQ_c}{dA_c} = h(T_s - T_c) \tag{6-14}$$

or integrated over the entire heat exchange surface, A_c, just as in a heat exchanger:

$$Q_c = UA_cLMTD \tag{6-15}$$

where:

h = local heat transfer coefficient, $Wm^{2\circ}C$

U = overall heat transfer coefficient, $Wm^{2\circ}C$

A_c = heat exchange area = surface area of the cooling channels, m^2

LMTD = logarithmic mean temperature difference, °C, defined as

$$LMTD = \frac{(T_S - T_C)_{in} - (T_S - T_C)_{out}}{ln\frac{(T_S - T_C)_{in}}{(T_S - T_C)_{out}}} \quad (6\text{-}16)$$

The temperature difference between the stack body, Ts, and the cooling fluid, T_c, may be constant (constant thermal flux case), or it may vary from one side of the stack to the other depending on the position of coolant inlets and outlets vs reactants inlets and outlets, internal coolant and reactants passages configuration, and current density configuration.

The same heat, Qc, has to be "absorbed" by the cooling fluid and carried out of the fuel cell stack:

$$Q_c = \dot{m} C_p (T_{c,out} - T_{in}) \quad (6\text{-}17)$$

The temperature difference $\Delta T_c = (T_{c,out} - T_{c,in})$ is a design variable that has to be selected in conjunction with the coolant flow rate. As usual in fuel cell design, in selecting the temperature difference between coolant outlet and inlet there are conflicting requirements. To achieve uniform temperature distribution through the stack, ΔT_c should be selected as small as practically possible, unless larger temperature gradients are required by stack design (for example, to facilitate water management). However, small ΔT_c would result in large coolant flow rate, which would increase parasitic power and reduce system efficiency. On the other side, larger ΔT_c would result in lower temperature to which the coolant must be cooled at, and there may be practical limits imposed by the ambient temperature and by the characteristics and performance of the heat rejection device.

The coefficient of convection heat transfer, h, depends on the Nusselt number, that is, properties of the coolant, geometry of the passages, and flow characteristics.

$$h = N_u \frac{k}{D_H} \text{ Or } h = N_{uL} \frac{k}{L} \text{ Or } \bar{h} = \overline{N_{uL}} \frac{k}{D_H}$$

The Nusselt number represents the ratio of convection heat transfer for fluid in motion to conduction heat transfer for a motionless layer of fluid.

Reference:

[1] Spiegel C., ***"PEM Fuel Cell Modelling and Simulation Using MATLAB",*** *Elsevier, 2008.*

[2] Frano Barbir., " **PEM Fuel Cells Theory and Practice**."

Section 7

Operating Conditions of Genport 300 Watt

7.1 Introduction

In this section the discussion will be made on the performance analysis of a polymer electrolyte membrane (PEM) fuel cell power system for portable applications. The analysis includes the operation of all the components in the system, which consists of two major modules: PEM fuel cell stack module and system module. System module includes air compressor, heat exchanger, humidifier and a cooling loop. A parametric study is performed to examine the effect of varying operating conditions (e.g., temperature and air stoichiometry) on the energy efficiencies of the stack and the system. In this analysis the fuel cell was operated between the current densities of 0.1 and 0.55 Acm^{-2}. The operating temperatures that are set in this experiment are 55, 60 and 65 ˚C while the air supply was at the stoichiometric ratio of 2. For another test the air is supplied to the system at the stoichiometric ratios of 1.5, 2, 2.5 and 3and the temperature was kept constant at 65 ˚C. The description of the system is given below.

7.2 Fuel cell System considered

The hydrogen PEM fuel cell power system that was used for this analysis is Genport 300W fuel cell system. The model consists of four major subsystems: the fuel cell stack, the air supply subsystem, the hydrogen supply subsystem, and the cooling subsystem. The fuel cell stack is the central component of the system—this is where the output power is generated and where the electrochemical reaction of hydrogen and oxygen takes place as follows:

$$\boldsymbol{H_{2(g)} + \frac{1}{2} O_{2(g)} \rightarrow H_2 O_{(l)}}$$

Here, the waste heat produced in the stack module is removed through the cooling loop. The air compressor component of the system module provides oxygen that is

contained in air, to the stack. The air is humidified in a humidifier before being fed to the stack. The compressed hydrogen stored on-board is fed to the stack in dry state. Humidification of inlet air is necessary to prevent dehydration of the membranes in the fuel cell stack. The hydrogen is supply to the stack in dead end mode at fixed pressure. This ensure stoichiometric ratio of 1, which keep the low possible consumption of fuel. A cycling purge expels water formed in the anode side to the environment. The purpose of the cooling loop is to remove the heat produced by the exothermic reaction of hydrogen and oxygen. The cooling loop consists of a radiator, cooling pump, radiator and fans. The cooling pump directs coolant (water/glycol) through the stack to remove the waste heat via radiator.

A block diagram of the system is shown in figure A.

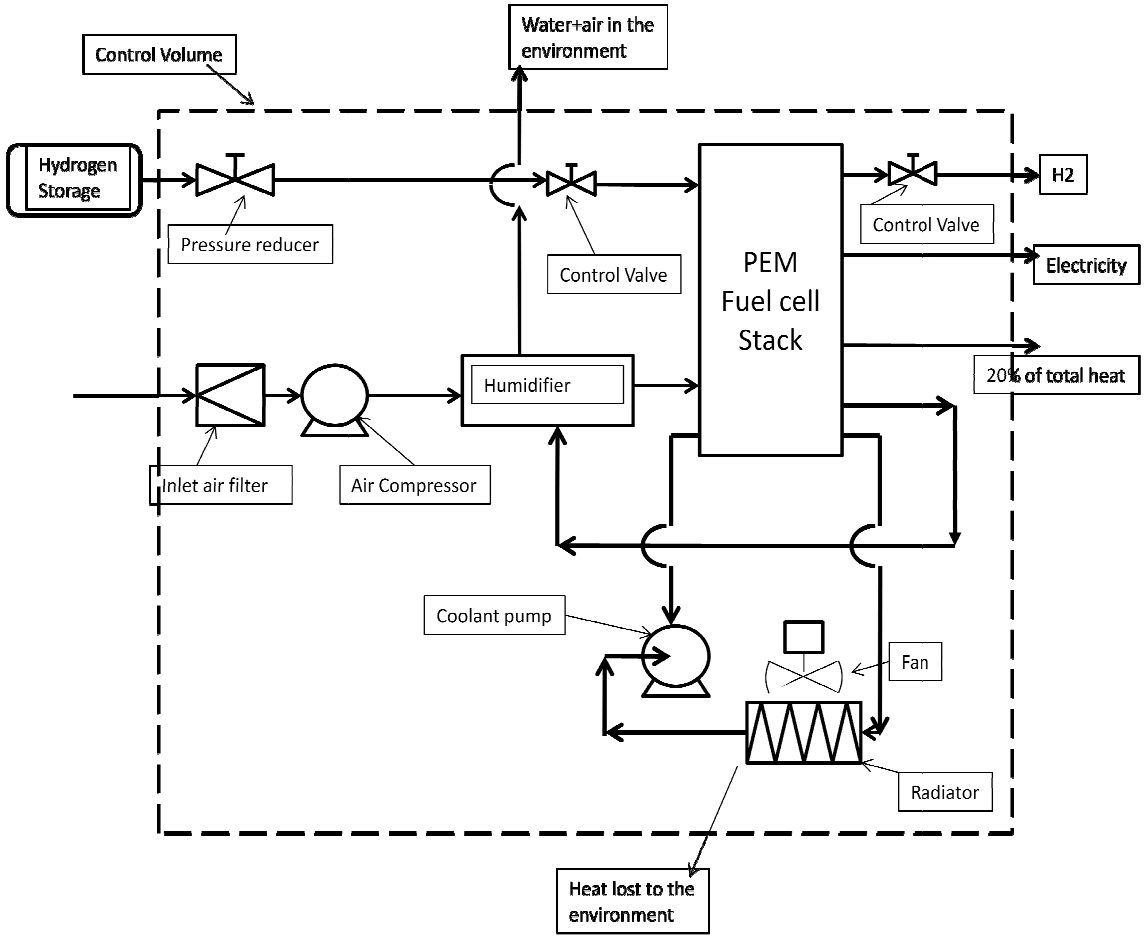

Figure A: Block diagram of the Genport 300W PEMFC System.

The test station was designed control, simulate and monitor the various phenomena that effect the fuel cell system performance. The system was operated an internally developed Lab View® control scheme. The control scheme has show in figure B.

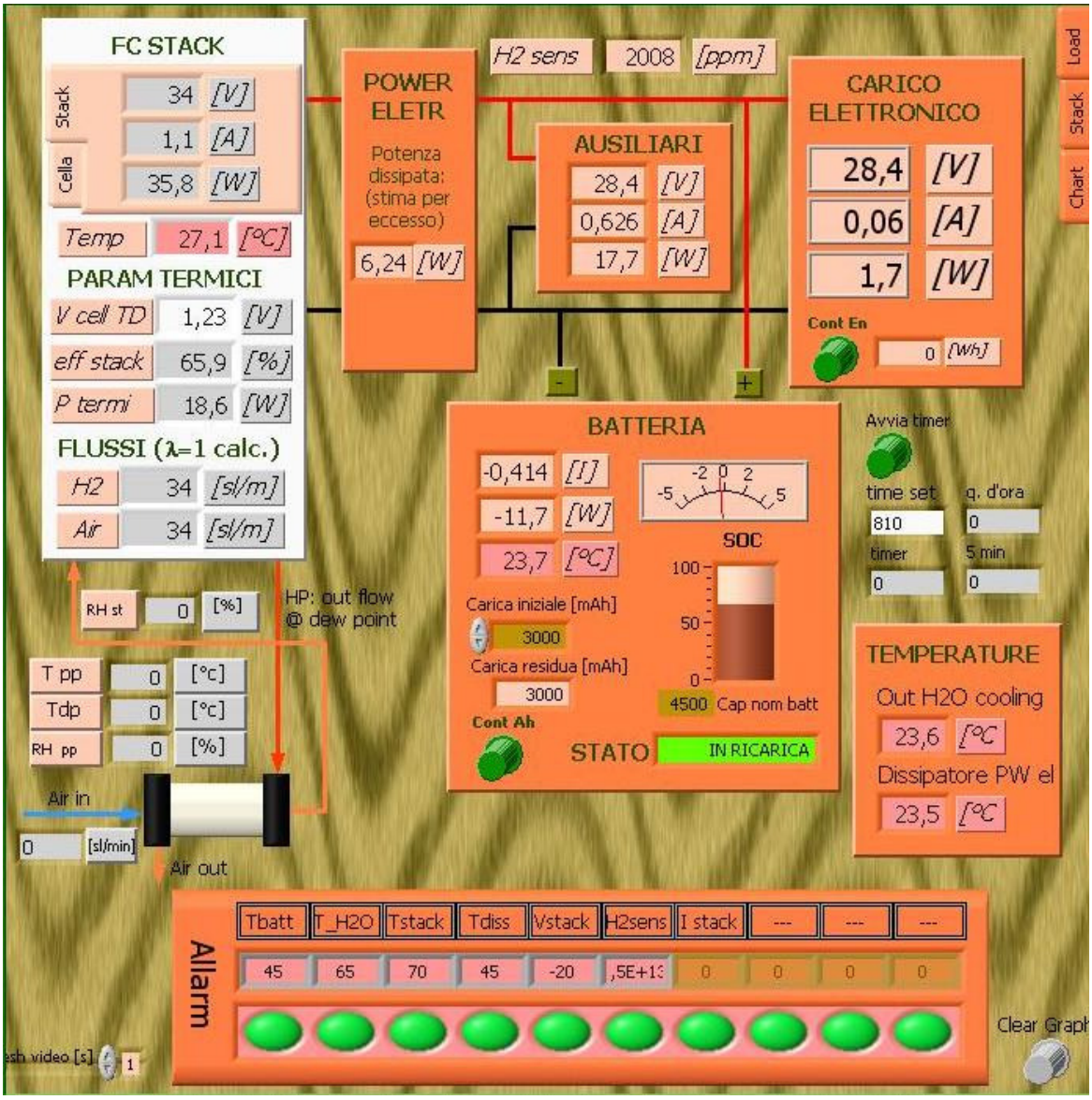

Figure B: Control scheme for the test bench of GP 300W

7.3 Assumptions

Some assumptions were made before carrying out the experiment. The most important of these are:

– A theoretical amount of hydrogen is required based on the current produced (using Faraday's constant). As well, a theoretical amount of oxygen can be calculated based on the required hydrogen.

– The environment consists of a gaseous mixture at 1 atm and 298.15 K, composed of 79% nitrogen and 21% oxygen, on a volume basis; and of liquid water at 298.15 K.

– The hydrogen storage tank is at a constant pressure of 200 bar and temperature of 298.15 K, the pressure of hydrogen is reduce to 300 mbar.

– The temperatures at the inlet and outlet of the water circulation pump are assumed to be equal.

– Heat transfer to the environment only occurs for three components—the fuel cell stack, the radiator, and the air compressor. Further, 20% of the total heat generated by the fuel cell is assumed to be lost via convection and radiation from the fuel cell stack, while the remainder is taken to be removed at the radiator.

– Heat transfer between the radiator and the environment is taken to occur at average temperature of 45 ◦C.

– The stoichiometric ratio of the hydrogen supplied to the system is one.

– The pressure of the air inside the stack is 50mbar.

– The pressure of the hydrogen inside the stack is 300mbar.

7.4 Approach and methodology

As mentioned above that the fuel cell system is composed of fuel cell stack, air supply system (compressor), hydrogen supply system and cooling system. In addition to these another system is the control system which consumes the energy from the stack. The net system power is equal to the gross stack power ($W_{\text{gross}} = iv$) less all of the parasitic loads. For this model, this expands to

$$W_{net} = iv - W_{ac} - \dot{W_{pump}} - W_{fan} - W_{control}$$

Where the parasitic electrical loads on the system are the air compressor, the water pump, the radiator fan and the control system. The output power is obtained by multiplying the voltage of the load and the current of the load. The power consumed by air compressor, cooling pump and fan is measured as auxiliary power collectively while the power dissipated due to joule heating effect and for the control of the system is measured as

$$W_{control} = (V_{stack} - V_{load}) * I_{stack}$$

Then the auxiliary power of the system that is collectively measured is given as

$$W_{aux} = W_{ac} + W_{pump} + W_{fan} = iv - W_{net} - W_{control}$$

7.5 Efficiency of the stack and efficiency of the system

The efficiency of the stack is calculated taking into account the Low Heating Value (LHV). The stack of the system consists of 42 cells and the area of each cell is 25cm^2. So, the cell voltage is calculated by the dividing the voltage of stack divided by the number of cells. So the efficiency of the stack is given by

$$\eta_{stack} = \frac{V_{stack}}{42 * 1.254}$$

Here the efficiency of the stack is less than 100% because the some part of the energy available from the fuel is converted into heat.

Efficiency of the system is given by

$$\eta_{sys} = \frac{W_{net}}{1.254 * 42 * I_{stack}}$$

Where W_{net} is the output work of the system for the load and I_{stack} is the current of the stack.

7.6 Results and Discussion

7.6.1 By varying the temperature

The results obtained from the experiments are summarized in graphs. First experiment is performed by varying the temperature and keeping the stoichiometric ratio as constant. The stoichiometric ratio of the supply of air is kept at two (Lam=2). The temperature is varied from 55 to 65 ˚C by the interval of 5˚C. The result for this experiment is shown below.

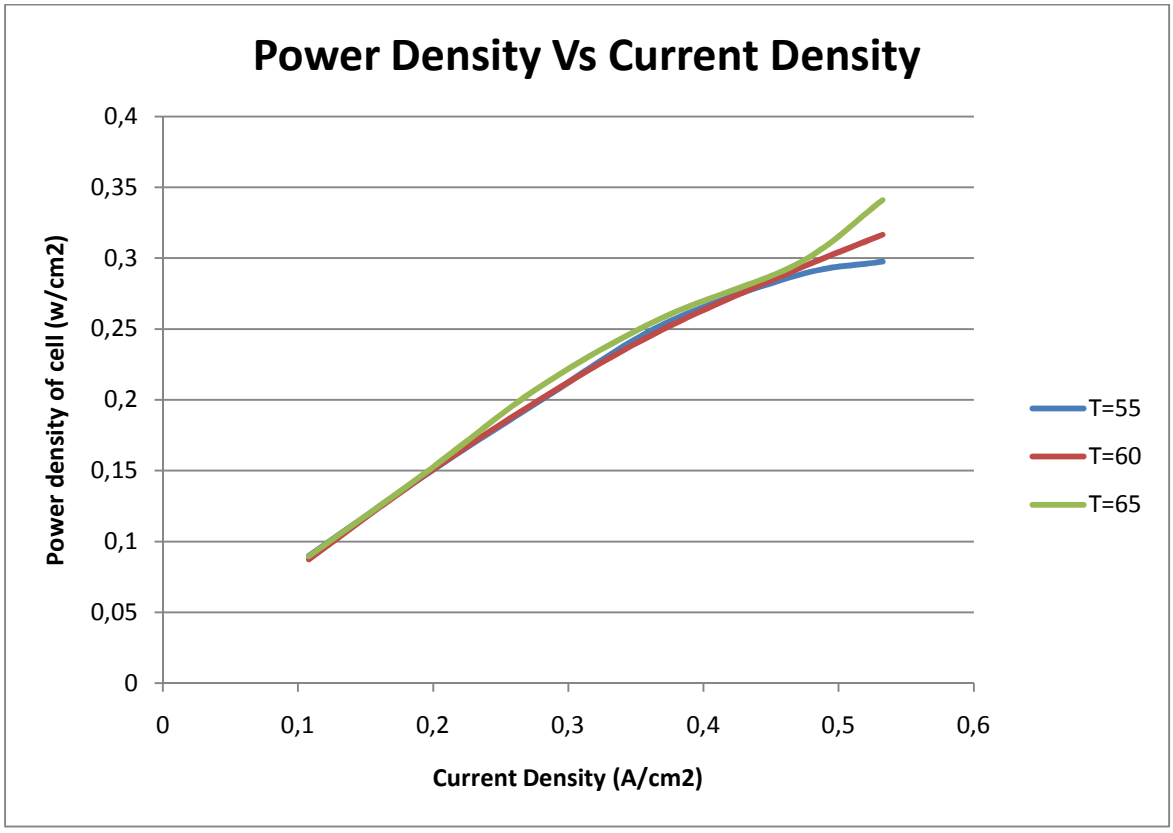

Fig: 1 comparison of power density of stack at various operating temperatures

From this graph it is clear that the power density is more at operating temperature of 65˚C and the difference is clearer at high current densities. This is because that at high temperature the kinetics of the reaction increases which significantly improves the mass transport properties. Also for all temperature ranges the power density increase by increasing the current density. This shows that this operating range of

current density has not reached in the region of concentration losses. The following graphs show the variation of some other parameters with current densities at different operating temperatures.

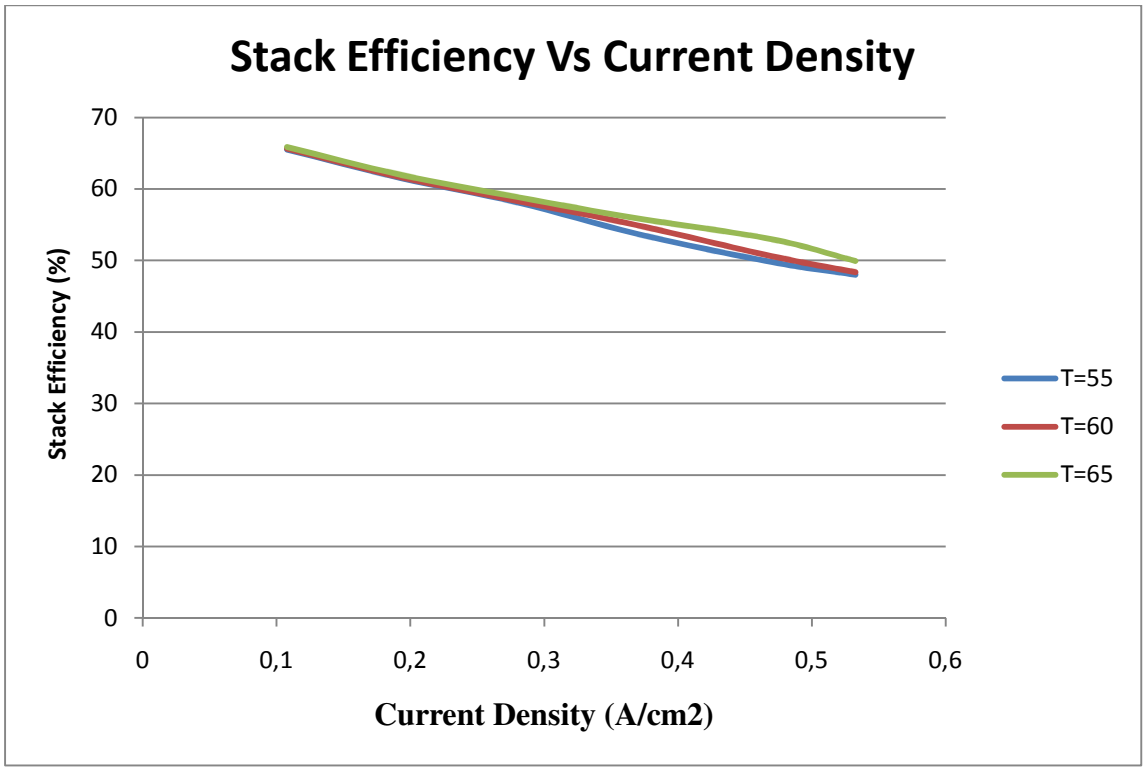

Fig:2 comparison of stack efficiencies at various operating temperatures

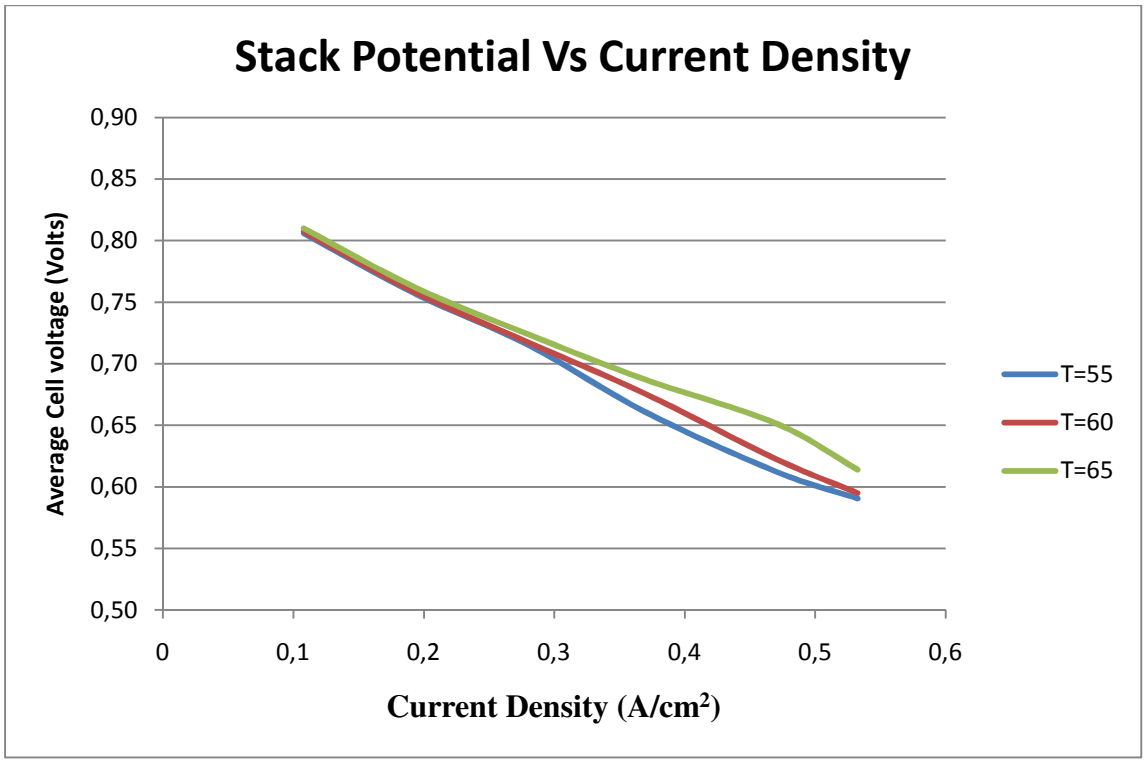

Fig:3 comparison of stack potential at various operating temperatures

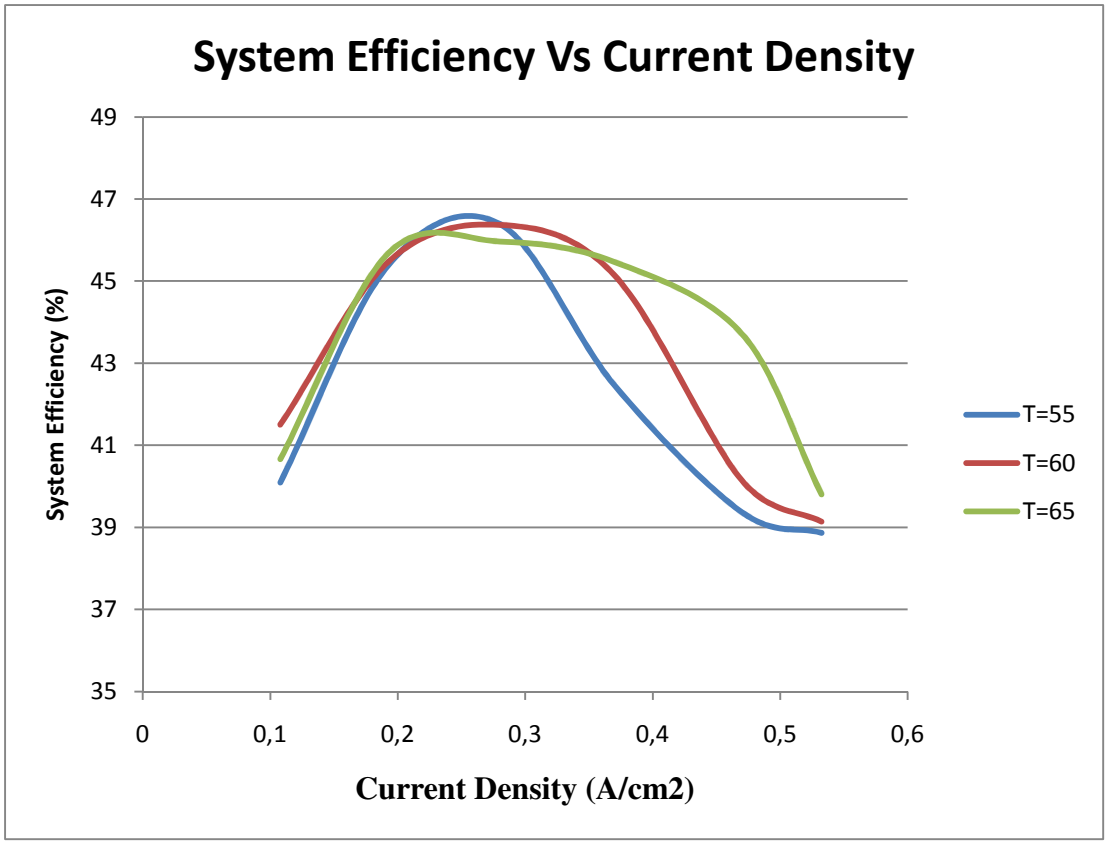

Fig:4 comparison of stack potential at various operating temperatures

Fig: 2 and fig: 3 almost contain the same information. The better performance of the stack is obtained at a temperature of 65˚C. Theoretically cell potential decreases with temperature (3-14). However, in operating fuel cells, in general, a higher cell temperature results in a higher cell potential for the same current generated. This is because the voltage losses in operating fuel cells decrease with temperature, and this more than compensates for the loss of theoretical cell potential. This is the reason that the stack efficiency is more at 65˚C.

In Fig. 3, the overall performance of the GP 300W PEM stack is reported in terms of voltage and electric power as a function of stack current. The voltage versus current diagram represents the polarization curve that describes the stack behavior for different loads. The output voltage decreases from .82 V at to about .58 V at the highest load tested (12 A), while the power increases with current and the highest power value (290 W) corresponds to a current value of 12 A. It can be noted that in all range of load conditions, the voltage is essentially linearly dependent on current, indicating that the voltage drop in this range is derived principally from resistive losses and heat generated.

Figure 4, contains very important information about the complete system. The efficiency of the system first increases and then decreases. The increase in efficiency is due to the fact that at low current densities, power used by the auxiliaries of the system is high compared to the output of the stack. But as the power output of the system increases, the power consumption of the auxiliaries increases in less proportion of the output value. The high efficiency is obtained at the value of 7.5 Amperes. After this value the efficiency of the system again decreases because the decrease in efficiency of the stack becomes dominant and results in overall decrease of system efficiency. Also the system is efficient at the operating temperature of 65˚C. It is because when the system is working at high temperature, less power is required by the cooling system to maintain the temperature.

7.6.2 By varying stoichiometric ratio

The next experiment is performed by maintaining the temperature of the stack constant at 65˚C. In this experiment the stoichiometric ratio (Lam) of the air is changed from 1.5 to 3 with the interval of 0.5. The results of this experiment in terms of graph are described from figure 5 to figure 8.

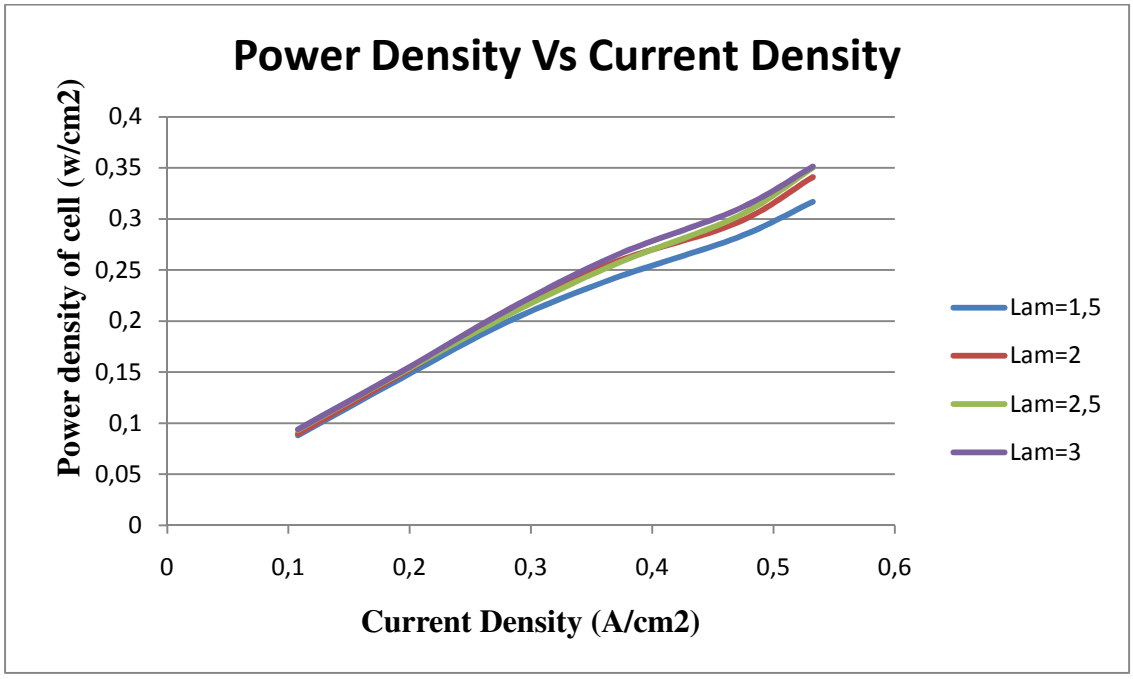

Fig: 5 comparison of power density of stack at various stoichiometric ratios of air

Fig: 5 show that the power density at air stoichiometric ratio of 1,5 is less as compared to the other values of air stoichiometric ratio. Increasing the air stoichiometry from 2.0 to 3.0 has almost no increase in power densities.

With the increase of air stoichiometry, molar flow rate of air increases resulting in the decrease of cathode overpotential and hence gross power produced by the stack increases which results in increase of stack efficiency. Figure: 6 and figure: 7 show that the stack performance has increased when the stoichiometric ratio of air has increased from 1,5 to 2. But increasing the stoichiometry value from 2 to 3 has no significant effects on the performance of the stack.

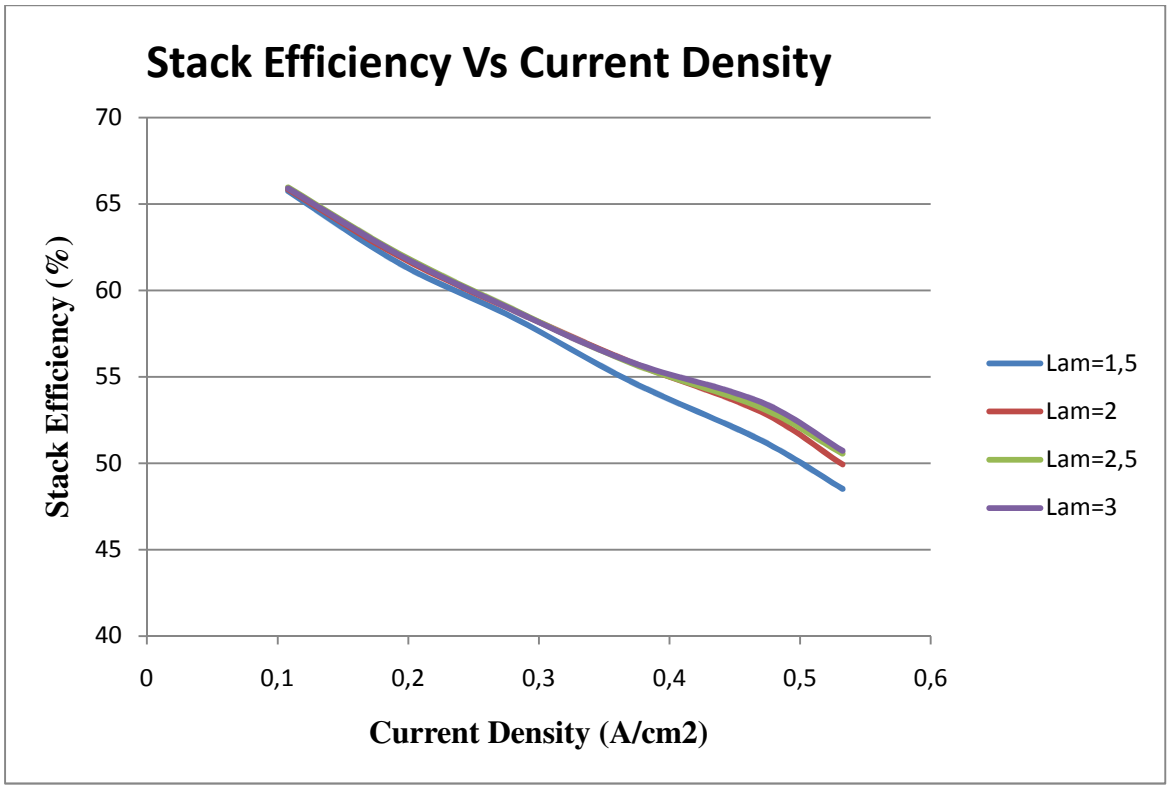

Fig: 6 comparison of stack efficiencies at various stoichiometric ratios of air.

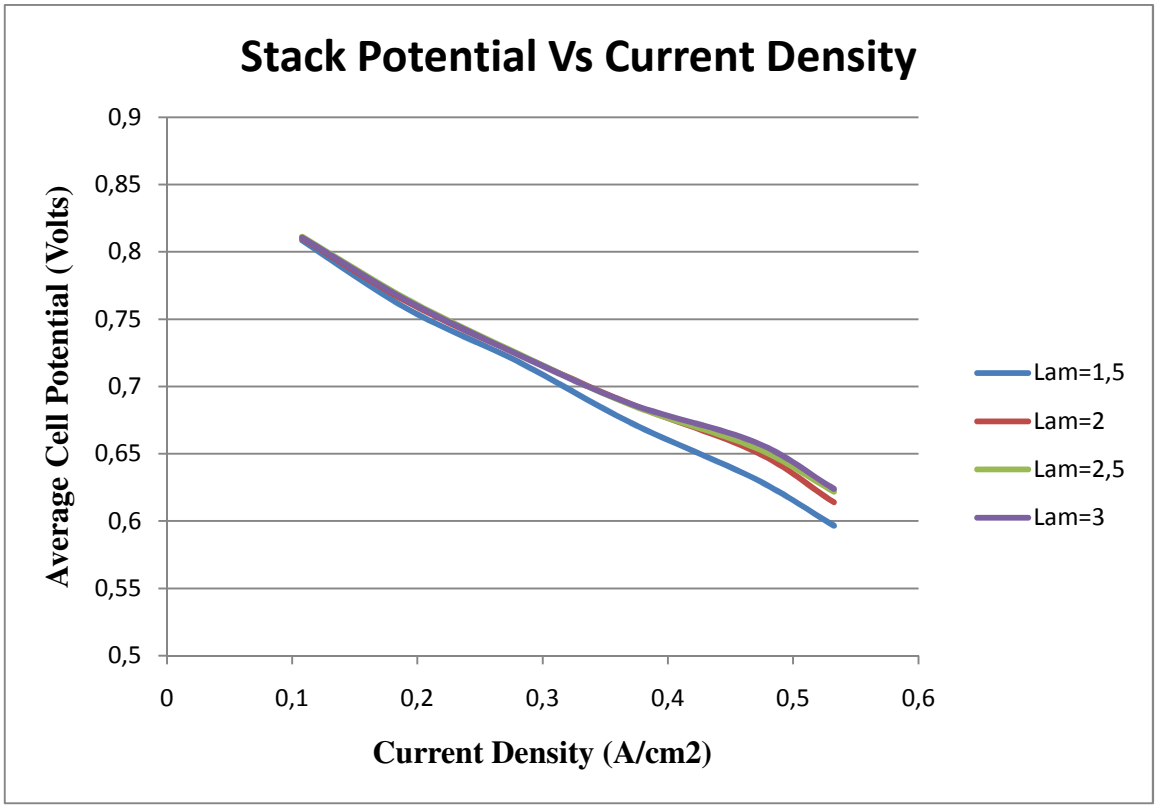

Fig: 7 comparison of stack potential at various stoichiometric ratios of air

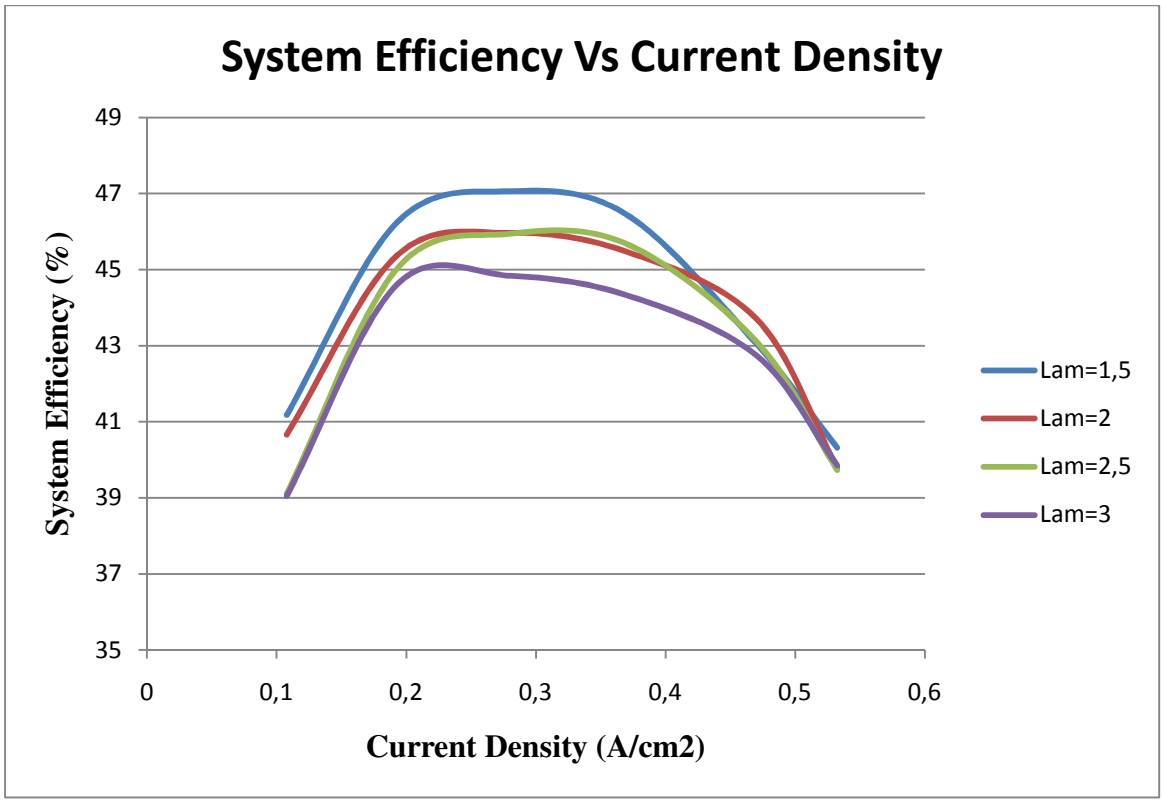

Fig: 8 comparison of system efficiency at various stoichiometric ratios of air

Figure: 8 is showing the efficiency of the fuel cell system at various stoichiometric ratio of air. The better efficiency of the system is achieved at stoichiometric ratio of 1,5 till the current density value of 0.4. This is because the work done by the compressor is less than the work at other stoichiometric ratios. But after that system has shown no effects of changing the stoichiometric ratio. Increasing the air stoichiometry from 2.0 to 3.0 result in decrease of net power produced by the system. This is again due to increase in parasitic load which is offsetting the increase in gross stack power with air stoichiometry, resulting no significant increase in energy and exergy efficiencies with increase in air stoichiometry.

7.7 Conclusion

A performance analysis of a PEM fuel cell power system for portable application has been carried out. In addition, a parametric study is conducted to examine the effect of varying operating conditions on the efficiencies of the system and of the stack. It was found that, with the increase of external load (current density), the best performance of the system is obtained at 65˚C. Both the efficiencies of the system and of the stack increase with the increase of stack operating temperature.

No appreciable increase in efficiency of stack was found with the increase of air stoichiometry beyond 2.0. Although the efficiency of the system is better at air stoichiometry of 1,5 but the power density is better at air stoichiometry of 2,0 than 1,5. Besides stoichiometric of 2.0 is better than 1.5 for to expel water from cathode side in order to avoid flooding of channel. To obtain the better power output from the system, a little compromise on the efficiency of the system can be made and air stoichiometry of 2,0 can be used for the operation of the system. The other reason is that it will improve the concentration of the oxygen.

More useful information can be obtained by considering the power generation and power losses at operating condition of 65˚C and stoichiometric ratio of 2.

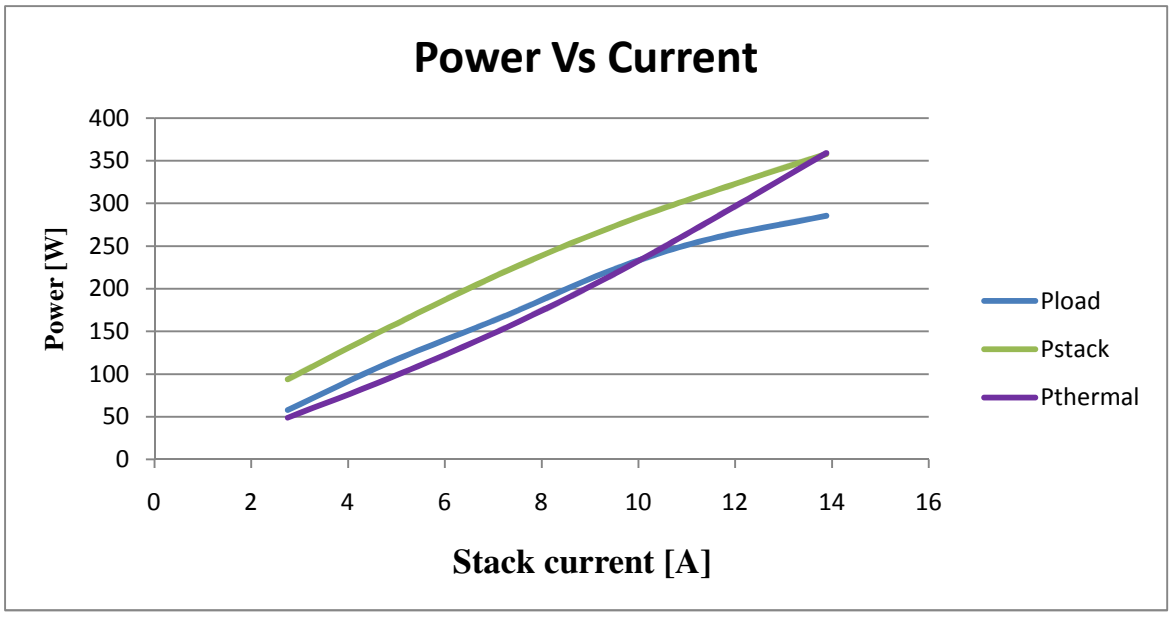

Figure 9: Stack current vs Power

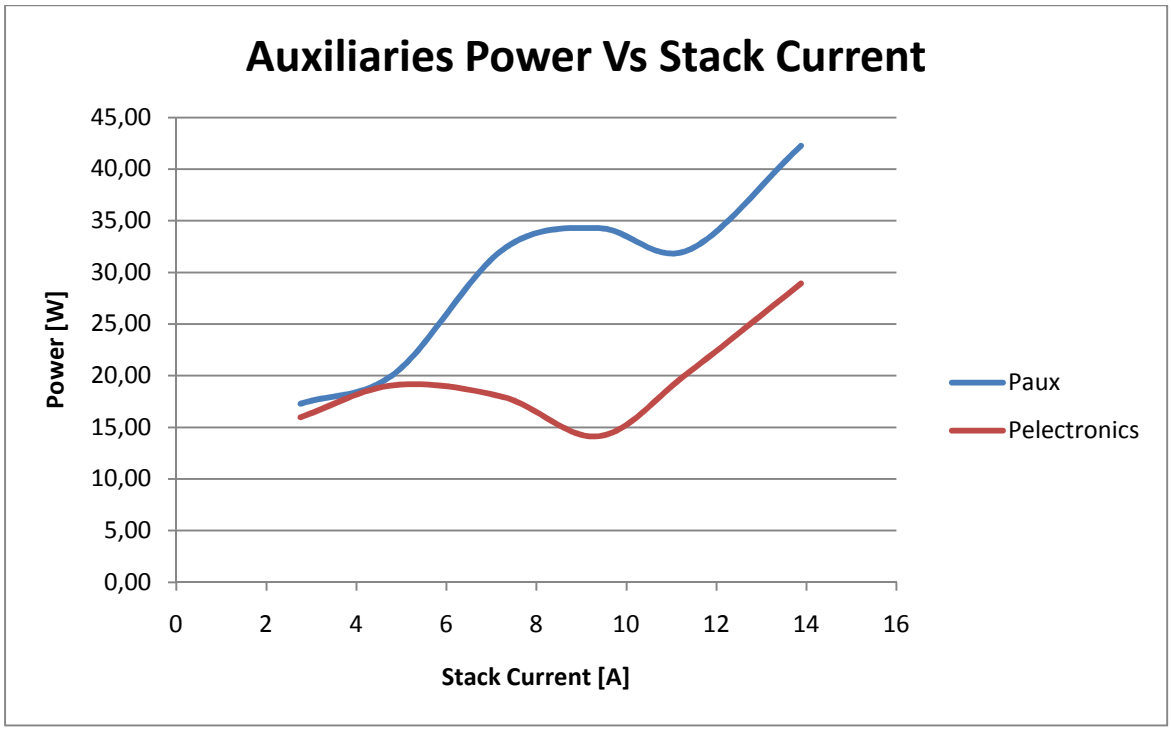

Figure 10: Power consumed by auxiliaries Vs current generated by stack.

Figure 9 shows the Power output of the stack and system and power that is lost in terms of heat energy. It can be seen that power of the stack and of the system increases linearly with stack current and after 10 Amp the power out of stack and system is not linear any more. This decrease is compensated by the increase in loss of thermal energy. And at maximum value of stack current the fifty percent of the fuel energy is wasted in heat energy and remaining is given as stack output power.

Figure 10 shows the power consumed by the control system and the power consumed by auxiliaries (air compressor, pump and fans).

The power required by the air compressor increases with stack output current because the more air has to be supplied to the stack to produce more current. The power consumed by the cooling system increases till the temperature of the stack is maintained at 65˚C at 6 Amp. Then auxiliary power stays constant and shows sudden increase after the stack current is reached at 10 Amp. This is because after this value the heat emitted by the electrochemical reaction increase and the cooling system takes more power in order to maintain the temperature at 65˚C.

The power consumption of electronics system has shown in figure 10. It can be explained by considering the following circuit arrangement.

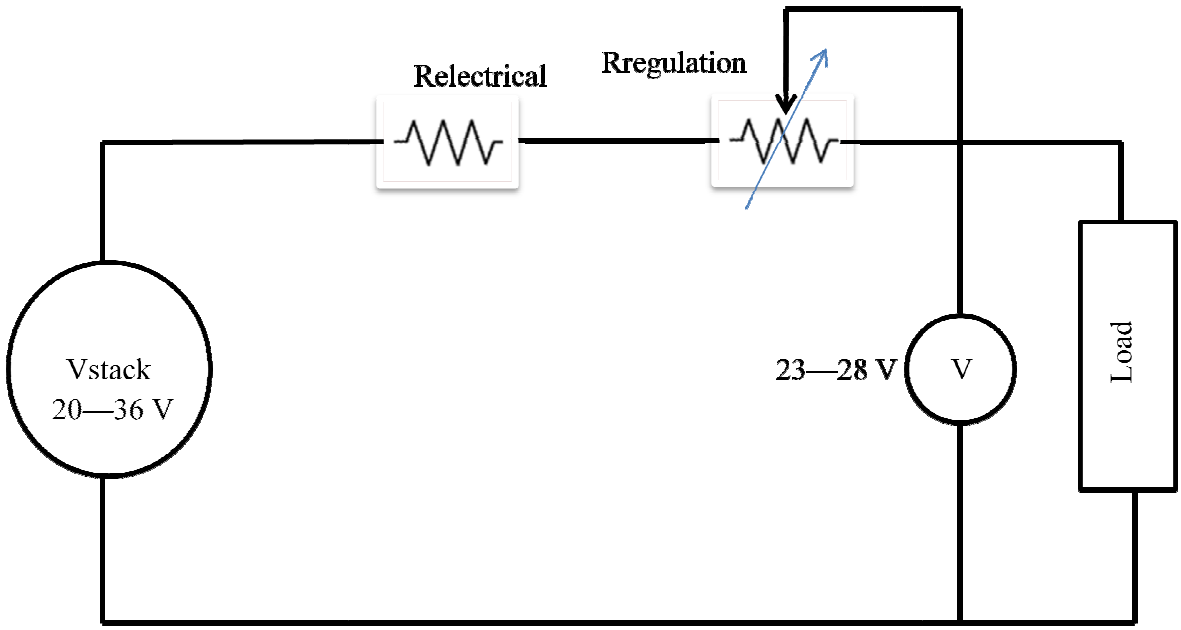

Figure C: Shows the electrical connection of the stack and the control system.

The resistance to regulate the voltage and electrical wiring of the fuel cell system are connected like resistances in series. The voltage of the stack varies 20 to 36Volts but these must be delivered to the load 23 to 28Volts. So the control system regulates these voltages and its resistance increase at lower values of stack current in order to control the voltage in the range of 23—28 volts before supplying to load. This results in power losses in control system. But at high values of current the voltage of the stack itself decrease to value lower than 28Volts. At the high current requested by load correspond parasitic ohmic losses into the circuit load that increase the Power losses due to Joule effect. These kinds of power losses increase with the current and it is possible to see their behavior just when the phenomenon is relevant as the current generated by the system.

References:

[1] M.M. Hussain a, J.J. Baschuka, X. Li a, I. Dincer b, “Thermodynamic analysis of a PEM fuel cell power system.”

[2] Ryan Cownden a, Meyer Nahon a, Marc A. Rosenb “Exergy analysis of a fuel cell power system for transportation applications.”

Section 8

Thermal Balance of Fuel Cell System Using FEM

In this section the discussion will be made on the thermal balance of the Genport 300W Fuel Cell System by using FEM. The 3D cad drawing of the system is shown below in figure 8.1. The detail about working of this system is already given in section 7.

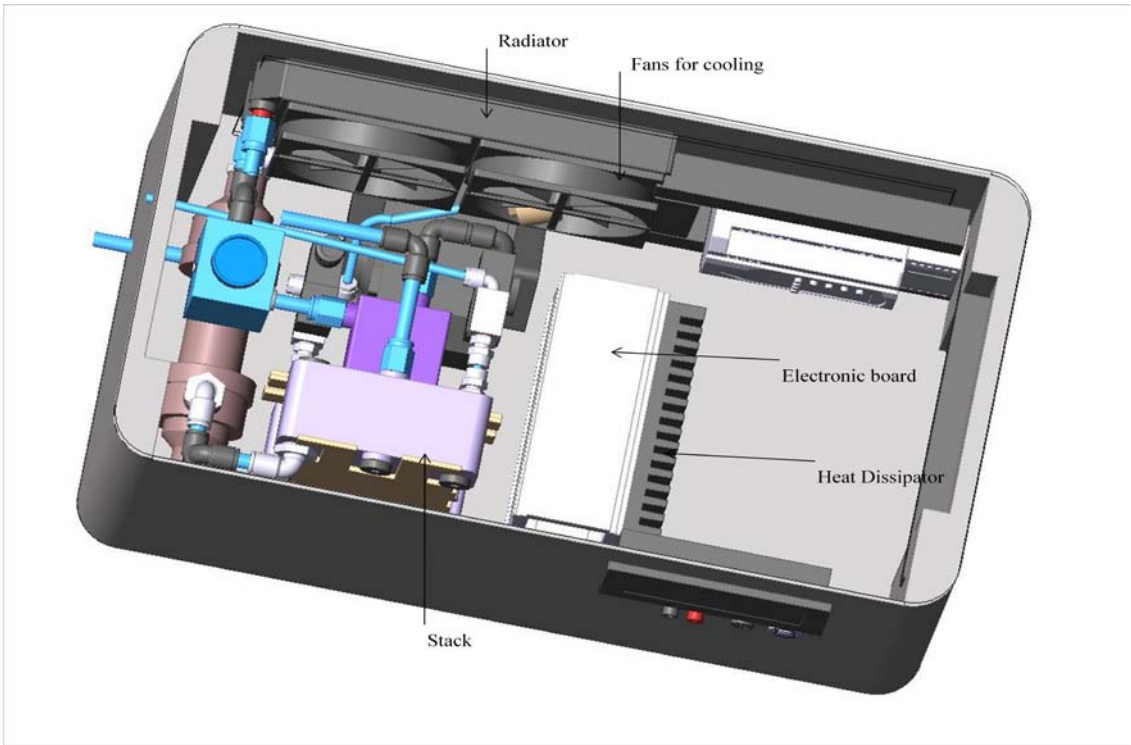

Figure 8.1: Genport 300W Fuel Cell System

8.1 What is Heat Transfer

Heat transfer is defined as the movement of energy due to a difference in temperature. It is characterized by the following three mechanisms:

8.1.1 Conduction

Heat conduction takes place through different mechanisms in different media. Theoretically it takes place in a gas through collisions of the molecules; in a fluid

through oscillations of each molecule in a “cage” formed by its nearest neighbors; in metals mainly by electrons carrying heat and in other solids by molecular motion which in crystals take the form of lattice vibrations known as phonons. Typical for heat conduction is that the heat flux is proportional to the temperature gradient.

8.1.2 Convection

Heat convection (sometimes called heat advection) takes place through the net displacement of a fluid, which transports the heat content in a fluid through the fluid’s own velocity. The term convection (especially convective cooling and convective heating) also refers to the heat dissipation from a solid surface to a fluid, typically described by a heat transfer coefficient.

8.1.3 Radiation

Heat transfer by radiation takes place through the transport of photons, which opaque surfaces can absorb or reflect. Surface-to-ambient radiation treats the ambient surroundings as a black body with known temperature.

In this analysis first two modes of heat transferred are considered only.

8.2 Model definition

The model for this analysis is simplified and the only heat generating components are considered. The model is analyzed in 3D system. As shown in above figure 8.1, the heat generating parts are fuel cell stack, air compressor, radiator and electronic board. All of these components are enclosed in a box which also contains a heat dissipater attached to the electronic board. The model is simplified in such a way that for each of the component like stack, air compressor, electronic board and heat dissipater a separate block has drawn. Each block corresponds to the dimension of each component. The radiator which is just located in front of the exit, and contains the holes for the flow of air is modeled in separate layers placed in front of the exit. All of the heat generating and heat dissipating components are placed in a close box which contains air as a fluid. This box has an inlet and an outlet for the flow of air.

Figure 8-2 shows an equal and simplified model of the GP 300W System made in Comsol Multiphysics.

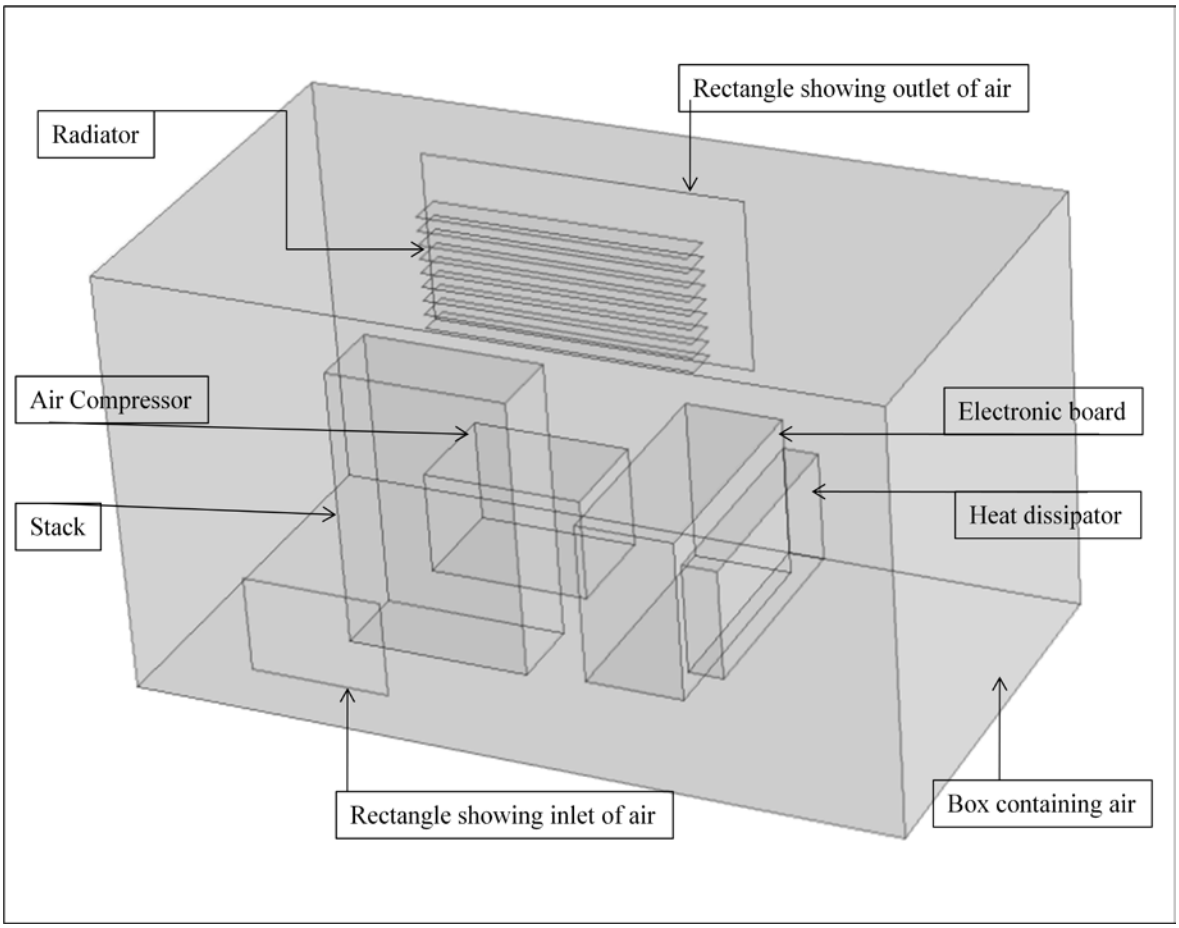

Figure 8-2: Simlified model of GP 300W for comsol

The model is solved using the conjugate heat transfer part of the Comsol Multiphysics 4.0. The air is considered as compressible fluid and the flow is assumed as laminar flow. And then the stationary analysis of the system is performed.

8.3 Definition of geometry

As mentioned above the model consists of a box which contains fuel cell stack, air compressor, radiator, electronic board and the heat dissipater. These all components (except the dissipater that is attached with the electronic board) that are contained in the box generate heat inside the box. The radiator is cooled by forced convection and the flow of air not only removes the heat from radiator but also from the box

which contains the fuel cell system. When the power output is required from the system, air is supplied to the stack through the compressor and hydrogen is also supplied to the stack from the storage vessel. Electrochemical reaction takes place and electricity is generated by stack and heat is produced as a result of the exothermic reaction. To remove the heat from stack, water is supplied by the pump which absorbs the heat from the stack and this water is fed to the radiator. To remove the heat from the radiator, forced convection is made by two fans which are attached just in front of the radiator. The box contains two rectangular holes, one for the inlet and other for the outlet of the air. To optimize the performance of this fuel cell system, a control system is added in the Fuel Cell System and electronic board is also a part of that control system. The heat is imparted by the electronic board in the system and a dissipater is attached to the electronic board to dissipate the heat produced. These are the main components in the box which generate heat. In addition to these, there are some other components like electrovalves which generate heat. But their contribution is very small as compared to the others and can be neglected. The dimensions of each component that are used for modeling the system are given in table 8.1below.

Table 8.1: Dimensions and position of each component of FC System.

	Dimentions			Position		
Component	Length (mm)	Width (mm)	Height (mm)	X (mm)	Y (mm)	Z (mm)
Box	550	300	290	0	0	0
Stack	130	55	190	130	60	25
Air Compressor	115	75	70	140	160	25
Electronic Board	70	170	110	300	65	25
Heat Dissipater	25	160	75	370	70	42.5
Radiator	200	25	9 layers	80	265	150

			spaced by 10 mm			

The boundary conditions that are applied are shown in table 8.2.

Table 8.2: Parameters used as boundary condition for the Computation

Boundary Condition	Value
Temperature of Stack	327 K
Temperature of Air compressor	323 K
Temperature of Electronic Board	317 K
Temperature of Radiator	317 K
Ambient Temperature	296 K
Flow rate at exit	.052 m^3/sec

Before going into the detail of the analysis, some features and equations of the Comsol Multiphysics 4.0 that are used for solving this model are discussed below.

8.4 The Heat Equation

The fundamental law governing all heat transfer is the first law of thermodynamics, commonly referred to as the principle of conservation of energy. However, internal energy, U, is a rather inconvenient quantity to measure and use in simulations. Therefore, the basic law is usually rewritten in terms of temperature, T. For a fluid, the resulting heat equation is:

$$\rho C_p \left(\frac{\partial T}{\partial t} + (u.\nabla)T\right) = -(\nabla.q) + \tau : S - \frac{T}{\rho}\frac{\partial p}{\partial T}\Big|_p \left(\frac{\partial p}{\partial t} + (u.\nabla)p\right) + Q \qquad (8\text{-}1)$$

Where

- ρ is the density (SI unit: kg/m3)
- Cp is the specific heat capacity at constant pressure (SI unit: J/(kg•K))

- T is absolute temperature (SI unit: K)
- u is the velocity vector (SI unit: m/s)
- q is the heat flux by conduction (SI unit: W/m2)
- p is pressure (SI unit: Pa)
- τ is the viscous stress tensor (SI unit: Pa)
- S is the strain rate tensor (SI unit: 1/s):

$$S = \frac{1}{2}(\nabla u + (\nabla u)^T)$$

- Q contains heat sources other than viscous heating (SI unit: W/m^3)

In deriving Equation 8-1, a number of thermodynamic relations have been used. The equation also assumes that mass is always conserved, which means that density and velocity must be related through:

$$\frac{\partial \rho}{\partial t} + \nabla.(\rho u) = 0 \qquad (8\text{-}2)$$

The heat transfer interfaces use Fourier's law of conduction, which states that the conductive heat flux, q, is proportional to the temperature gradient:

$$q_i = -k\frac{\partial T}{\partial x_i} \qquad (8\text{-}3)$$

Where k is the thermal conductivity (SI unit: W/(m·K)). In a solid, the thermal conductivity can be anisotropic (that is, it has different values in different directions). Then k becomes a tensor

$$k = \begin{bmatrix} k_{xx} & k_{xy} & k_{xz} \\ k_{yx} & k_{yy} & k_{yz} \\ k_{zx} & k_{zy} & k_{zz} \end{bmatrix} \qquad (8\text{-}4)$$

and the conductive heat flux is given by

$$q_i = -\sum_j k_{ij}\frac{\partial T}{\partial x_j} \qquad (8\text{-}5)$$

The second term on the right of Equation 8-1 represents viscous heating of a fluid. An analogous term arises from the internal viscous damping of a solid. The operation ":" is a contraction and can in this case be written on the following form:

$$a{:}\, b = \sum_n \sum_m a_{nm} b_{nm} \tag{8-6}$$

The third term represents pressure work and is responsible for the heating of a fluid under adiabatic compression and for some thermo-acoustic effects. It is generally small for low Mach number flows. A similar term can be included to account for thermo-elastic effects in solids.

Inserting Equation 8-2 into Equation 8-1, reordering the terms and ignoring viscous heating and pressure work puts the heat equation on a perhaps more familiar form:

$$\rho C_p \frac{\partial T}{\partial t} + \rho C_p \mathrm{u}\nabla \mathrm{T} = \nabla(\mathrm{k}\nabla \mathrm{T}) + Q \tag{8-7}$$

The Heat Transfer interface with the Fluid feature (using the Heat Transfer in Fluids entry point) solves this equation for the temperature, T. If the velocity is set to zero, you get the equation governing pure conductive heat transfer in a solid:

$$\rho C_p \frac{\partial T}{\partial t} + \nabla.\,(-\mathrm{k}\nabla \mathrm{T}) = Q \tag{8-8}$$

Heat is not a conserved property. The conserved property is instead the total energy. There is hence heat flux and energy flux which are similar, but not identical.

8.5 The Navier-Stokes Equations

The single-phase fluid-flow interfaces described in this section are based on the Navier-Stokes equations, which in their most general form read

$$\frac{\partial \rho}{\partial t} + \nabla.\,(\rho u) = 0 \tag{8-9}$$

$$\rho \frac{\partial u}{\partial t} + \rho(u.\nabla)u = \nabla.\,[-pI + \tau] + F \tag{8-10}$$

$$\rho C_p \left(\frac{\partial T}{\partial t} + (u.\nabla)T\right) = -(\nabla.q) + \tau : S - \frac{T}{\rho}\frac{\partial p}{\partial T}\Big|_p \left(\frac{\partial p}{\partial t} + (u.\nabla)p\right) + Q \qquad (8\text{-}11)$$

Where

- ρ is the density (SI unit: kg/m3)
- u is the velocity vector (SI unit: m/s)
- p is pressure (SI unit: Pa)
- τ is the viscous stress tensor (SI unit: Pa)
- F is the volume force vector (SI unit: N/m3)
- Cp is the specific heat capacity at constant pressure (SI unit: J/(kg·K))
- T is the absolute temperature (SI unit: K)
- q is the heat flux vector (SI unit: W/m2)
- Q contains the heat sources (SI unit: W/m3)
- S is the strain rate tensor:

$$S = \frac{1}{2}(\nabla u + (\nabla u)^T)$$

The operation ":" denotes a contraction between tensors defined by

$$a : b = \sum_n \sum_m a_{nm} b_{nm} \qquad (8\text{-}6)$$

Equation 8-9 is the continuity equation and represents the conservation of mass. Equation 8-10 is a vector equation and represents the conservation of momentum. Equation 8-11 describes the conservation of energy, formulated in terms of temperature. This is an intuitive formulation that facilities specification of boundary conditions.

To close the equation system 8-9 through 8-11, some constitutive relations are needed. A common relation is derived by assuming that the fluid is Newtonian. Together with Stokes' assumption, the viscous stress tensor becomes:

$$\tau = 2\mu S - \frac{2}{3}\eta(\nabla.u)\mathrm{I} \qquad (8\text{-}12)$$

The dynamic viscosity μ (SI unit: Pa·s) is allowed to depend on the thermodynamic state but not on the velocity field. All gases and many liquids can be considered Newtonian. Examples of non-Newtonian fluids are honey, mud, blood, liquid metals, and most polymer solutions. Air that is the only fluid present in this analysis is also assumed as Newtonian fluid.

Other commonly used constitutive relations are Fourier's law of conduction and the ideal gas law.

8.6 Compressible Flow

The Navier-Stokes equations solved by default in all single-phase flow interfaces are the compressible formulation of the continuity:

$$\frac{\partial \rho}{\partial t} + \nabla.(\rho u) = 0 \qquad (8\text{-}13)$$

and the momentum equations:

$$\rho \frac{\partial u}{\partial t} + \rho u.\nabla u = -\nabla p + \nabla \left[\mu(\nabla u + (\nabla u)^T) - \frac{2}{3}\mu(\nabla.u)\mathrm{I}\right] + F \qquad (8\text{-}14)$$

These equations hold for incompressible as well as compressible flows where the density varies.

8.7 Laminar Outflow Condition

In order to prescribe an outlet velocity profile, this boundary conditions adds a weak form contribution corresponding to a one-dimensional Navier-Stokes equations projected on the boundary. The applied condition corresponds to the situation shown in Figure 8-3: assume that a fictitious domain of length L_{exit} is attached to the outlet of the computational domain. This boundary condition uses the assumption that the flow in this fictitious domain is laminar plug flow. If you select the option that constrains outer edges or endpoints to zero, the assumption is instead that the flow in the fictitious domain is fully developed laminar channel flow (in 2D) or fully developed laminar internal flow (in 3D). This does not affect the boundary

condition in the real domain, Ω, where the boundary conditions are always fulfilled.

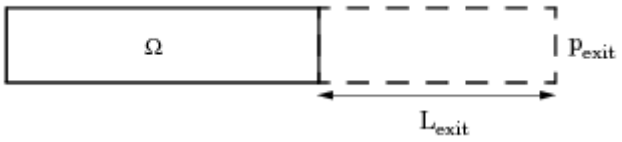

Figure 8-3: Sketch of the physical situation simulated when using Laminar outflow boundary condition. Ω is the actual computational domain while the dashed domain is a fictitious domain.

If you specify an average outlet velocity or outlet volume flow instead of the pressure, the software adds an ODE that calculates p_{exit} such that the desired outlet velocity or volume flow is obtained.

8.8 Solution of the Model

The Conjugate Heat Transfer interface is a predefined multiphysics coupling consisting of a single-phase flow interface, using a compressible formulation, in combination with a Heat Transfer interface is applied. When Conjugate Heat Transfer interface for laminar flow is added, it creates the Conjugate Heat Transfer node with default Heat Transfer in Solids, Wall, and Thermal Insulation nodes added. There is also a default Initial Values node added. Other featured nodes like boundary conditions, Fluid and volume force can be added as required.

8.8.1 Heat Transfer in Solids

The Heat Transfer in Solids node uses the following version of the heat equation as the mathematical model for heat transfer in solids:

$$\rho C_p \frac{\partial T}{\partial t} - \nabla.(k\Delta T) = Q \qquad (8\text{-}15)$$

with the following material properties:

- ρ is the density.
- Cp is the heat capacity.

- k is the thermal conductivity (a scalar or a tensor if the thermal conductivity is anisotropic).
- Q is the heat source (or sink). You can add one or several heat sources as separate features.

For a steady-state problem the temperature does not change with time and the first term disappears.

8.8.2 Fluid

The node 'fluid' is added on the box whose material is specified as air. The Fluid feature adds both the momentum equations and the temperature equation but without volume forces, heat sources, pressure work or viscous heating. The thermal conductivity of the material is defined and the thermal conductivity *k* describes the relationship between the heat flux vector **q** and the temperature gradient ∇T as in

$$q = -k\Delta T \qquad (8\text{-}16)$$

which is *Fourier's law of heat conduction*.

Further specified properties are the density, the heat capacity at constant pressure, and the ratio of specific heats for air.

8.8.3 Inlet

Another feature 'inlet' is added to describe the fluid flow condition at an inlet. As the fans are installed at the exit so the boundary condition for inlet selected is '*Pressure, No Viscous Stress'*

This boundary condition specifies vanishing viscous stress along with a Dirichlet condition on the pressure:

$$\left[\mu(\nabla u + (\nabla u)^T) - \frac{2}{3}\mu(\nabla . u)\mathrm{I}\right] n = 0 \qquad p = p_0 \qquad (8\text{-}17)$$

using the compressible formulation.

Zero pressure at the boundary (SI unit: Pa) in the p_0 edit field is entered.

This boundary condition is physically equivalent to a boundary that is adjacent to a large container. It is numerically stable and admits total control of the pressure level along the entire inlet boundary.

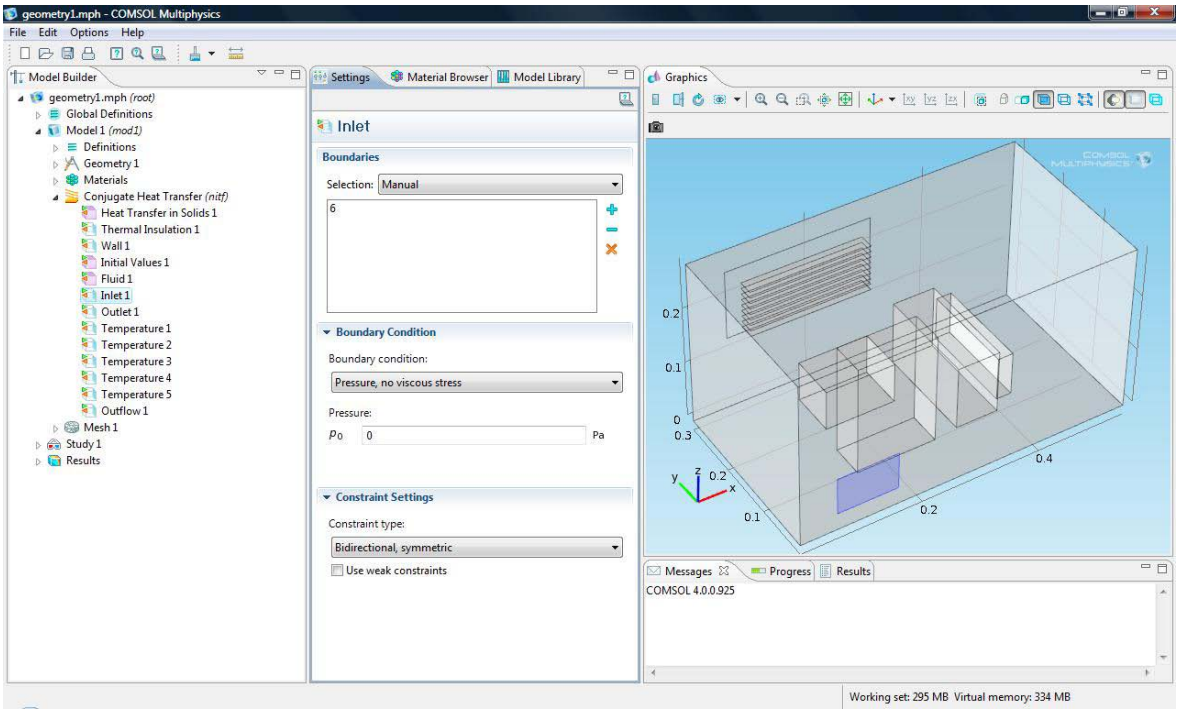

Figure 8-4: showing the boundary at which inlet node is applied

8.8.4 Outlet

The next feature that is added is the 'outlet' which includes a set of boundary conditions describing fluid flow conditions at an outlet. And the boundary condition that is applies is *Laminar Outflow*

This boundary prescribes a laminar velocity profiles using the implementation described in "Laminar Outflow Condition".

The flow rate V0 (.053: m3/s) through the outlet which is the flow rate of the fans installed in GP 300W Fuel Cell System is applied at the outlet boundary condition.

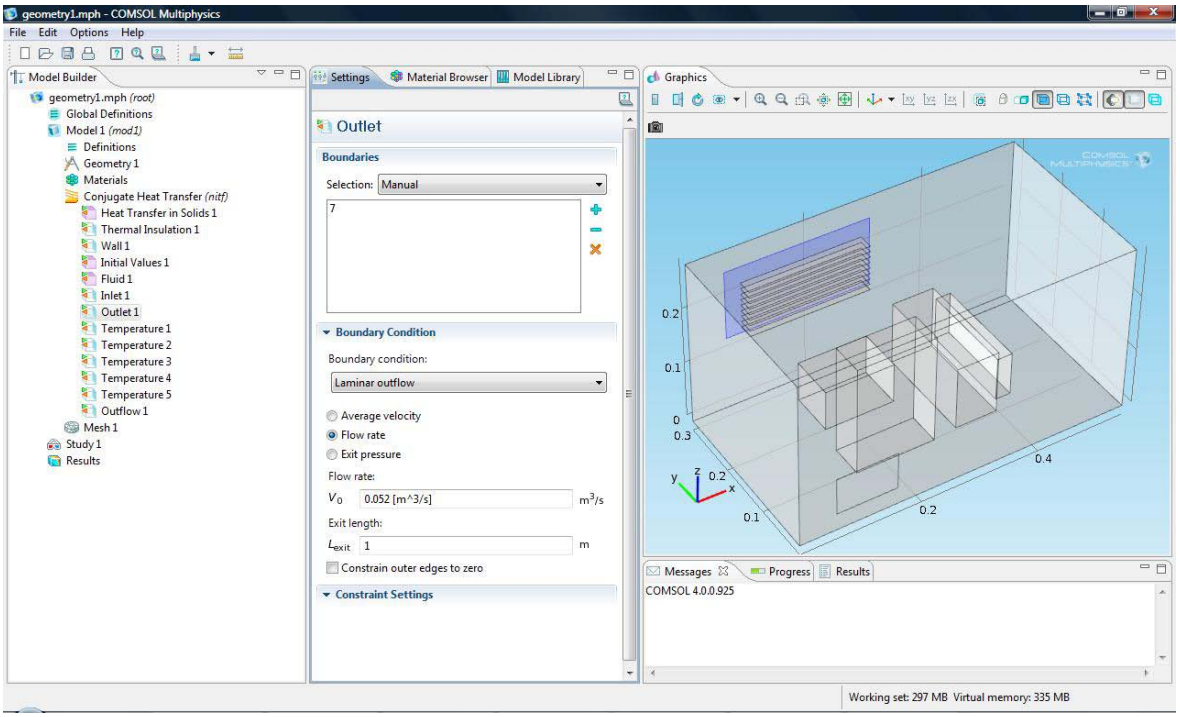

Figure 8-5: showing the boundary at which inlet node is applied

8.8.5 Temperatures

Another feature that is added is the temperature. The Temperature feature node prescribes a temperature on a boundary.

The Temperature boundary condition is applied on stack, electronic board, radiator, inlet boundary of air and the air compressor. And for each component the value of the corresponding temperature is entered. All the temperature values of the components were practically measured. The temperature values for each component are mentioned above in the table 8-2.

The equation for this condition is

$$T = T_0$$

where T_0 is the prescribed temperature (SI unit: K) on the boundary.

8.8.6 Outflow

The Outflow node is applied at the outlet boundary. The Outflow feature node provides a suitable boundary condition for convection-dominated heat transfer at outlet boundaries. In a model with convective heat transfer, this condition states that the only heat transfer over a boundary is by convection. The temperature gradient in the normal direction is zero, and there is no radiation. This is usually a good approximation of the conditions at an outlet boundary in a heat transfer model with fluid flow.

The Outflow node does not require any user input.

8.8.7 Creating Meshes

A mesh is a discretization of the geometry model into small units of simple shapes, referred to as *mesh elements*.

The mesh generator discretizes the domains into tetrahedral, hexahedral, or prism mesh elements whose faces, edges, and corners are called mesh faces, mesh edges, and mesh vertices, respectively.

The boundaries in the geometry are discretized into triangular or quadrilateral boundary elements.

The geometry edges are discretized into edge elements.

In this case the normal mesh size is used for the objects inside the box and the fine mesh size is used at the boundaries of the box. The free tetrahedral mesh is applied.

The meshed model is shown in the figure 8-6.

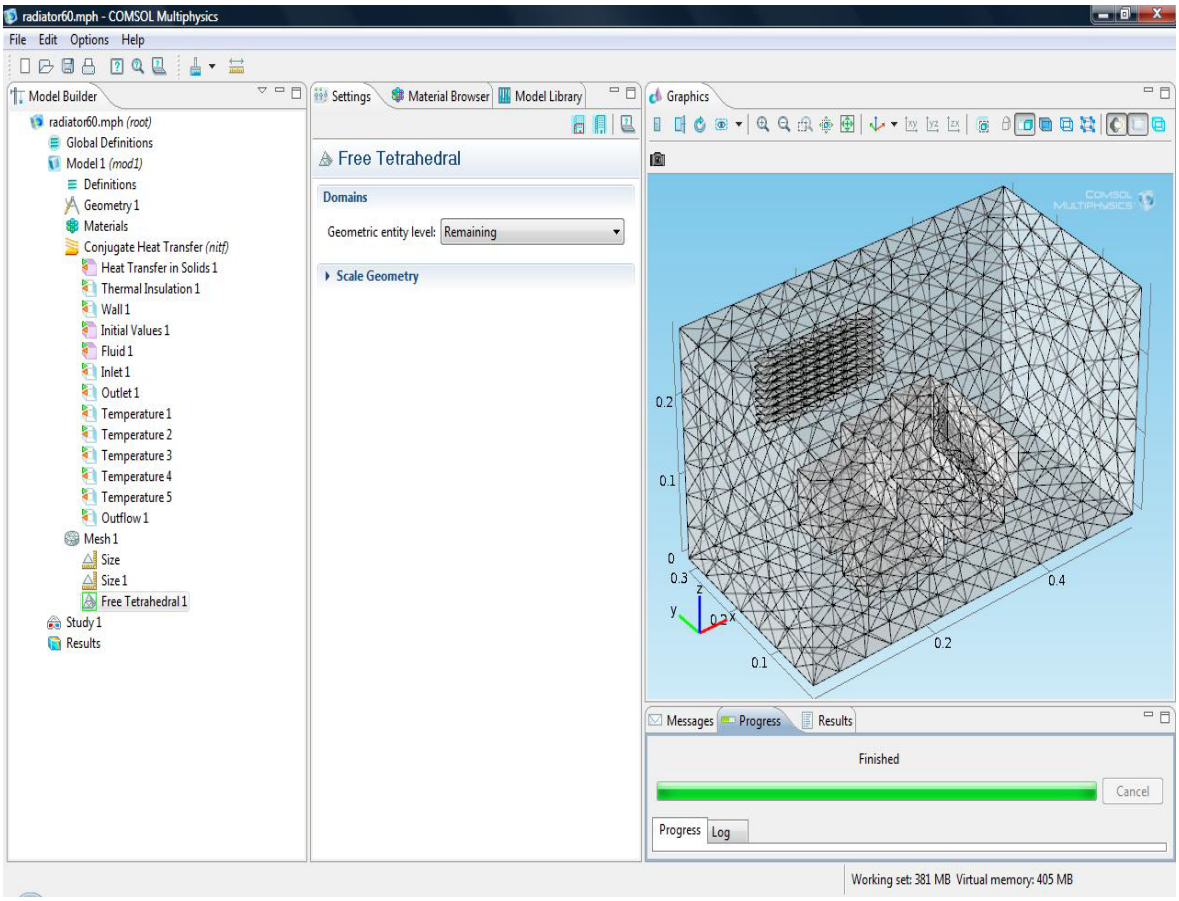

Figure 8-6: The free tetrahydral mesh is applied on the model.

8.8.8 Computing the solution

To compute the solution of the model the stationary study is used. A Stationary study node corresponds to a stationary solver (default) or a parametric solver. The Stationary study generates a solver sequence that is used to solve a stationary problem. Then the solver sequence is generated from the study in which fully coupled solution feature attribute is used. This attribute uses a damped version of Newton's method and is used together with the Stationary operation features. Here the maximum numbers of iterations were increased to 50 because the model to solve was too big and the defualt maximum numbers of iterations are not sufficient to make the solution. After the solution is computed several plots can be made to analyse the results.

8.9 Results and Discussions

The results obtained from this computation are summarized in the following figure 8-7:

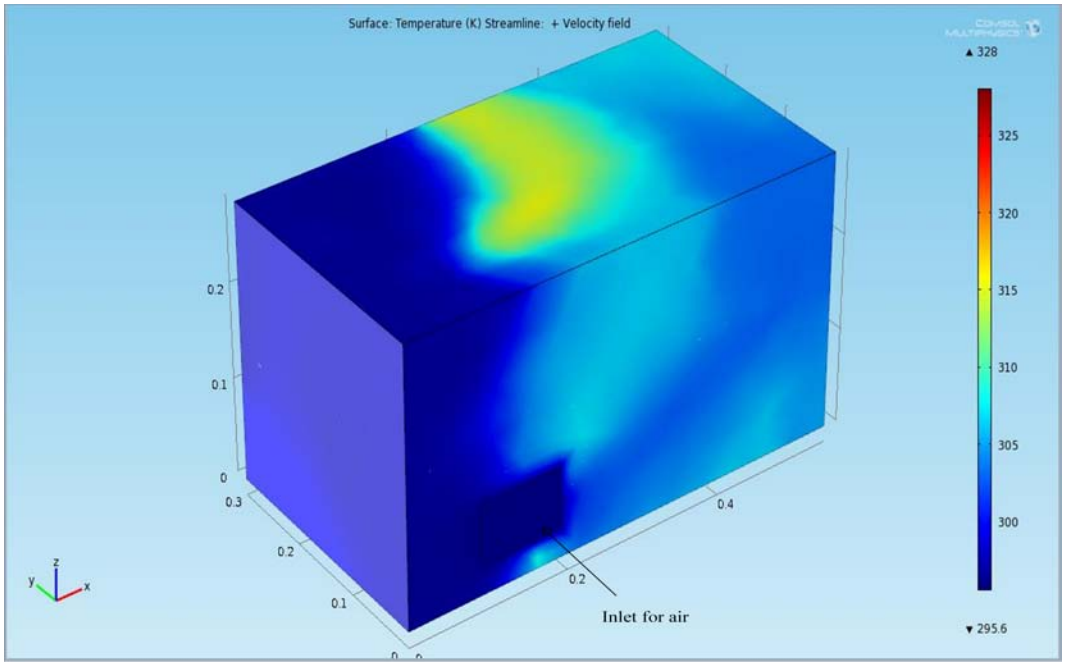

Figure 8-7a: Temperature distribution of the box containing FC System

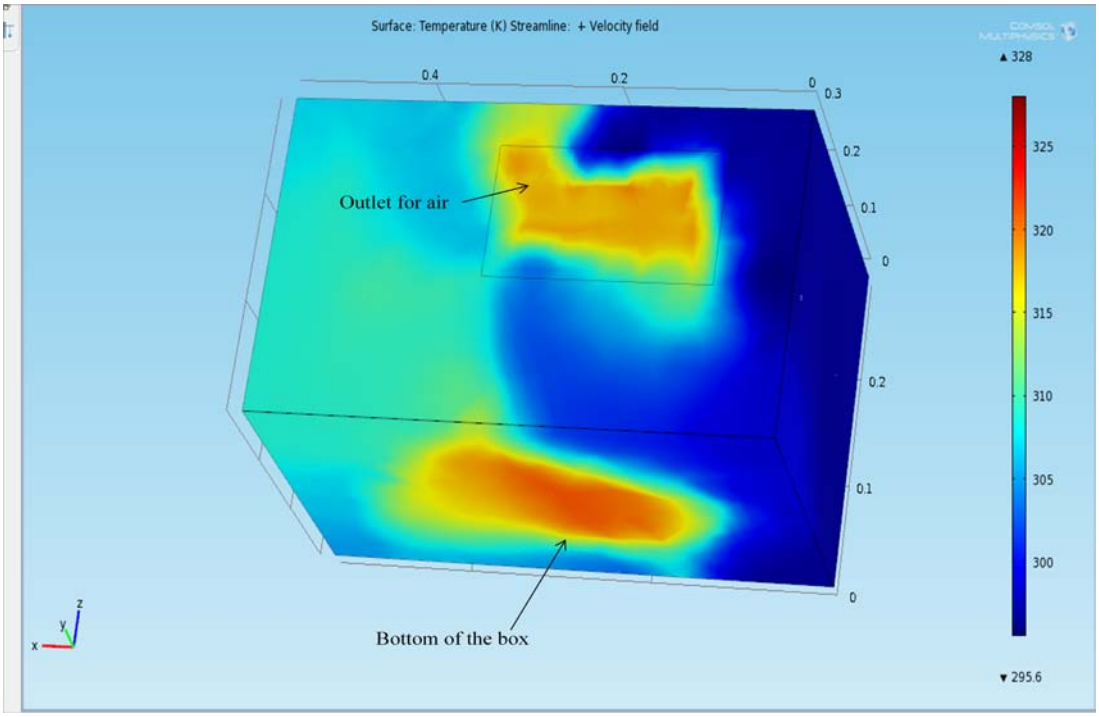

Figure 8-7b: Temperature distribution of the box containing FC System

Figure 8-7a shows the temperature distribution at the surface of the box, if viewed from inlet and figure 8-7b shows the temperature distribution, if viewed from outlet. The temperature of the air leaving the system was 319 [K] but the radiator usually have the average temperature of 318 [k]. If the air will be at temperature of 319 [K], it will not absorb the heat from the radiator effectively. The reason for the high temperature of the inlet is that the inlet of the air is just located in front of the stack and the temperature of the stack is 327[K]. So when the air enters in the Fuel Cell System it gets heat from stack and the temperature of the air increases. This can be clearly seen from the following figure 8-8.

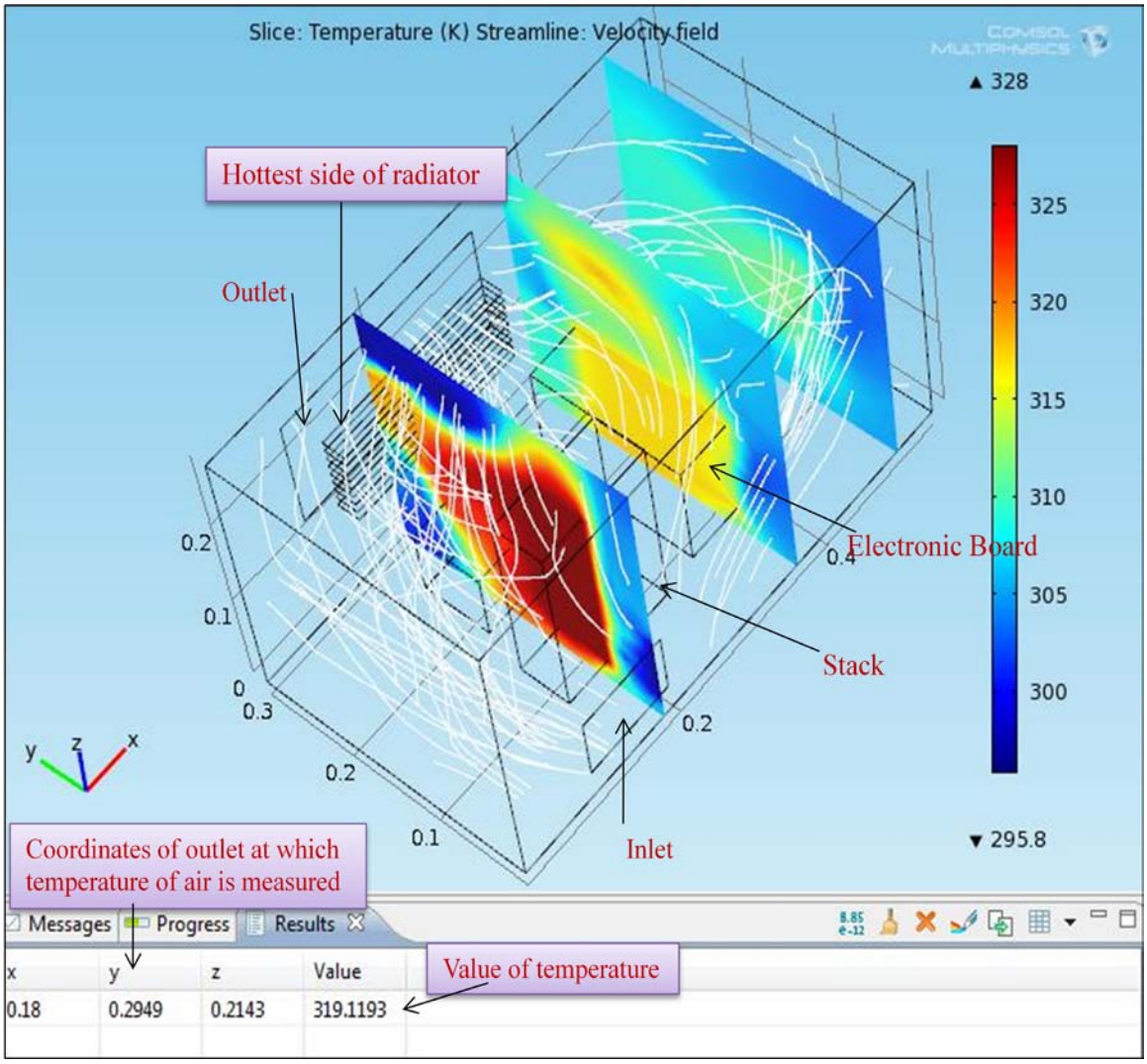

Figure 8-8: Slice plot of the system at different cross sections.

Figure 8-8: Shows the slice plot of the cross section of the fuel cell system in which white lines represent the velocity field of the air. Hottest part of the radiator is also

mentioned in this figure. It can be seen that the stack is between the inlet of air and the high temperature point of the radiator. After entering into the system, air first absorbs the heat from stack which increases the temperature of the air to the extent which is not suitable for the cooling of the radiator. This inlet or stack position is not suitable for the cooling system to work efficiently. The position of the stack cannot be changed but it is possible to change the position of the inlet. The computation with same configuration of the system was performed at low operating temperature of the stack. The stack temperature was at 318 K and 323 K and the outlet air temperature was found almost the same as the temperature of the radiator (shown in figure: 8-9 and Figure8-10) which shows this air inlet position is not a problem for the performance of the cooling system. But for the high operating temperature which is 338K inside the stack and suitable for the efficiency of the system this air inlet position is not suitable.

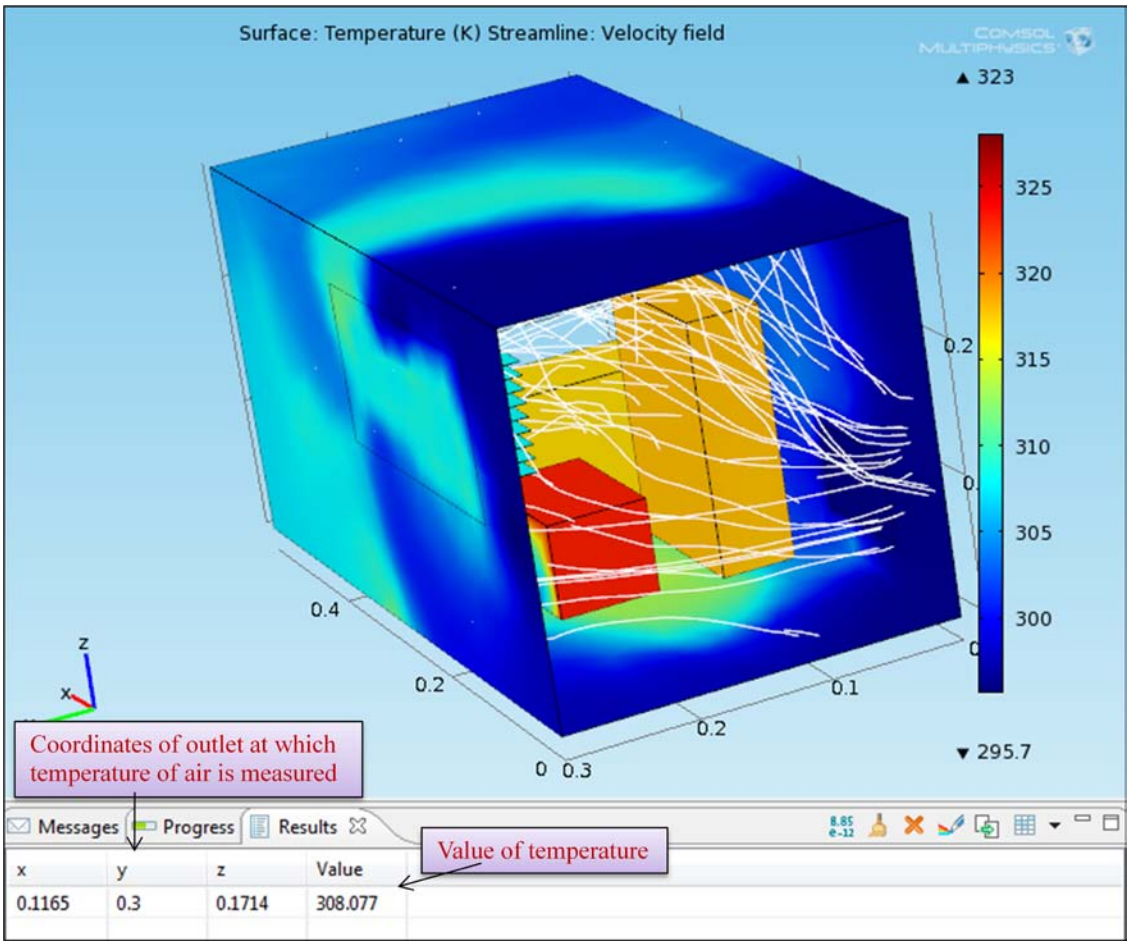

Figure 8-9: Stack temperature 318K and radiator temperature 308K.

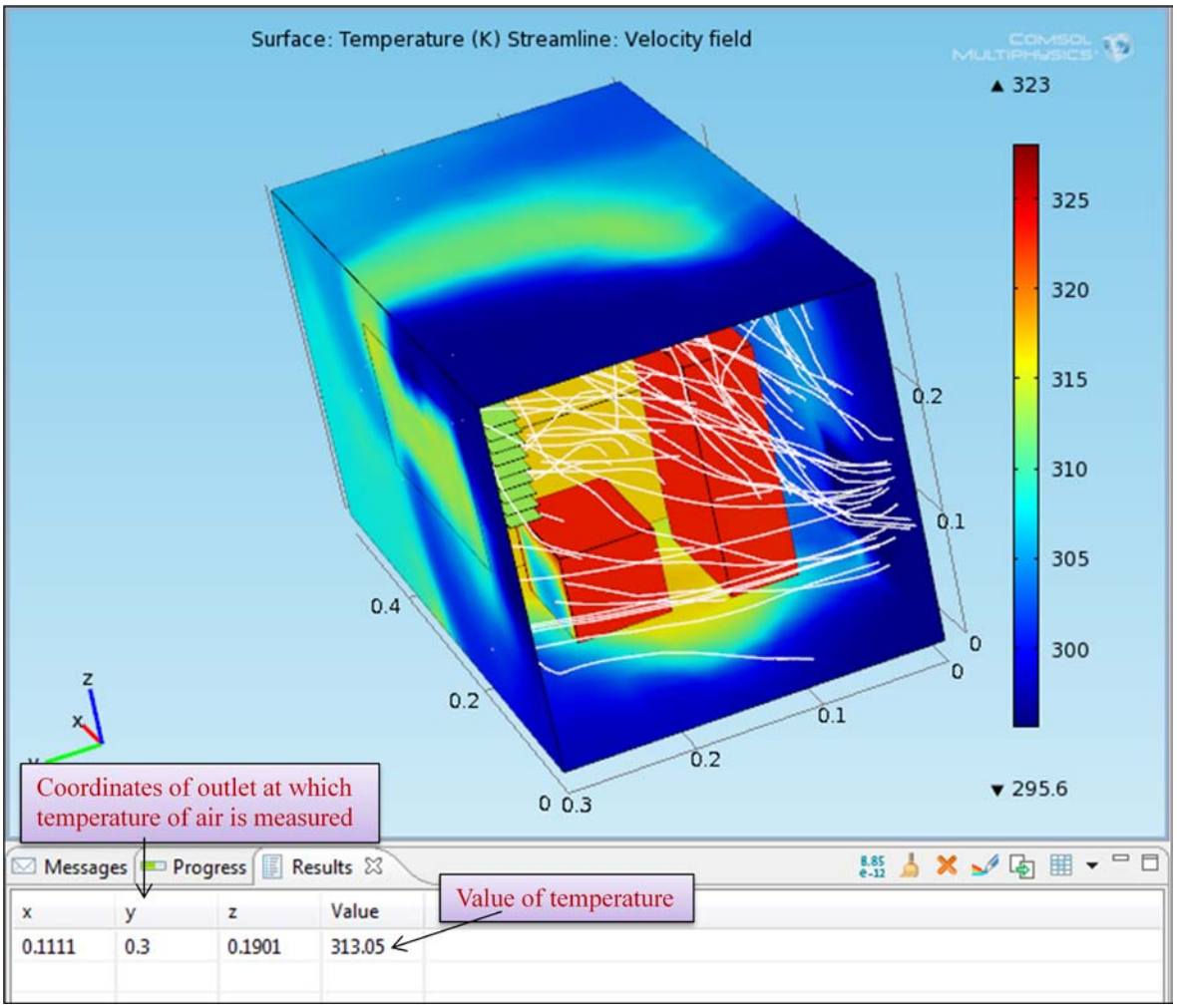

Figure 8-10: Stack temperature 323K and radiator temperature 313K.

Next possible solution is analyzed by changing the possible position of the inlet. For this computation the inlet position is considered parallel to the y-axis in the yz-plane as shown in the following figure 8-11.

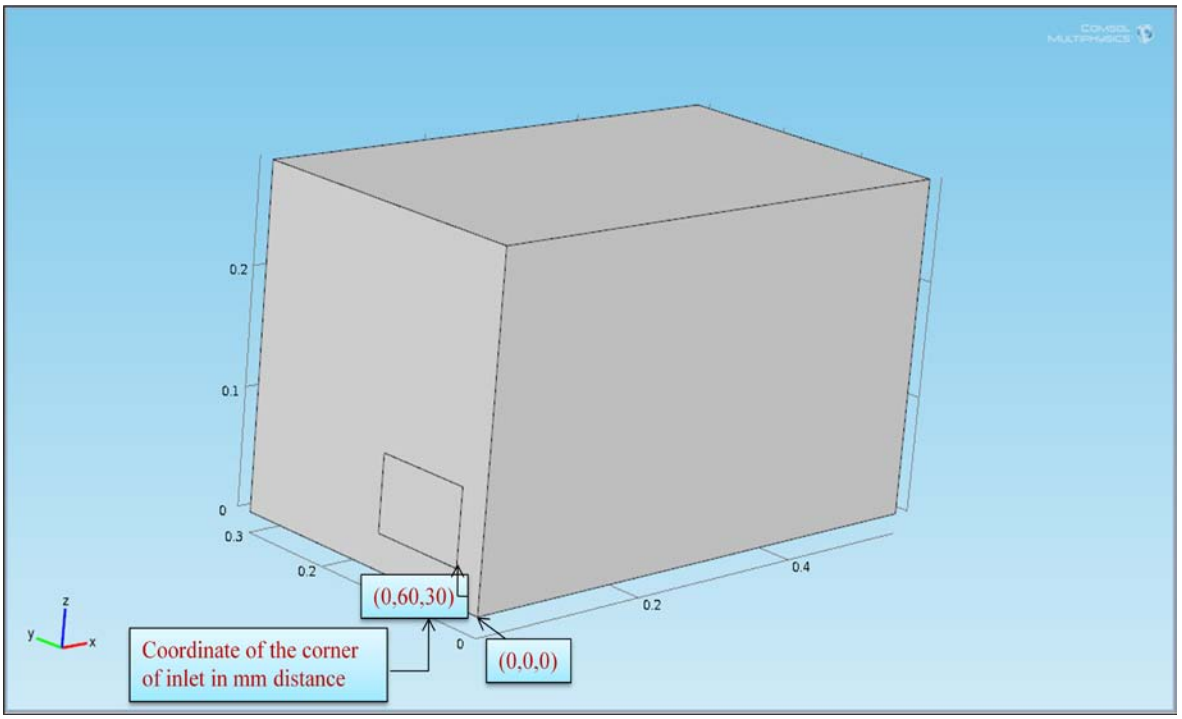

Figure 8-11: New position for the inlet air with coordinates

Figure 8-11 shows the new position for the air inlet in yz-plane. The corner that is pointed out in the figure has y-coordinate 60mm, z-coordinate 30mm and the x-coordinate is zero.

The computation for this possible configuration has been performed and the following results were obtained.

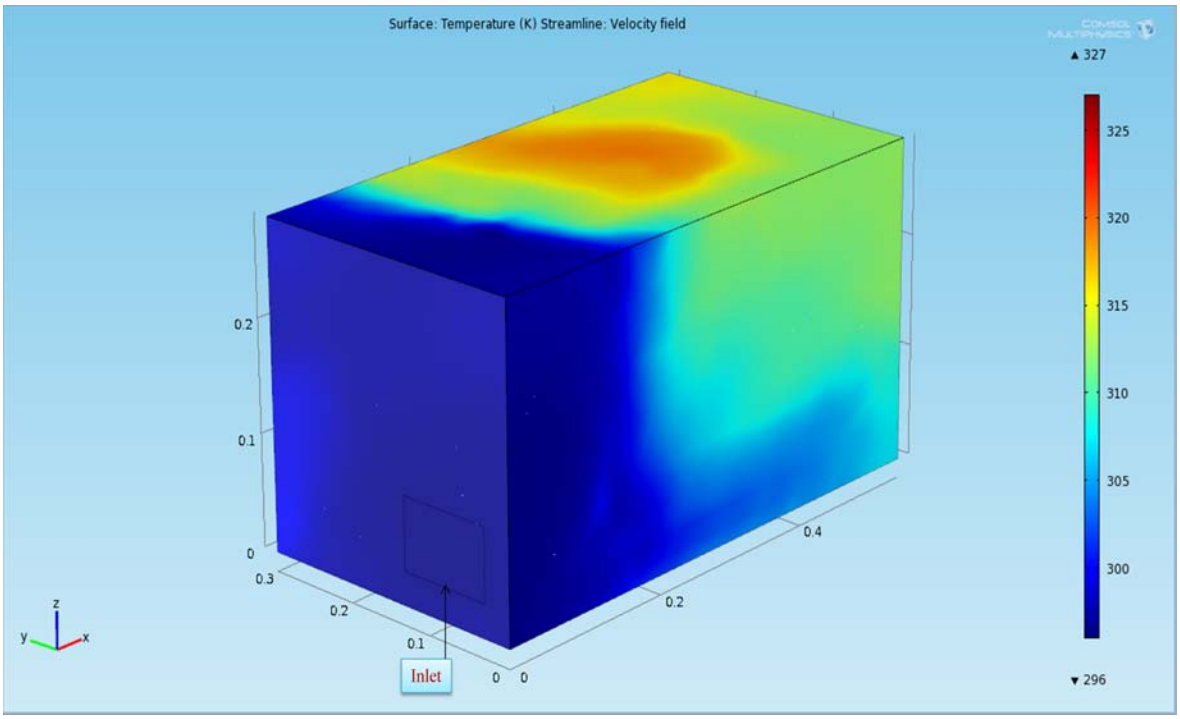

Figure 8-12: Temperature distribution near the surface of the box.

Figure 8-12 shows the view of the surface of the controlled volume of air. This is a view from inlet and top surface. Another view of outlet and bottom is shown in Figure 8-13.

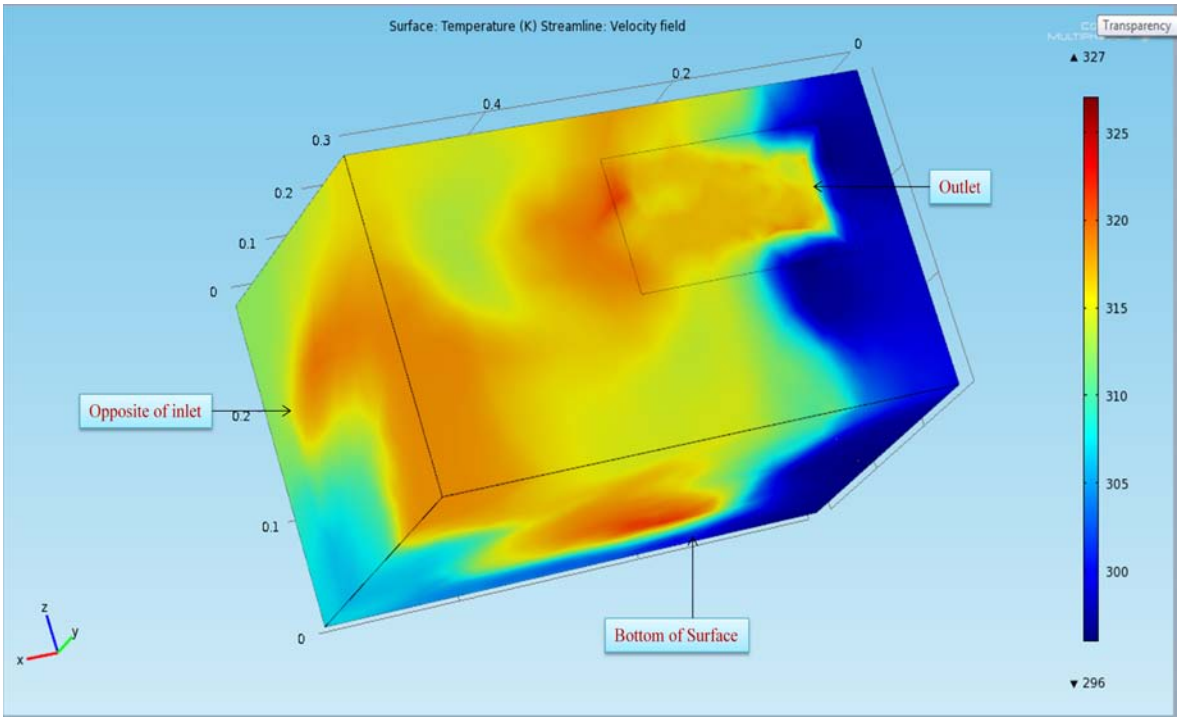

Figure 8-13: Temperature distribution at outlet and bottom side of the system.

We can see that in this case more temperature in the opposite side of the radiator which reaches to 320 K at some points. But on these sides this temperature will not make any effect on the performance of the system. To see the inside distribution of temperature slice plot is drawn.

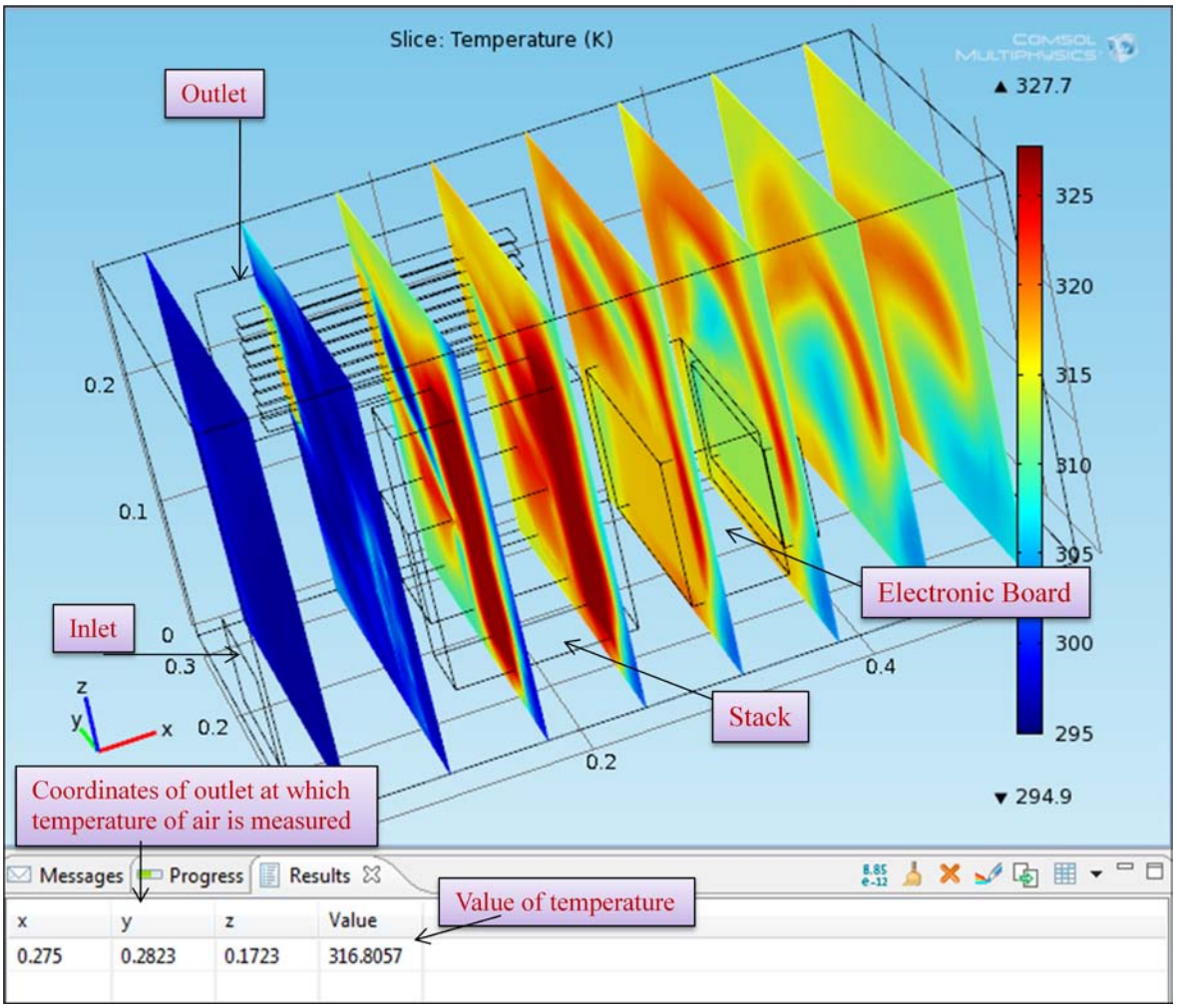

Figure 8-14: Slice plot to show the temperature distribution at different positions inside the system.

Figure 8-14 contains little information about the air that touches the hot part of the radiator. To show the velocity field of the air that flows towards the radiator, stream line plot is shown in figure 8-15.

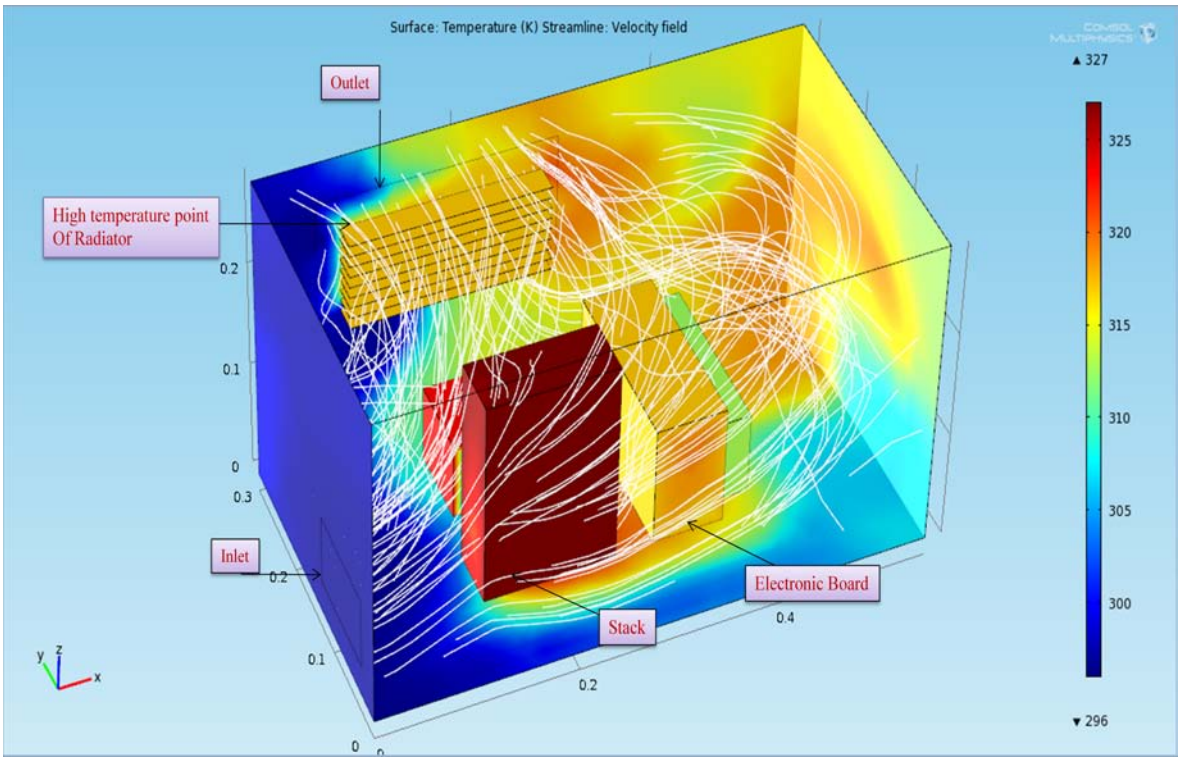

Figure 8-15: Velocity field of the air in the system.

It is clear from the figure that much part of inlet air is touching to the radiator without taking heat from the stack and in this way it can take heat more efficiently from the radiator and the performance of the cooling system will improve.

As it is shown in figure 8-14, the temperature of the air leaving the cooling system is less than 317 K. An important point to note is that the air temperature of the air is after touching the radiator whose temperature is 317 K. To know the heat removing capacity of the air from the radiator another computation is performed and in this computation the radiator is not present in the system. The heat removing capacity of the air can be judged by calculating the temperature difference of the radiator operating temperature (317 K) and the air leaving the system.

Figure 8-16 shows the computation model used for another analysis. There is not radiator present in this model. The result of this computation is shown in figure 8-17 and figure 8-18.

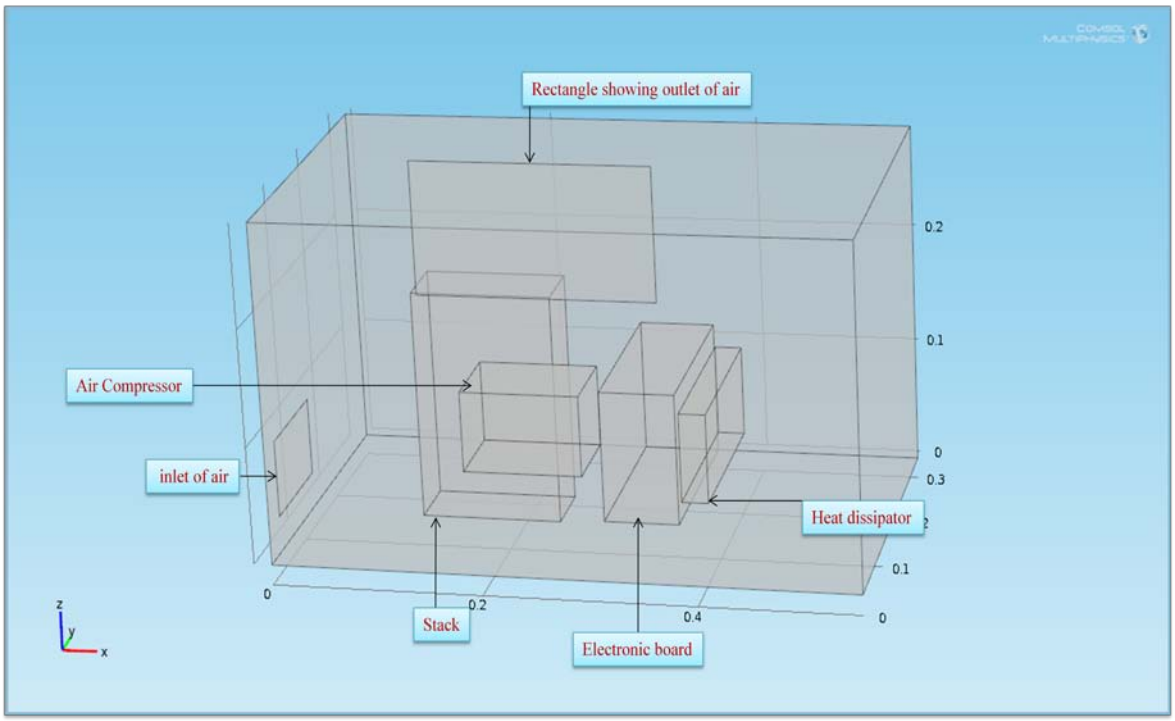

Figure 8-16: Model without radiator used for the computation.

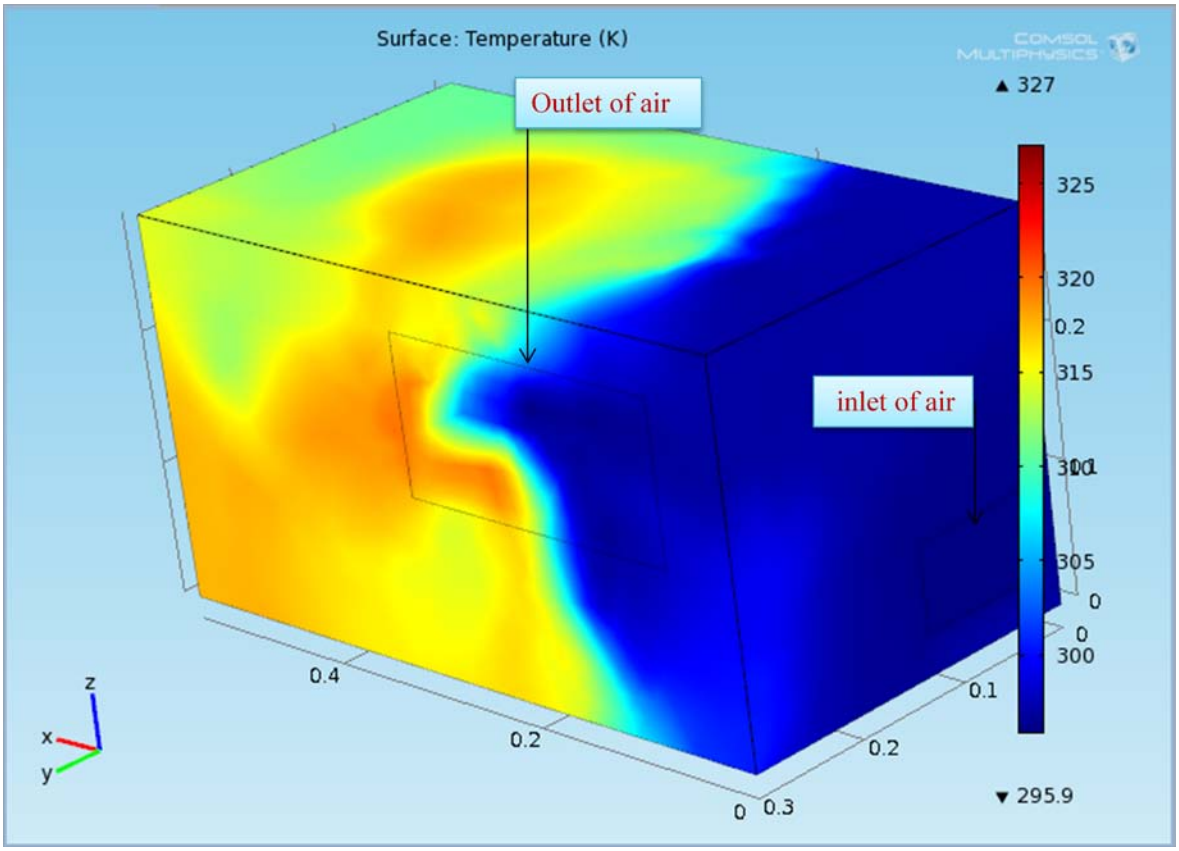

Figure 8-17: Temperature distribution at the outlet and top surface of the system

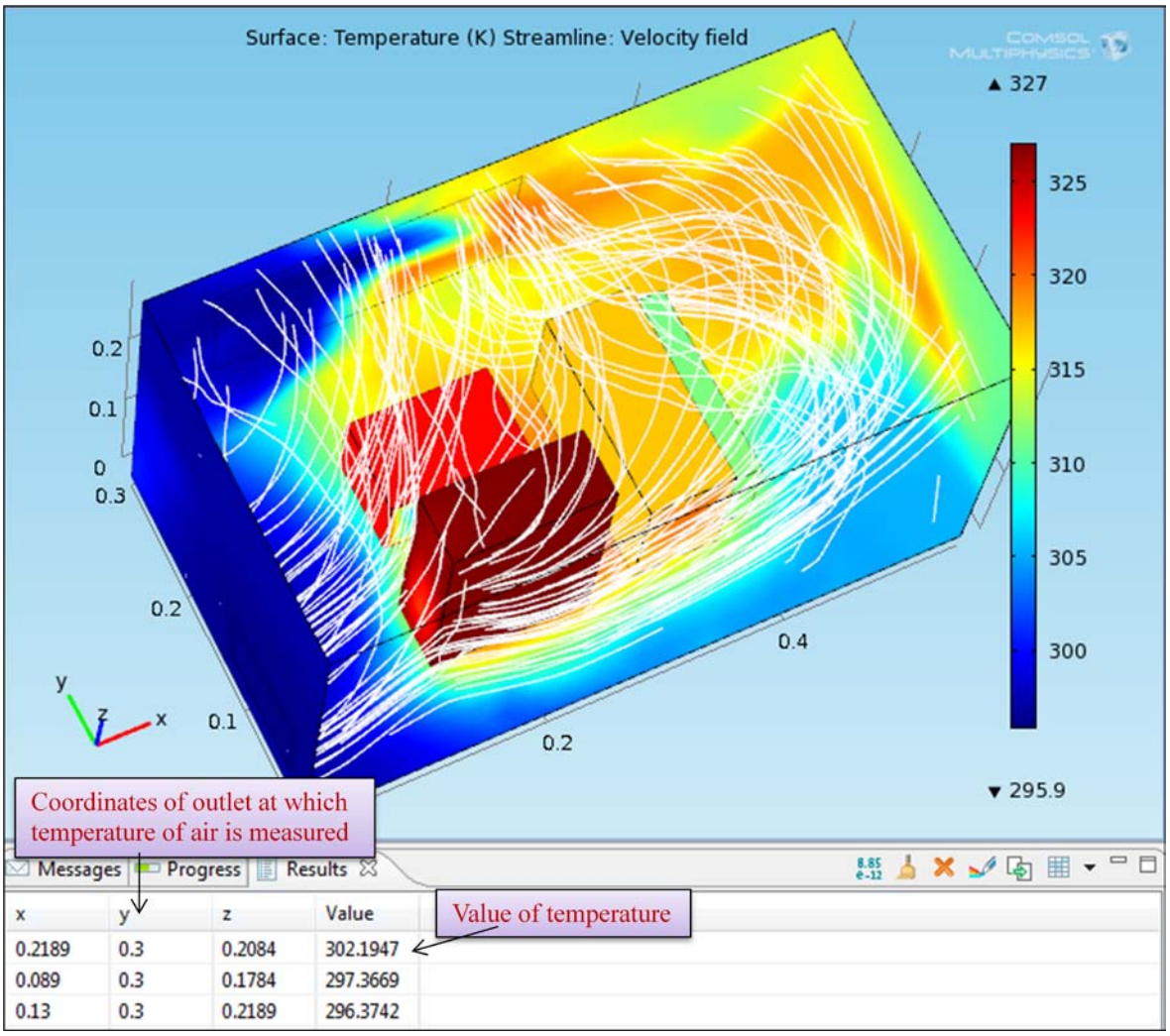

Figure 8-18: Air velocity field and measured temperature of air leaving the system.

The velocity field is same as the one shown in figure 8-15 but the temperature of the air leaving the system is very close to the ambient temperature especially in the area where the radiator has high temperature point. So the air has maximum capacity of removing heat for this layout. In this configuration the temperature on the opposite side of the inlet face increases but increase of the temperature in that area will not affect the performance of the system.

The slice plot in longitudinal direction and the air velocity field is shown in figure 8-19 and figure 8-20.

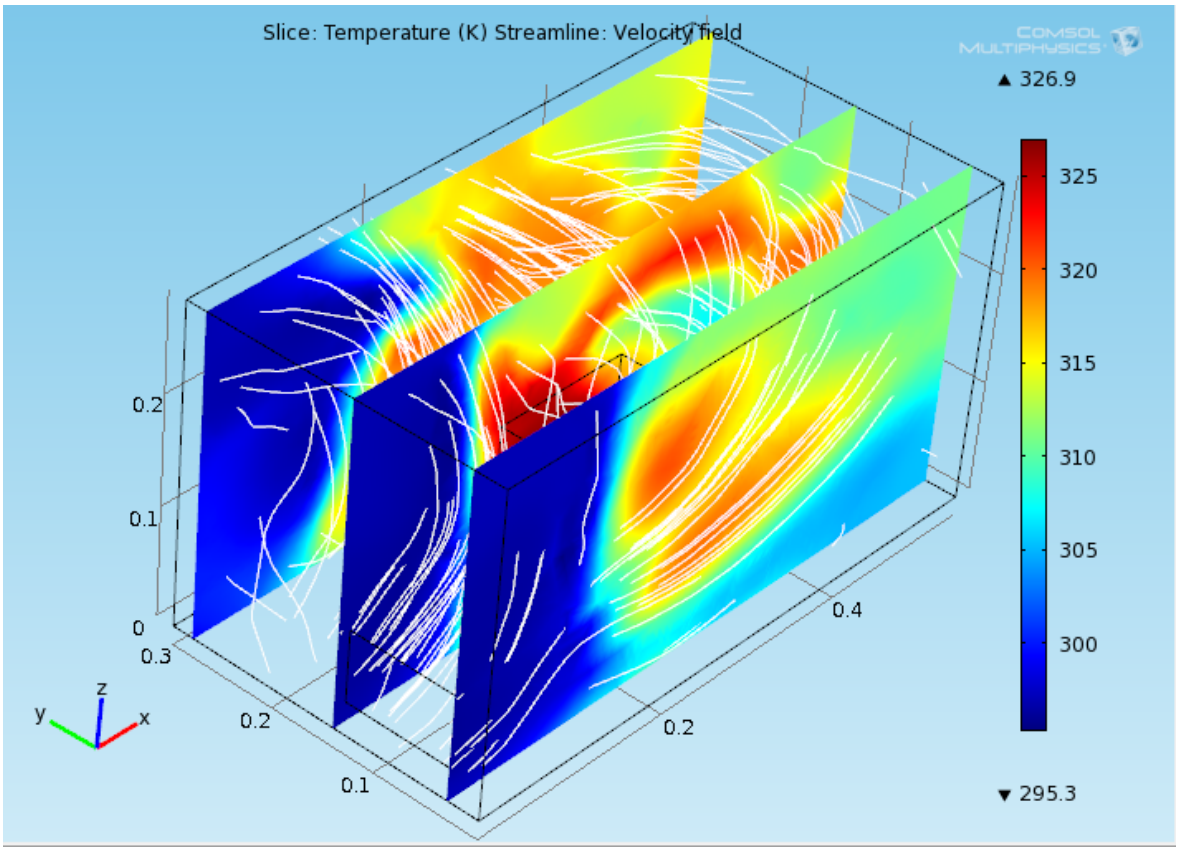

Figure 8-19: A view of Slice plot along longitudinal direction from inlet side

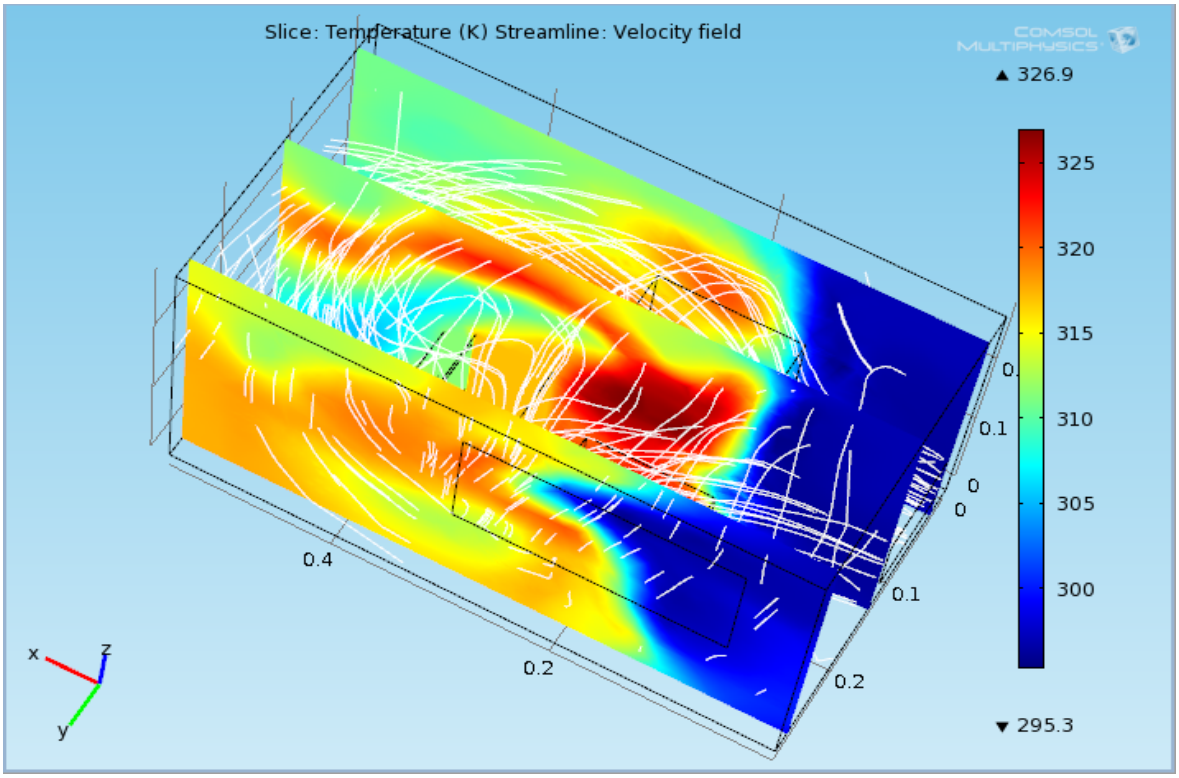

Figure 8-20: A view of Slice plot along longitudinal direction from outlet side

Reference:

[1] Comsol multiphysics 4.0 user's guide.

[2] Comsol heat transfer user's guide.

[3] http://www.comsol.com